bioengineering

MDPI

Review

Recent Advances in the Application of Nanocatalysts for the Hydrodeoxygenation of Lignin and Its Derivatives to Jet-Fuel-Range Cycloalkanes and Aromatics

Kexin Gu [1], Dongyu Zhang [1], Meiting Yin [1], Shu Yan [1,2,*], Wenjun Fang [1,2,3] and Yongsheng Guo [1,2,3,*]

[1] Department of Chemistry, Zhejiang University, Hangzhou 310058, China; 12537019@zju.edu.cn (K.G.); 12537073@zju.edu.cn (D.Z.); 22437027@zju.edu.cn (M.Y.); fwjun@zju.edu.cn (W.F.)
[2] Center of Chemistry for Frontier Technologies, Zhejiang University, Hangzhou 310058, China
[3] Zhejiang Key Laboratory of Low-Carbon Synthesis of Value-Added Chemicals, Zhejiang University, Hangzhou 310058, China
* Correspondence: 21637062@zju.edu.cn (S.Y.); wjjw@zju.edu.cn (Y.G.); Tel.: +86-13588839326 (Y.G.)

Abstract

Lignin is the sole renewable organic carbon resource that is intrinsically rich in aromatic rings. Its catalytic hydrodeoxygenation (HDO) to produce jet-fuel-range cycloalkanes and aromatics represents a pivotal route toward achieving sustainable aviation fuel. The central challenge of HDO lies in achieving selective C-O bond cleavage while precisely controlling the hydrogenation of aromatic rings. This review systematically summarizes recent advances in nanocatalysts for this application, covering molybdenum-based catalysts (edge-site engineering and oxygen vacancy regulation in MoS_2), nickel-based catalysts (optimization of low-temperature activity in nickel phosphide and hydrogen spillover strategies), bimetallic catalysts (geometric/electronic/stabilization/synergistic effects), and bifunctional catalysts (synergy between acid sites and metal sites), with particular emphasis on the emerging single-atom catalysts (coordination environment and charge density regulation). The functional roles of nanocatalysts in cascade conversion processes are also discussed. Finally, the future directions for the rational design of highly efficient nanocatalytic systems are outlined, aiming to provide insights for the targeted synthesis of lignin-based jet-fuel-range cycloalkanes and aromatics.

Keywords: lignin; hydrodeoxygenation; nanocatalysis; sustainable aviation fuel (SAF)

Check for updates

Academic Editor: Reeta Rani Singhania

Received: 2 September 2026
Revised: 1 October 2026
Accepted: 15 October 2026
Published: 19 October 2026

Copyright: © 2026 by the authors. Licensee MDPI, Basel, Switzerland. This article is an open access article distributed under the terms and conditions of the Creative Commons Attribution (CC BY) license.

1. Introduction

Biomass is defined as any organic matter that is regenerable on a timescale relevant to human use. Among various renewable resources (such as solar energy and wind power, etc.), biomass stands out as the sole naturally occurring renewable organic carbon resource, conferring a unique advantage in producing high-value-added products [1–4]. In the energy sector, amid pressing challenges such as the energy crisis and climate deterioration, biomass holds a significant position in the context of energy transition and the "dual carbon" goals. Globally, the transportation sector currently accounts for approximately one-quarter of energy-related CO_2 emissions, with aviation and shipping together contributing about 4–5%. Within the aviation sector, sustainable aviation fuel (SAF) accounts for only 0.1% [5]. SAF represents a practical and immediately deployable solution for aviation decarbonization, as its life-cycle CO_2 emissions can be reduced by up to 80% compared to conventional jet fuel [6]. The World Economic Forum's 2025 Global Aviation Sustainability Outlook

particularly emphasizes the critical role of SAF in advancing aviation decarbonization, and identifies the availability and cost of SAF as one of the top ten challenges impeding this process (Figure 1) [7]. Therefore, the importance of developing biomass-derived jet fuel is self-evident.



Figure 1. The top ten challenges impeding the decarbonization of aviation. Reproduced with permission from [7].

Conventional aviation jet fuel is composed of paraffins, cycloalkanes and aromatics, with a carbon number range of approximately C9 to C16 [8,9]. Among these, cycloalkanes exhibit higher thermal stability, greater energy density, and shorter ignition delay time compared to *n*-alkanes [10–13]. Additionally, the favorable low-temperature properties of cycloalkanes help maintain fuel fluidity at low temperatures while preserving energy density [10]. Natelson et al. [14] demonstrated that alkyl-substituted cyclohexanes generate various unsaturated alkyl radicals and cycloalkenes during low-temperature combustion decomposition pathways, thereby conferring two-stage ignition capability. Aromatic hydrocarbons, despite their inferior thermal oxidative stability, play a crucial role in determining the fuel system safety, lubricity, and the swelling of elastomeric O-ring seals in fuel tanks [15]. Studies have indicated low-molecular-weight alkylbenzenes as ideal aromatic components for fully synthetic aviation turbine fuels [8,16]. Furthermore, monocyclic aromatics exhibit advantages over polycyclic aromatics in terms of heat release profile and emissions performance [16,17].

However, the current mainstream technical routes for producing jet fuel from biomass components are each confronted with a distinct set of challenges: the biomass gasification–Fischer–Tropsch (FT) synthesis hydroprocessing route suffers from limited and unstable feedstock supply, as well as high processing costs [18]. The hydroprocessed esters and fatty acids (HEFA) route, which relies on vegetable oils and animal fats, directly competes with the food supply chain, and is further plagued by catalyst deactivation, high production costs, and relatively higher carbon emissions [19,20]. The alcohol-to-jet (ATJ) route, based on bio-derived light alcohols, faces issues such as complex and multi-step processes, high energy intensity, low Technology Readiness Level (TRL), and carbon emissions that are significantly higher than those of other mainstream SAF pathways [21]. The power-to-liquid (PtL/e-fuels) route encounters challenges that primarily originate from the upstream electrolysis stage, including high capital costs, low energy conversion efficiency with a substantial portion of electrical energy being dissipated as heat, and a similarly low TRL [22,23]. Furthermore, a common shortcoming across these routes is that the resulting products are predominantly paraffinic hydrocarbons, with insufficient contents of cycloalkanes and aromatics to meet fuel specifications, thereby necessitating blending with conventional

petroleum-based jet fuel [24]. Relevant studies suggest that the blending ratio of such alternative fuels should not exceed 50%, and that the volume fraction of aromatics should not fall below 8% [25,26].

In contrast, the lignocellulosic biomass conversion (LCBC) route, which utilizes lignocellulosic biomass, including lignin, as feedstock, offers inherent advantages for producing SAF: 1. Abundant and underutilized feedstock. The global annual production of lignocellulosic biomass is approximately 182 billion tonnes, of which only about 8 billion tonnes are currently utilized [27]. Lignocellulose mainly consists of three components: hemicellulose, cellulose, and lignin (Figure 2) [28]. Lignin accounts for about 15–35% of the total mass and up to 40% of the total energy content [3]. Moreover, lignin is non-edible, and its use does not compete directly with the food supply chain; it is therefore recognized as a promising alternative to fossil-based fuels and chemicals [1]. 2. Intrinsic structural compatibility with jet-fuel aromatic and cycloalkane fractions. Lignin is the only naturally occurring polymer that is rich in aromatic rings, which endows it with an intrinsic structural advantage for "naturally matching" the aromatic and cycloalkane fractions required in jet fuel [28,29]. This inherent compatibility provides a feasible pathway toward developing fully drop-in jet fuel that can be used at 100% without blending limitations [24]. 3. Superior carbon footprint. The LCBC route can achieve up to 94% greenhouse gas emission reduction over its life cycle, significantly outperforming the HEFA route and the PtL route in terms of carbon performance [20].

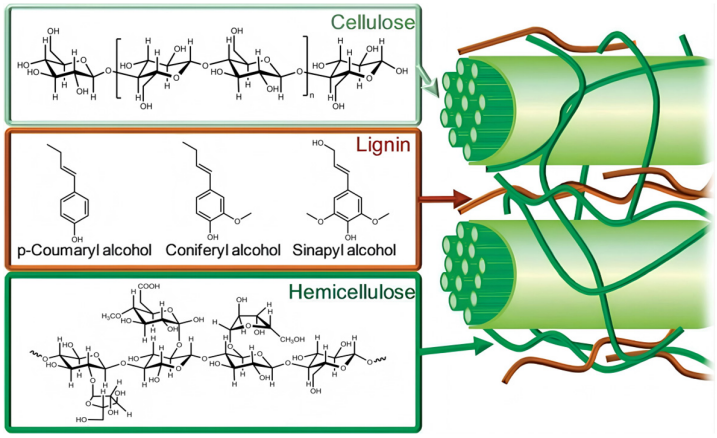


Figure 2. The structure of cellulose, hemicellulose and lignin in woody cellulose. Reproduced with permission from [28]; published by Royal Society of Chemistry, 2012.

Although the composition and content of lignin vary among different plant species, it is generally composed of three basic C9 structural units: p-coumaryl alcohol (H), coniferyl alcohol (G), and sinapyl alcohol (S). These units are linked through ether bonds (C-O-C) and carbon–carbon bonds (C-C) (Figure 2) [28,29]. In native lignin, ether bonds account for two-thirds or more of the total linkages. Lignin can be depolymerized via various approaches, including pyrolysis [30], gasification [31–33], hydrogenolysis [34–36], oxidation [37], as well as photo-/electrocatalytic degradation [38–40], microwave-assisted degradation [41–43], or enzymatic hydrolysis [44,45] (Figure 3) [1]. The primary products are oxygenated aromatic compounds, which cannot be directly utilized as jet fuel. Among the various upgrading strategies, hydrodeoxygenation (HDO) is recognized as the most effective approach for upgrading lignin-derived oils [1,46]. The HDO process proceeds via two parallel reaction pathways: direct deoxygenation (DDO) and hydrogenation–deoxygenation (HYD). In the DDO pathway, the aromatic ring structure is preserved through hydrogenolysis of the C-O bonds in the side chains, yielding aromatics as the main products. In the HYD pathway, the aromatic ring is first hydrogenated to saturation, followed by hydrogenolysis of the

C-O bonds in the side chains, producing cycloalkanes such as cyclohexane and propylcyclohexane [47], which are key components of aviation kerosene. However, direct HDO of lignin-derived monomers typically yields lower-molecular-weight aromatics and cycloalkanes such as benzene (C6), toluene (C7), cyclohexane (C6), and methylcyclohexane (C7). Although these compounds fall below the ideal jet-fuel carbon range, they can be upgraded to jet-fuel-range hydrocarbons through C-C coupling reactions such as alkylation or aldol condensation, followed by HDO [48,49]. Therefore, in this review, the term "jet-fuel-range products" is used broadly to denote hydrocarbons that can ultimately be converted into jet fuel components, either directly or after appropriate C-C coupling/upgrading steps. We do not strictly distinguish C6-C8 and C9-C16 products in the subsequent discussion. Instead, we focus on the catalytic strategies that enable selective C-O cleavage and controlled hydrogenation, with the understanding that low-molecular-weight products can be further upgraded to meet jet fuel specifications.

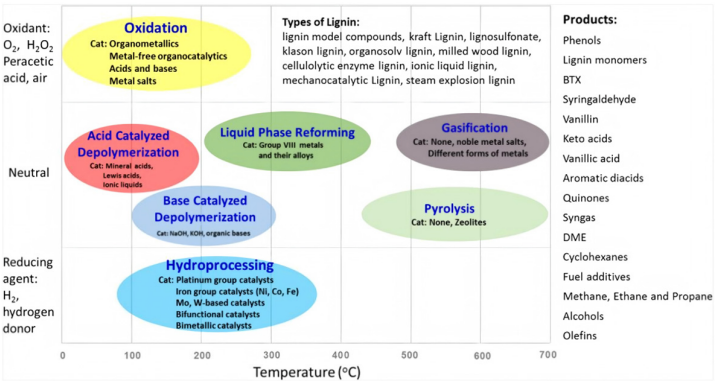


Figure 3. Summary of the lignin conversion process. Reproduced with permission from [1]; published by American Chemical Society, 2015.

However, achieving the desired selectivity control in the aforementioned pathways remains a formidable challenge. The HDO reaction involves competing C-O bond cleavage and aromatic ring hydrogenation, which impose markedly different requirements on the geometric configuration and electronic density of the catalyst active sites [50]. Catalysts developed for lignin HDO include noble metals, non-noble metals, and their nitrides, carbides, and phosphides. Studies have demonstrated that nanocatalysts, in which the active sites or active phases are controlled at the nanoscale (typically 1–100 nm), exhibit unique reactivity in lignin HDO reactions [51]. Taking metal catalysts as an example, nanoscale metal particles (typically < 5 nm) expose a high density of unsaturated coordination sites, with a significantly increased proportion of surface steps and edge sites, which can substantially lower the energy barrier for C-O bond cleavage [52,53]. Mondelli et al. [52], from the perspective of fundamental catalyst design, pointed out that the particle size and chemical state of the metal played a decisive role in determining the activity, selectivity, and stability of the catalyst. Owing to the unique structure-sensitive nature of competing reactions, tuning the size of metal nanoparticles can effectively modulate the product distribution in many hydrogenation, oxidation, and reforming reactions. Moreover, smaller particle sizes also imply a higher density of accessible surface metal atoms, which enhances the catalytic activity for both C-O bond cleavage and hydrogenation, highlighting the importance of precisely tailoring the particle size of metal and metal–support interactions for achieving high target product selectivity and catalytic efficiency in lignin valorization. In fact, the strong metal–support interaction (SMSI) is a size-dependent phenomenon: the interfacial contact area and the extent of charge transfer between metal and support are governed by the dimensions of the active phase, endowing it with a critical role in enhancing the

reactivity and stability of the catalyst [54,55]. In addition to geometric and interfacial effects, electronic and defect-related effects are likewise intimately tied to the nanoscale and play a decisive role in catalysis. When metal particles are reduced to the nanoscale, the proportion of surface atoms increases dramatically, and the electronic structure undergoes substantial changes, including shifts in the d-band center, alterations in oxidation state, and quantum size effects, which in turn determine adsorption energies and reaction barriers [51,56]. Similarly, defect chemistry, including oxygen vacancies, coordinatively unsaturated sites, and cationic vacancies, is also intimately linked to nanoscale structure, as the formation and stabilization of these defects depend on particle size, morphology, and surface reconstruction [57]. Begum et al. [58] demonstrated that the particle size of Ru significantly influenced its catalytic performance in the HDO of lignin-derived compounds: specifically, undercoordinated Ru sites were more favorable for C-O bond cleavage, whereas ring hydrogenation occurred preferentially on coordinatively saturated sites.

This review systematically summarizes recent research progress on nanocatalysts for the HDO of lignin to produce jet-fuel-range cycloalkanes and aromatics. First, molybdenum-based catalysts are introduced, with a focus on edge-site engineering of MoS_2 and strategies for activating inert basal planes, oxygen vacancy regulation in molybdenum oxides, and the noble-metal-like catalytic behavior of molybdenum carbides and nitrides. Second, nickel-based catalysts are discussed, emphasizing hydrogen spillover and transfer hydrogenation strategies, as well as activity modulation in C-O/C-C bond cleavage. Third, the metal–metal interaction (geometric, electronic, stabilization, and synergistic effects) of bimetallic catalysts and their influence on deoxygenation selectivity are explored. Subsequently, bifunctional catalysts (including metal–zeolite, metal–metal oxide, and metal–polyoxometalate composite systems) are highlighted, elucidating the synergistic mechanisms between acid sites and metal active sites in cascade deoxygenation, isomerization, and selectivity control. Furthermore, emerging single-atom catalysts are reviewed for their cutting-edge achievements to achieve precise product selectivity via fine-tuning of electronic structure. Finally, the current challenges are summarized, and future directions for the rational design of high-performance nanocatalytic systems are envisioned, with the aim of providing theoretical foundations and technical references for the targeted synthesis of aromatic and cycloalkane components in lignin-based SAF.

2. Nanocatalysts

Platinum-group metals (PGMs, such as Ru, Rh, Pd, and Pt) and certain non-noble metals (e.g., Mo, Ni, and Co) possess excellent hydrogenation and deoxygenation capabilities and have been widely used in the HDO of bio-oil [59–62]. However, the use of PGMs alone as catalysts is not an optimal choice for HDO processes [63–65], owing to their high cost and their excessively strong hydrogenation activity, which readily saturates aromatic rings and thereby compromises the retention of the aromatic fraction required in jet fuel. Consequently, PGMs are often employed supported on functional supports, such as zeolites, metal oxides, and polyoxometalates, etc. [1], a strategy that will be elaborated in Section 2.4 (Bifunctional Catalysts). In contrast, non-noble metals like Mo and Ni are abundant and cost-effective. Nevertheless, these catalysts typically suffer from issues such as partial hydrogenation and a high propensity for coke deposition, necessitating performance modulation through approaches such as facet engineering or heteroatom doping. Furthermore, it should be emphasized that, although some of the studies cited below also examine lignin-derived oil or raw/technical lignin, mechanistic work in this field has largely relied on model compounds. This is a reasonable starting point: model compounds allow specific C-O linkages and reaction pathways to be isolated, from which broader design principles can be distilled to guide the rational design of future catalysts.

By contrast, studies on the HDO of real lignin remain relatively scarce and less mature. Reaction conditions are often incompletely reported, and performance metrics vary widely across studies. As a result, the data compiled in the table are difficult to compare and interpret consistently. For this reason, the table includes only data for lignin model compounds, while real-lignin studies are discussed in more detail in Section 3.

2.1. Molybdenum-Based Catalysts

Molybdenum-based catalysts include sulfides, oxides, nitrides, carbides, and others, and have been studied since as early as the 1980s, with molybdenum sulfides being the most extensively studied among them [66]. Layered MoS_2 is currently one of the most widely reported transition metal sulfide catalysts for the HDO of lignin (Figure 4). For MoS_2 (Figure 5a), the dominant exposed planes are predominantly the inert basal planes, while the density of active edge sites is governed by the extent of the edge planes. The number of stacked layers is a crucial factor in increasing the edge plane surface area [67–70]. Therefore, maximizing the exposure of edge sites through controlled growth of MoS_2 nanostructures represents a viable strategy for enhancing the catalytic activity of MoS_2-based catalysts. Table 1 summarizes recent studies on the application of molybdenum-based catalysts in the HDO of lignin and its derivatives.

Table 1. A summary of recent literature on the application of molybdenum-based catalysts in the catalytic HDO of lignin.

Year	Catalyst	Substrate	Major Product	Catalyst to Biomass Ratio (C:B)	Size (nm)	Reaction Conditions				Conv. (%)	Sel. (%)	Ref.
						T (°C)	P (MPa)	Time (h)	Solvent			
2023	CoS-MoS_2	4-Methylphenol	Toluene	1:24	n.r.	180	4	7	Dodecane	85	99.5	[71]
2022	Pt-MoS_2-x	*p*-Cresol	Methylcyclohexane	1:12	1.6	120	5	10	Dodecane	100	96.3	[72]
2026	Co_xS_y-*n*-MoS_2	*p*-Cresol	Toluene	1:2	<2	170	3	10	Dodecane	99.9	96.7	[73]
2022	Mo-Co_9S_8/Al_2O_3	Diphenyl ether	Benzene	1:4	n.r.	300	4	4	Methylcyclohexane	98.9	87.2	[74]
2025	Mo/Ti	Phenol	Benzene	N/A	26	330	0.1	1	None (gas phase)	22	100	[75]
2022	Mo_2C-PC	Guaiacol	Benzene	N/A	7.4	350	0.1	2.5	Decalin	100	70	[76]
2023	Mo_2N@NC500/SBA-15	Guaiacol	Aromatic compounds	N/A	2–3	380	2	3	Decane	99	92	[77]

n.r.: not reported; N/A: not applicable.

Among the various strategies, the introduction of promoters at the MoS_2 edges to construct metal–sulfide interfaces has proven to be an effective approach for enhancing the intrinsic activity of the edge sites. Wang et al. [71] developed a novel strategy for the scalable fabrication of Co-promoted MoS_2 catalysts by exploiting sulfur vacancies in MoS_3 and their preferable adsorption of Co ions. Specifically, the CoS-MoS_2 catalyst was prepared via decomposition of MoS_3 followed by in situ sulfidation of cobalt oxides. HRTEM observations revealed that CoS tended to cover the edges of MoS_2, facilitating the formation of CoS–edge interfaces. Compared with pristine MoS_2, the MoS_2 fringes in the Co-Mo-0.5-400 catalyst exhibited increased discontinuity and curvature, indicating basal plane rupture and the generation of additional edge sites. This suggested that the addition of Co reduced the catalyst particle size and produced more intrinsic edges, primarily due to the inhibitory effect of Co on MoS_2 crystallite growth (Figure 6a). Density functional theory (DFT) calculations (Figure 6b) demonstrated that the formation of CoS–edge interfaces enhanced the adsorption of 4-methylphenol and lowered all reaction energy barriers

compared to pristine MoS_2, enabling a toluene yield as high as 100% at a low temperature of 120 °C (Figure 6c). The catalysts synthesized based on this principle exhibited excellent stability, with negligible changes in 4-methylphenol conversion and toluene selectivity over eight consecutive runs. XRD and HRTEM analyses confirmed that no significant agglomeration or sulfur loss occurred. This approach opens up a new scalable strategy for the fabrication of iron family-element-promoted MoS_2-based catalysts, provides an effective route for lignin oil upgrading, and demonstrates promising potential for applications in industrial catalysis and biomass conversion.

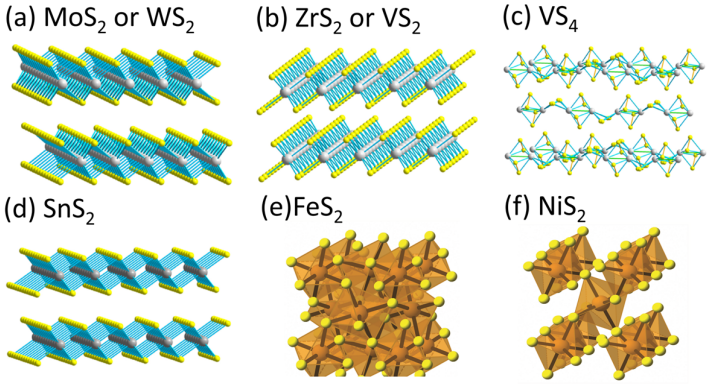


Figure 4. Schematic diagram of the three-dimensional structures of selected transition metal sulfides. (**a**–**d**) Layered structures. Reproduced with permission from [78]; published by RSC Publishing, 2013. (**e**,**f**) Non-layered structures. Reproduced with permission from [79]; published by Elsevier, 2014.

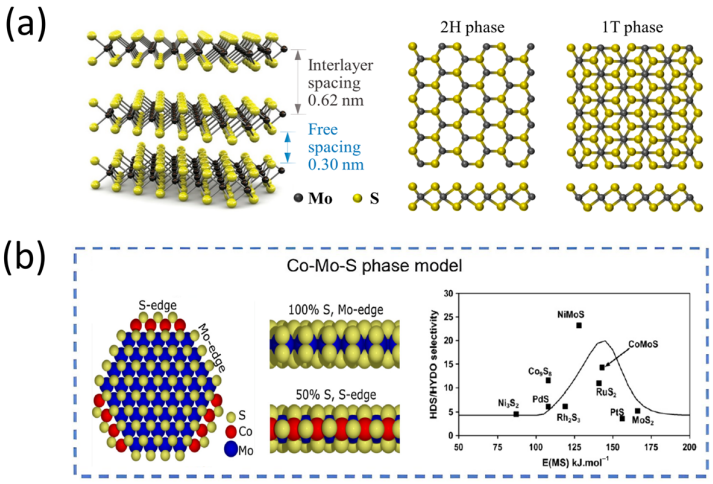


Figure 5. (**a**) MoS_2 structure and HDO reaction mechanism of p-cresol on MoS_2. Reproduced with permission from [80]; published by American Chemical Society, 2017. (**b**) Co-Mo-S active phase model. Reproduced with permission from [81]; published by Elsevier, 2008. Reproduced with permission from [82]; published by Elsevier, 2016.

As mentioned above, two-dimensional MoS_2 catalysts exploit edge sites for their catalytic activity, while the basal planes remain inert in heterogeneous catalysis. To activate these inert basal planes, Wu et al. [72] developed a metal intercalation–deintercalation process to prepare a Pt-MoS_2-x catalyst. HAADF-STEM images revealed that Pt^{4+} partially substituted Mo^{4+} in the basal planes of 1T-MoS_2-x; upon reduction, Pt was deintercalated from the basal planes, ultimately generating abundant edge sites within the originally inert basal planes of MoS_2 and forming numerous Pt–edge interfaces (Figure 7a–j). This Pt-MoS_2-x catalyst exhibited high activity in the HDO of *p*-cresol, achieving 100% oxygen removal at 120 °C, with negligible sulfur loss or deactivation over recycling runs (Figure 7k). DFT calculations indicated that the hydrogenation of the aromatic ring and conjugated

diene exhibited the highest energy barriers on MoS_2-x, identifying these two hydrogenation steps as the primary rate-determining steps. However, owing to the formation of Pt–edge interfaces, dissociated H species on Pt clusters could rapidly spill over to sulfur vacancies at the edge sites to participate in hydrogenation reactions. Consequently, the energy barriers for the aforementioned two rate-limiting hydrogenation steps on the Pt-MoS_2-x catalyst were significantly reduced, correlating well with the observed catalytic performance and highlighting the critical role of Pt–edge interface formation (Figure 7l). The Pt-MoS_2-x catalyst was also effective for the HDO of various lignin model compounds and lignin-derived bio-oils. This approach opens up an innovative strategy for designing durable MoS_2 catalysts with activated basal planes and provides an efficient alternative for the synthesis of lignin-based jet-fuel-range cycloalkanes.

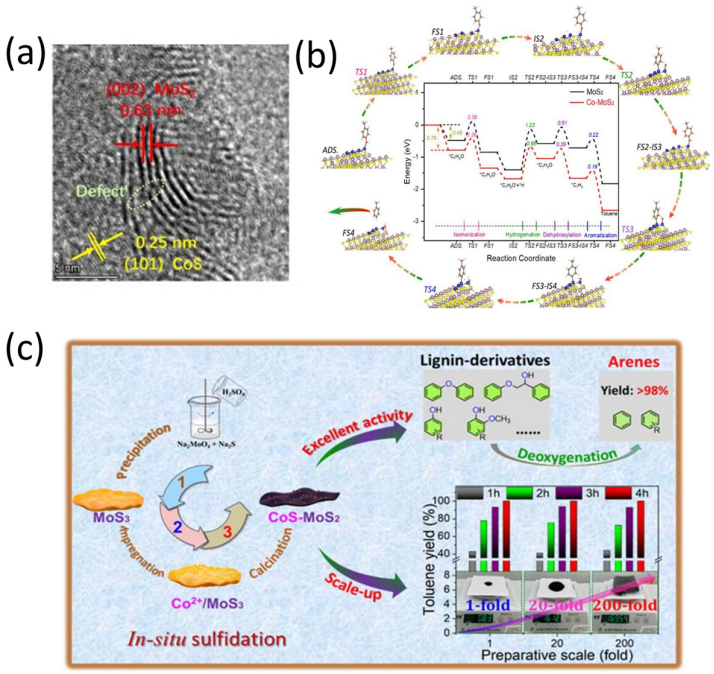


Figure 6. (**a**) HRTEM image of Co-Mo-0.5-400. (**b**) Calculated energy profile for the direct deoxygenation of 4-methylphenol on MoS_2 and CoS-MoS_2 catalysts and DFT-optimized structure for the initial state (IS), transition state (TS), and final state (FS) on CoS-MoS_2 catalyst. (**c**) Flowchart of the preparation process and overview of the properties of CoS-MoS_2 catalysts. Reproduced with permission from [71]; published by American Chemical Society, 2023.

In addition, Diao et al. [73] proposed an alternative one-step approach for activating the inert basal planes of MoS_2, which involves creating nanopores within the basal planes and confining ultra-small Co_xS_y clusters in close proximity to the nanopores through adjacent Co-S covalent bonds. In this work, a catalyst composed of Co_xS_y clusters supported on a nanoporous MoS_2 substrate (designated as Co_xS_y-*n*-MoS_2) was synthesized via a phase transition of 1T-MoS_2 and in situ sulfidation of a cobalt dimethylimidazole complex (Figure 8a). This catalyst exhibited excellent performance in the HDO of lignin and its derivatives to aromatic hydrocarbons. In the HDO of *p*-cresol, the catalyst achieved 99.9% conversion and 96.7% toluene selectivity under mild conditions (170 °C, 3 MPa H_2, 10 h), and maintained its performance over eight consecutive cycles. Moreover, the catalyst demonstrated general applicability to G-type (guaiacyl) and H-type (*p*-hydroxyphenyl) lignin monomers with various side-chain groups, representing state-of-the-art performance among reported catalysts (Figure 8e–i). Mechanistic studies revealed that Co was anchored as Co_xS_y clusters via Co-S covalent bonds adjacent to the nanopores on the MoS_2 basal planes (Figure 8b–d). The ultra-small Co_xS_y clusters served as the primary active

sites, while the nanopores contributed to weakening the C-O bonds through a unique stretching effect on the electron-rich aromatic rings (Figure 8j). This work opens up new opportunities for exploring advanced functional MoS_2-based catalysts for the synthesis of lignin-derived aromatics.

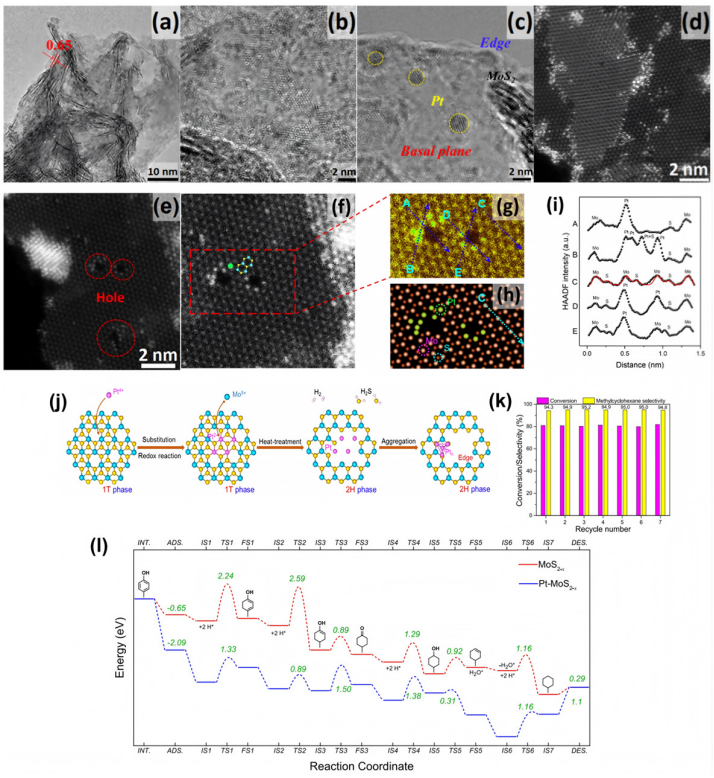


Figure 7. (**a**) TEM image of Pt-Mo. HRTEM images of (**b**) Pt-Mo and (**c**) Pt-Mo-200. HAADF-STEM image of (**d**) Pt-Mo and (**e**) Pt-Mo-200. (**f**,**g**) enlarged and (**h**) simulated HAADF-STEM images of Pt-Mo-200. (**i**) Measured intensity profile along four lines labeled in (**g**), (**h**), and (**j**) schematic illustration of the formation of the Pt-MoS_2-x catalyst. (**k**) Stability test of Pt-Mo-200 in the HDO of *p*-cresol. (**l**) Energy barrier profiles for the HDO of *p*-cresol on MoS_2-x and Pt-MoS_2-x. Reproduced with permission from [72]; published by American Chemical Society, 2022.

In industry, CoMoS and NiMoS are two conventional transition metal sulfide catalysts used in hydrotreating processes, exhibiting good conversion performance (Figure 5b) [82]. However, these sulfide catalysts suffer from sulfur loss and poor stability under industrial operating condition [83,84]. Therefore, to facilitate the practical application of MoS_2-based catalysts, effective strategies are urgently needed to substantially enhance their high-temperature stability without compromising catalytic activity. Diao et al. [74] developed a facile synthesis strategy to fabricate a Mo-Co_9S_8/Al_2O_3 catalyst assembled from isolated MoS_2 slabs and Mo-Co_9S_8 structures, which served as a highly selective and stable catalyst for converting lignin model compounds, lignin bio-oil, and even raw lignin into aromatic hydrocarbons. The Mo-Co_9S_8/Al_2O_3 catalyst was prepared by loading Mo onto a hydrotalcite-derived Co_3O_4/Al_2O_3 support, followed by subsequent sulfidation. In this catalyst, Mo existed in two forms: isolated MoS_2 slabs and Mo-Co_9S_8 structures, which are chemically connected via Mo-S-Co type covalent bonds on the Co_9S_8 surface (Figure 9a). This multifunctional assembled Mo-Co_9S_8/Al_2O_3 catalyst exhibited electron transfer from Co to Mo sites within the Mo-Co_9S_8 structure, and the Mo-Co_9S_8 interface possessed a unique affinity for adsorbing oxygenated compounds, thereby conferring exceptional HDO performance (Figure 9b,c). Moreover, owing to the anchoring effect of the Al_2O_3 matrix and the electronic effect of Co_9S_8, the catalyst demonstrated excellent resistance to high

reaction temperatures (265 °C) and H_2O poisoning. After 10 cycles, the conversion and benzene yield remained at approximately 99.8% and 91.0%, respectively, with no significant deactivation observed (Figure 9d,e). Characterization by XRD, Raman, TEM, and ICP-OES confirmed that both the surface Mo active centers and the overall catalyst structure remained stable after reaction, with no appreciable sulfur loss. Overall, this work provides a facile strategy for designing MoS_2-based catalysts with exceptional high-temperature stability and HDO activity, highlighting their promising potential for application under harsh high-temperature conditions.

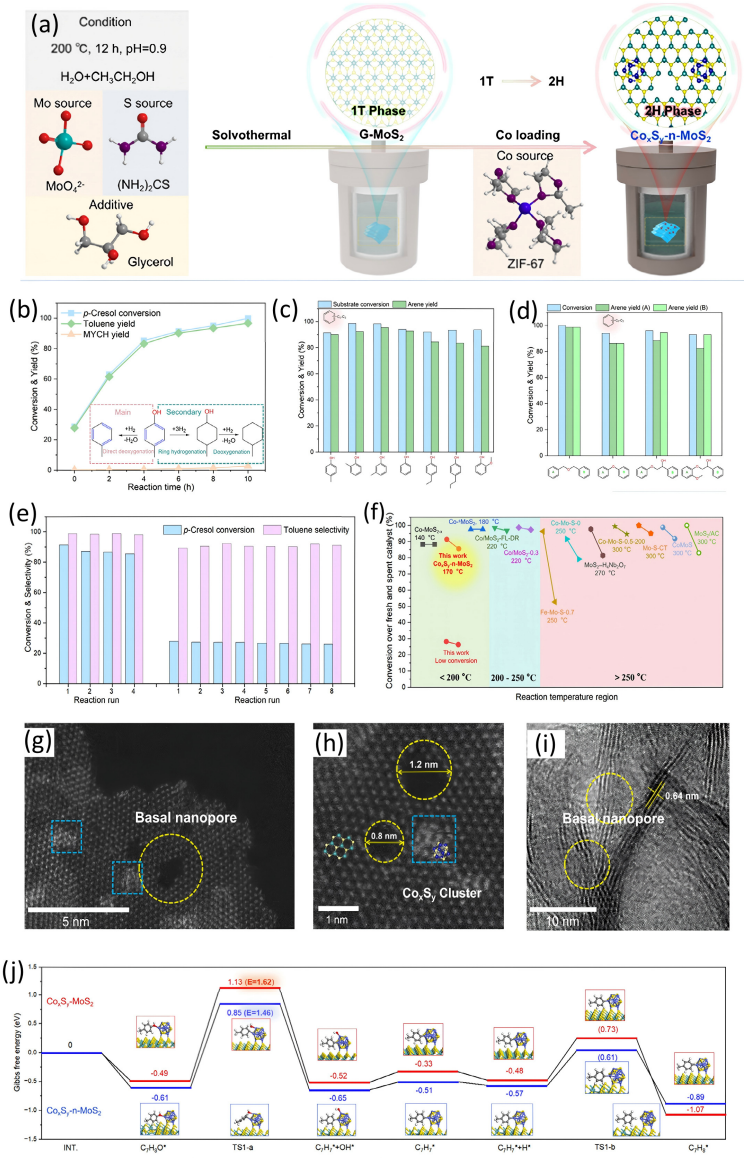


Figure 8. (**a**) Schematic illustration of the preparation procedure of Co_xS_y-*n*-MoS_2. (**b**) Product distributions as a function of reaction time for Co_xS_y-*n*-MoS_2. (**c**) HDO result of *p*-cresol over Co_xS_y-*n*-MoS_2 at different reaction temperatures. (**d**) HDO result of *p*-cresol over Co_xS_y-*n*-MoS_2 under different initial H_2 pressure. (**e**) Stability test of Co_xS_y-*n*-MoS_2 in the HDO of *p*-cresol at 170 °C for 6 h under 3 MPa (full conversion) and 1 MPa (low conversion), respectively. (**f**) The comparison of the activity over various MoS_2-based catalysts in HDO of lignin derivatives. (**g**,**h**) HAADF-STEM images of Co_xS_y-*n*-MoS_2. (**i**) HRTEM images of Co_xS_y-*n*-MoS_2. (**j**) Energy barrier profiles for the HDO of *p*-cresol on Co_xS_y-MoS_2 and Co_xS_y-*n*-MoS_2. The yellow and green represent electron accumulation and depletion, respectively. Reproduced with permission from [73]; published by John Wiley and Sons, 2026.

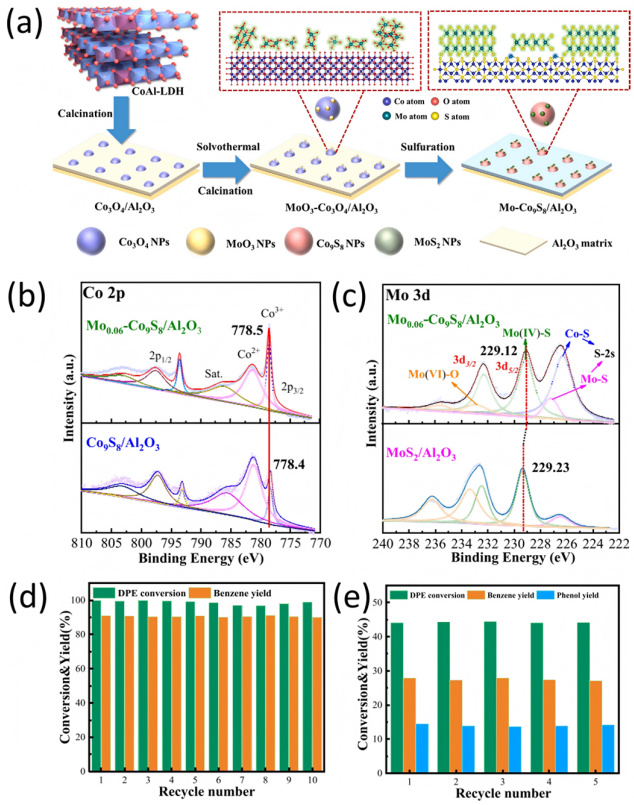


Figure 9. (**a**) Schematic illustration of the preparation procedure of Mo-Co_9S_8/Al_2O_3 catalyst. (**b**) XPS spectra for Co 2p. (**c**) XPS spectra for Mo 3d. (**d**) Stability test of $Mo_{0.06}$-Co_9S_8/Al_2O_3 in the HDO of diphenyl ether (DPE) at 265 °C for 10 h. (**e**) Stability test of $Mo_{0.06}$-Co_9S_8/Al_2O_3 in the HDO of DPE at 265 °C for 2 h. Reproduced with permission from [74]; published by Elsevier, 2022.

Overall, by virtue of the inherent selectivity toward aromatic hydrocarbons, cost-effectiveness, and sulfur resistance imparted by the edge–rim structure of MoS_2 itself, together with the morphological tunability arising from its layered structure [85], MoS_2-based catalysts can achieve efficient and selective deoxygenation of lignin derivatives under mild conditions. However, these systems require high hydrogen pressures and the continuous addition of sulfur to maintain activity, which in turn necessitates additional purification steps to eliminate sulfur contaminants [86]. Moreover, owing to the high oxygen-to-sulfur ratio in lignin oil, sulfide catalysts are susceptible to deactivation through oxidation of the active sites [87]. In contrast, oxides, carbides, and nitrides exhibit activities comparable to those of sulfides and have therefore attracted considerable attention for their application in HDO reactions.

Studies have revealed that molybdenum oxides can selectively cleave C-O bonds under low hydrogen pressures while avoiding saturation of the aromatic rings in lignin-derived compounds, and they also exhibit strong resistance to water and coke formation [88–93]. Molybdenum oxides exist in multiple oxidation states, such as MoO_2 and MoO_3, and the activity of molybdenum-based oxides is closely related to the electron density of Mo in the catalyst. A comparative study on the HDO performance of various unsupported molybdenum-based compounds toward 4-methylphenol revealed that the turnover frequency (TOF), based on CO uptake, decreased in the order MoP > MoS_2 > MoO_2 > MoO_3, whereas the activation energy increased in the reverse order [94]. Several studies have demonstrated the HDO activity of MoO_2/C catalysts and their excellent selectivity toward C-O bond cleavage without causing saturation of C=C bonds, thereby reducing hydrogen consumption during the reaction. Ansaloni et al. [88] conducted mechanistic investigations on molybdenum oxides and attributed the HDO performance of MoO_2/C toward

guaiacol to active sites formed by oxygen vacancies (also referred to as coordinatively unsaturated sites, CUS), which simultaneously served as selectivity-determining sites. The surface modifications induced by the formation of CUS influenced both selectivity and activity, and these oxygen vacancies were generated by the surface reduction of specific Mo (IV) species. Furthermore, MoO_2 exhibits superior resistance to CO formation and water poisoning [88,92,93].

Bulk molybdenum oxides are highly effective for the HDO of various biomass-derived compounds, primarily yielding aromatic hydrocarbons and olefins [95]. The influence of supports on the HDO performance of molybdenum oxide catalysts for lignin-derived compounds has also been subject to preliminary investigation. Studies have indicated that MoO_x catalysts supported on SiO_2, γ-Al_2O_3, TiO_2, ZrO_2, and CeO_2 exhibit exceptionally high selectivity for cleaving the C-O bond of m-cresol without hydrogenating the aromatic ring [91]. In addition, Dionizio et al. [75] conducted a comparative study on the HDO of phenol over molybdenum oxides supported on titania, activated carbon, and silica. The catalytic activity decreased in the order Mo/Ti > Mo/C > Mo/Si, whereas the selectivity to benzene remained 100% across all catalysts, indicating that the molybdenum active phase did not directly influence the reaction selectivity and that the reaction proceeded predominantly via the direct deoxygenation pathway rather than the aromatic ring hydrogenation route. Hydrogen pretreatment exerted a significant effect on catalyst activity: for Mo/Ti, high-temperature reduction ($\geq$400 °C) led to decreased activity, which may be attributed to the SMSI effect; for Mo/C, however, high-temperature reduction ($\geq$400 °C) substantially enhanced the activity, possibly due to the formation of MoO_2 active sites. In conjunction with H_2O-TPD results, the amount of hydrogen desorbed followed the order Mo/Ti > Mo/C > Mo/Si and showed a positive correlation with the HDO rate, suggesting that a higher concentration of oxygen vacancies was associated with higher HDO activity. This finding is consistent with the previously discussed influence of oxygen vacancies on the HDO of lignin-derived substrates.

Recently, molybdenum carbide (Mo_2C) catalysts have attracted considerable attention due to their Pt-like behavior in HDO reactions [96]. Mo_2C catalysts have been applied not only to the production of aromatic hydrocarbons [97] but also to the generation of phenolic monomers [98]. However, conventional carburization synthesis methods often lead to carbon deposition on the Mo_2C surface [99]. To address this issue, Yu et al. [76] employed low-temperature plasma generated from H_2 and CH_4 to reduce and carburize molybdenum oxide precursors, yielding β-Mo_2C, designated as Mo_2C-PC. For comparison, a molybdenum carbide catalyst (Mo_2C-TPC) was also prepared via conventional temperature-programmed reduction carburization. According to calculations based on the Scherrer equation from XRD patterns and XPS measurements, Mo_2C-PC exhibited a smaller crystallite size (7.4 nm) and a higher density of active sites (Mo^{2+}) (Figure 10a). TEM characterization revealed that Mo_2C-PC particles showed no significant agglomeration, whereas aggregated particles and carbon layers were observed in Mo_2C-TPC (Figure 10b,c). The HDO performance of Mo_2C-PC and Mo_2C-TPC was evaluated using guaiacol, phenol, and anisole as substrates in a stainless-steel tubular reactor. The results demonstrated that at low temperatures (<300 °C), Mo_2C-PC exhibited higher conversion of phenolic compounds and higher selectivity to aromatics compared to Mo_2C-TPC (Figure 10d,e). In the HDO of guaiacol, the TOF of Mo_2C-PC (0.37 s^{-1}) was comparable to that of Mo_2C-TPC (0.32 s^{-1}), indicating that the intrinsic reaction rate per active site did not differ significantly between the two catalysts. This suggested that the enhanced performance could be attributed to the reduced particle size, increased Mo sites (Mo^{2+}), and suppressed carbon deposition. This work provides new insights into the controlled synthesis of molybdenum carbide catalysts

and opens up a viable pathway for the low-temperature and high-efficiency production of lignin-based aromatic hydrocarbons.

Mo_2N exhibits catalytic properties similar to those of platinum-group metals, a feature attributed to the incorporation of nitrogen atoms into the interstitial sites of the molybdenum lattice. Through hybridization between Mo d-orbitals and N p-orbitals, the d-band center of Mo is downshifted, thereby weakening the excessive adsorption of reaction intermediates on the surface and achieving optimized adsorption energetics [100,101]. Consequently, Mo_2N is also considered a promising catalyst for the HDO of bio-oil [102–106]. Wang et al. [77] employed $MoCl_5$ and dicyandiamide as the Mo source and C/N source, respectively, to prepare Mo_2N@NC/SBA-15 with high stability and dispersity. Mo_2N was formed in situ during high-temperature carburization under H_2, while dicyandiamide was converted into nitrogen-doped carbon (NC) (Figure 10f,g). The formation of ultra-fine Mo_2N nanoparticles (NPs) was attributed to the N-doped carbon species surrounding the Mo_2N NPs, which prevented their aggregation at the high carburization temperature (Figure 10e). The Mo_2N@NC/SBA-15 catalyst exhibited high HDO activity and selectivity toward aromatic compounds (Figure 10h,i). At 380 °C and 2 MPa, the selectivity to aromatic products reached 92%, with a guaiacol conversion of 99%, fully demonstrating the great potential of molybdenum-based nitrides for the HDO of lignin to aromatic hydrocarbons.

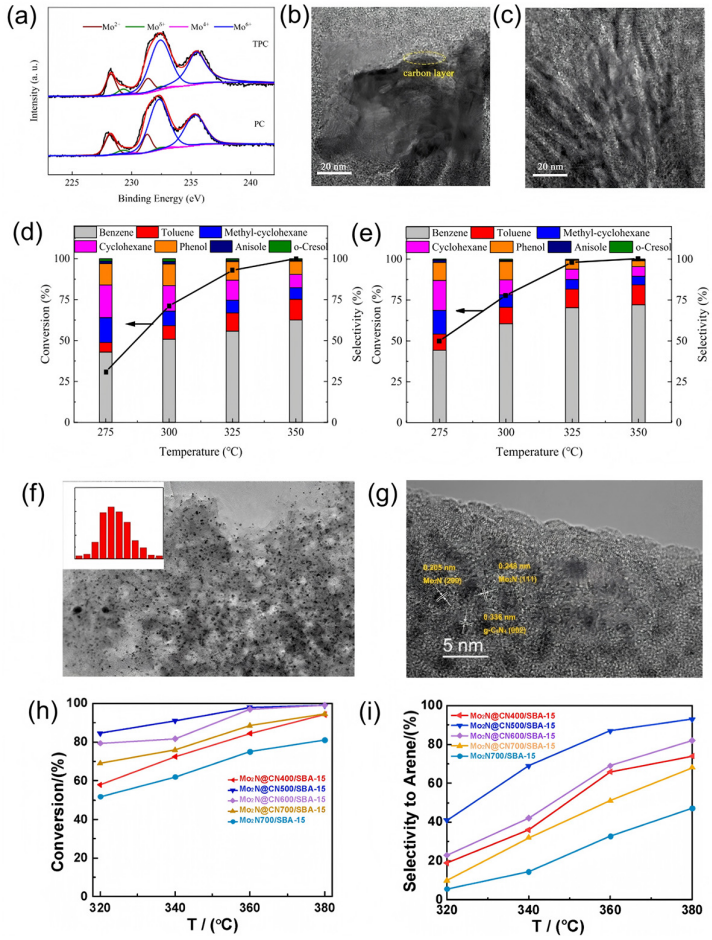


Figure 10. (**a**) Deconvolution of Mo 3d XPS spectra for Mo_2C-TPC and Mo_2C-PC. (**b**,**c**) TEM images of Mo_2C-TPC. HDO of guaiacol over (**d**) Mo_2C-TPC and (**e**) Mo_2C-PC. Reproduced with permission from [76]; published by Springer Nature, 2022. (**f**) TEM images of Mo_2N@CN500 after removing SBA-15. (**g**) HRTEM images of Mo_2N@CN500/SBA-15 catalyst. Conversion of guaiacol (**h**) and selectivity to arene (**i**) on different Mo_2N catalyst. Reproduced with permission from [77]; published by Elsevier, 2023.

Across the Mo-based family, the deliberate engineering of undercoordinated Mo sites—edge sites, basal-plane defects, and oxygen vacancies—together with tuning of the Mo oxidation state and support interaction, emerges as the recurring design strategy. These sites govern the balance between C-O cleavage and aromatic-ring hydrogenation: edge-site density and oxygen vacancies favor direct deoxygenation, whereas excessive reduction or sulfur loss can alter selectivity and stability [66–72]. Therefore, molybdenum-based sulfides exhibit excellent sulfur resistance and HDO performance, rendering them promising for the processing of industrial lignin. However, their practical application is constrained by a series of issues arising from S-O exchange, including sulfur loss, product contamination, water poisoning, poor high-temperature stability, and insufficient activity. Meanwhile, oxides, carbides, and nitrides also suffer from certain drawbacks, including complex preparation procedures and deactivation via oxidation induced by water formation during the HDO process [95,107]. Furthermore, current research has largely focused on the conversion of lignin-derived monomers and model compounds. Although excellent conversion rates and HDO product selectivity have been achieved, the direct application of these catalysts to the HDO of actual lignin for the production of aromatic and cycloalkane fuels holds greater promise for industrial applications and warrants further development [108].

2.2. Nickel-Based Catalysts

Nickel-based catalysts have been widely employed in the HDO of lignin derivatives owing to their cost-effectiveness and strong hydrogen dissociation capability. However, in most cases, these catalysts require harsh reaction conditions (e.g., 250 °C, 5 MPa) to convert lignin monomers and C-O bond dimers into cycloalkanes through complete deoxygenation and aromatic ring hydrogenation [109]; their activity under mild conditions remains insufficient and requires further enhancement. In addition, the recalcitrant C-C bonds inherent in the lignin structure are generally difficult to cleave using non-noble metal catalysts, which restricts the product yield from the HDO of raw lignin [29]. Furthermore, nickel-based catalysts are reported to be susceptible to oxidation and agglomeration during application, resulting in decreased stability, which limits their practical utility to some extent. Therefore, enhancing the C-O and C-C bond cleavage capability along with the cycling stability of nickel-based catalysts constitutes a critical challenge that must be addressed [110,111]. Table 2 summarizes recent studies on the application of nickel-based catalysts in the catalytic HDO of lignin and its derivatives.

Table 2. A summary of the recent literature on the application of nickel-based catalysts in the catalytic HDO of lignin.

Year	Catalyst	Substrate	Major Product	Catalyst to Biomass Ratio (C:B)	Size (nm)	Reaction Conditions				Conv. (%)	Sel. (%)	Ref.
						T (°C)	P (MPa)	Time (h)	Solvent			
2025	$Ni@AlPO_4/Al_2O_3$	Guaiacol	Cyclohexane	1:2.5	7.1	230	1	2	*n*-Hexane	99.1	92.9	[112]
2022	Ni_2P-Al_2O_3	Guaiacol	Cyclohexane	1:2.5	8.4	250	5	3	*n*-Hexane	100	94.5	[113]
2026	NiNPs-SAs/NC	PPE [a]	Ethylbenzene	1:1.25	n.r.	200	none	3	Isopropanol	99.90	86.3	[114]

[a] 2–2-phenoxy-1-phenylethane. n.r.: not reported.

To address this issue, Diao et al. [112] developed a $Ni@AlPO_4/Al_2O_3$ catalyst, in which the surface of Ni nanoparticles was modified with $AlPO_4$ species. This catalyst exhibited excellent catalytic activity and stability in both C-C and C-O bond cleavage. Under conditions of 230 °C, 1 MPa H_2, and 2 h, it achieved a guaiacol conversion of 99.1% and a cyclohexane yield of 92.9%. Half-conversion experiments demonstrated that the catalyst maintained good performance after five cycles, showing its robust recyclability. Mechanistic studies revealed that the formation of $Ni^{\delta+}$-$AlPO_4$ interfaces and the moderate surface

coverage of Ni by $AlPO_4$ significantly promoted the conversion of methoxycyclohexanol and cyclohexanol to cyclohexane. Notably, the $AlPO_4$ coverage exhibited an "optimal window", that is, insufficient coverage led to inadequate $Ni^{\delta+}$-$AlPO_4$ interfaces, whereas excessive coverage blocked Ni sites, resulting in a sharp decline in cyclohexane yield. Furthermore, Ni@$AlPO_4$/Al_2O_3 demonstrated broad substrate applicability in the HDO of various typical lignin monomers and dimers to cycloalkanes. This work provides a successful example of a highly stable and active nickel-based catalyst for converting lignin derivatives into cycloalkanes and lays a foundation for the development of lignin-based sustainable aviation fuel.

Numerous studies have demonstrated that nickel phosphide (Ni_2P) exhibits superior HDO performance compared to other transition metal phosphide catalysts, a property attributed to the higher surface metal site density and electron density in Ni_2P [115–117]. Ni_2P contains two distinct types of Ni sites, designated Ni(1) and Ni(2) [118], among which the pyramidal Ni(2) sites preferentially favor the hydrogenation pathway [119]. In general, Ni_2P catalysts can achieve high alkane yields in the HDO of oxygenated lignin model compounds at relatively elevated temperatures [115]; however, the cyclohexane yield drops sharply when the reaction temperature falls below 300 °C [120]. Studies have revealed that reducing the Ni_2P particle size while simultaneously enhancing the dispersion of the active phase plays a crucial role in improving the low-temperature catalytic performance [121]. Jia et al. [113] developed a strategy for the low-temperature synthesis of a hydrotalcite-derived nickel phosphide catalyst with a flower-like porous structure (Ni_2P-Al_2O_3). Benefiting from the high dispersibility of hydrotalcite, the resulting Ni_2P catalyst, obtained after in situ reduction with red phosphorus at 500 °C, exhibited small particle sizes (Figure 11a,b) and abundant active and acidic sites, which facilitated the activation of both substrates and H_2. Under conditions of 5 MPa H_2 and 250 °C for 3 h, Ni_2P-Al_2O_3 achieved a guaiacol conversion of 100% and a cyclohexane yield of 94.5% (Figure 11c). Additionally, Ni_2P-Al_2O_3 also displayed high HDO activity in the conversion of lignin oil and poplar lignin. DFT calculations further revealed that, compared to Ni(1) sites, the highly exposed Ni(2) sites on the Ni_2P-Al_2O_3 surface possess a stronger capability for C-O bonds cleavage during the HDO of guaiacol (Figure 11d). This work demonstrates that through nanoscale regulation of particle size and dispersion, Ni_2P-based catalysts can achieve efficient and selective conversion of lignin derivatives into jet-fuel-range cycloalkanes under mild conditions.

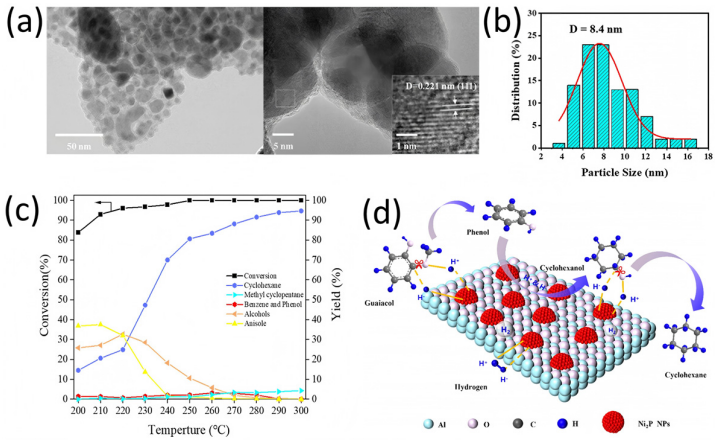


Figure 11. (**a**) TEM images and (**b**) the size distribution of Ni_2P-Al_2O_3(H)71. (**c**) Hydrogenation and deoxygenation performance of Ni_2P-Al_2O_3(H)71. (**d**) Proposed mechanisms for cleavage of C-O bonds and hydrogenation in guaiacol. Reproduced with permission from [113]; published by American Chemical Society, 2022.

Conventional HDO of lignin is typically conducted under relatively high hydrogen pressures (>2 MPa) [122,123], which poses significant safety and engineering challenges. To circumvent these issues, catalytic transfer hydrogenation (CTH) has been proposed as an alternative approach, wherein hydrogen atoms are supplied by sacrificial hydrogen-donor solvents (such as methanol, ethanol, and isopropanol) instead of gaseous H_2, enabling lignin hydrogenolysis under mild or atmospheric pressure [124,125]. Zeng et al. [114] prepared a NiNPs-SAs/NC catalyst, comprising Ni single atoms (SAs) and Ni nanoparticles (NPs) embedded in nitrogen-doped carbon, through an adsorption–aggregation and dispersion–capture strategy (Figure 12a). This catalyst was capable of cleaving C-O bonds in lignin under mild conditions (200 °C, with isopropanol as the hydrogen donor) while suppressing over-hydrogenation of the resulting aromatic monomers, thus affording high selectivity toward aromatic compounds (Figure 12b,c). Furthermore, DFT calculations (Figure 12d–f) were employed to elucidate the catalytic mechanism, revealing a strong synergistic interaction between Ni SAs and Ni NPs within the NiNPs-SAs/NC catalyst. Specifically, isopropanol preferentially adsorbed and dissociated on Ni NP sites to generate H* species, while the C-O bonds of the lignin model compound (PPE) were activated on Ni SA sites. Subsequently, H* species could spill over from Ni NPs to Ni SAs to complete the HDO reaction. This work provides a catalyst capable of selectively cleaving C-O bonds under mild conditions and offers a new strategy for the production of jet-fuel-range aromatics from lignin.

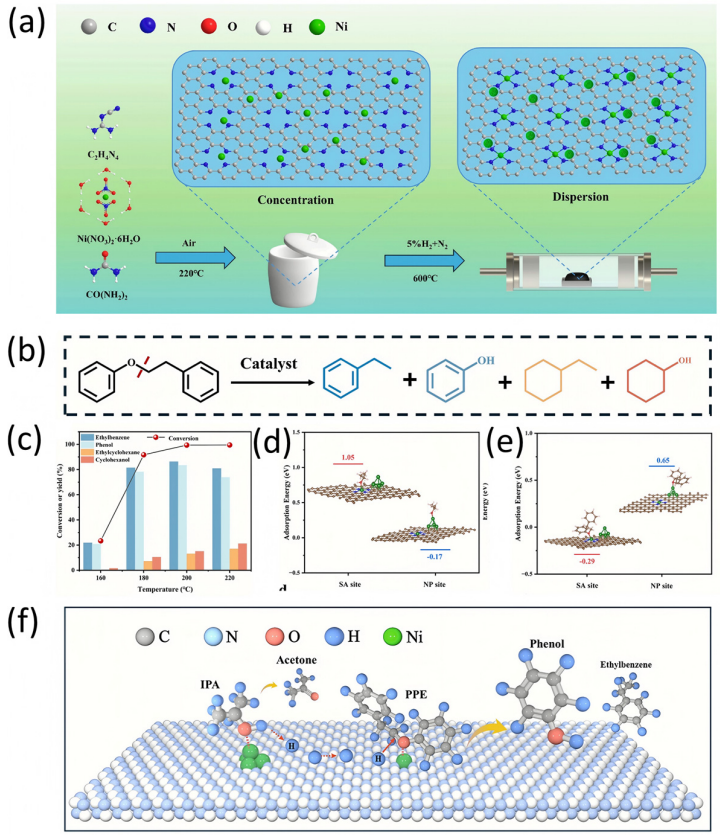


Figure 12. (**a**) Schematic diagram of the preparation method of NiNPs-SAs/NC catalyst. (**b**) Schematic of PPE hydrogenolysis reaction. (**c**) The effect of reaction temperature on hydrogenation deoxygenation of PPE. (**d**) Adsorption energy of isopropanol on different sites of the NiNPs-SAs/NC model. (**e**) Adsorption energy of PPE on different sites of the NiNPs-SAs/NC model. (**f**) Relative energy plots of PPE hydrogenolysis on NiNPs-SAs/NC and NiNPs/NC. Reproduced with permission from [114]; published by Elsevier, 2026.

Nickel-based catalysts face a recurring tension: strong hydrogen activation is necessary for C-O cleavage, yet excessive hydrogenation saturates aromatic rings. Size control, site geometry, and spatial separation of functions are the most effective ways to reconcile these competing demands. Although non-noble metals such as Ni are abundant and cost-effective, their synthesis routes are generally more complex, leading to increased process costs. Moreover, most transition metals are typically extracted from sulfides and arsenides, processes that may incur additional environmental costs. Furthermore, unsupported Ni active sites are prone to deactivation via coke deposition and agglomeration in the absence of strong metal–support interactions [126]. In addition, the efficiency of the catalytic conversion of macromolecular lignin over unsupported Ni catalysts is highly dependent on the solvent design and mass-transfer conditions of the reaction system [127]. Consequently, the introduction of a second metal with distinct hydrotreating or oxophilic properties to form bimetallic catalysts, or the incorporation of supports bearing tunable acid sites or redox sites to construct bifunctional catalysts, serves both to modify the active sites of the primary metal and to simultaneously generate additional active sites [46].

2.3. Bimetallic Catalysts

Compared with monometallic catalysts, bimetallic catalysts represent an intriguing strategy for HDO, as they offer the possibility to tune catalytic performance and tailor product selectivity. Bimetallic catalyst systems formed by Co, Ni, Mo, W, and noble metals in combination, such as PtSn [128], PtRh [64], NiRe [129], PtRe [130], and ZnPd [131], are among the most commonly employed for lignin HDO, and these bimetallic catalysts generally exhibit high selectivity.

For bimetallic catalysts, the activation effects induced by the addition of a second metal can range from a simple promotional role, e.g., assisting in the reduction of the first metal via hydrogen spillover, to more complex metal–metal interactions. These interactions can generally be classified into five distinct phenomena [28]:

(1) Geometric (or ensemble) effects, wherein the addition of the metal activator alters the geometric structure (or ensemble size) of the active sites composed of the catalytically active metal.
(2) Electronic (or ligand) effects, wherein the metal activator modifies the electronic properties of the active sites composed of the catalytically active metal through inter-metal electron transfer (or by functioning as a ligand).
(3) Stabilization effects, wherein the introduction of the metal additive enhances the stability of the catalytically active metal (e.g., by inhibiting sintering or suppressing the formation of carbonaceous deposits on the catalyst surface).
(4) Synergistic effects, wherein both metal species participate in the chemical bonding with reaction intermediates and transition states.
(5) Bifunctional effects, in which each metal provides a distinct function in the reaction mechanism (e.g., one metal catalyzes hydrogenation–dehydrogenation reactions, while the second metal catalyzes C-O hydrogenolysis), which will be detailed in the following section.

In general, geometric and electronic effects influence catalytic activity and selectivity, whereas stabilization effects enhance catalyst stability. Synergistic and bifunctional effects typically increase reaction rates but may also give rise to new reaction pathways. Table 3 summarizes recent studies on the application of bimetallic catalysts in the catalytic HDO of lignin and its derivatives.

Table 3. A summary of the recent literature on the application of bimetal catalysts in the catalytic HDO of lignin.

Year	Catalyst	Substrate	Major Product	Catalyst to Biomass Ratio (C:B)	Size (nm)	Reaction Conditions				Conv. (%)	Sel. (%)	Ref.
						T (°C)	P (MPa)	Time (h)	Solvent			
2020	RuNi/SiO_2-ZrO_2	Guaiacol	Hydrocarbons	1:2	n.r.	260	1	4	Octane	100	99.9	[132]
2021	Ni-Mo-0.1	Guaiacol	Cyclohexane	1:3.7	7.0	230	3	1	*n*-Decane	100	98.3	[133]
2025	$Pd_{1.7}$-$Pt_{0.3}$/NiO	Guaiacol	Cyclohexane	1	3.35	210	0.1	6	*n*-tetradecane	99.7	97.2	[134]

n.r.: not reported.

Ru-based catalysts have been widely employed in the HDO of lignin and its derivatives owing to their high performance and relatively lower cost compared to other noble metals [135–138]. Moreover, the addition of a second, less expensive metal to Ru not only reduces the overall catalyst cost but also allows for the modulation of catalytic performance (including selectivity, activity, coke resistance, and durability) through electronic effects [139]. Li et al. [132] applied a bimetallic RuNi/SiO_2-ZrO_2 catalyst to the HDO of guaiacol and observed a strong interaction between the two metals, with electron transfer from Ru to Ni. This resulted in a shift in the d-band center of the surface Ni atoms, thereby endowing the catalyst with adsorption properties distinctly different from those of monometallic Ru and Ni, particularly significantly enhanced adsorption of both the substrate and hydrogen, leading to a cyclohexane yield approaching 100%. Furthermore, the bimetallic RuNi catalyst also exhibited good HDO performance toward other phenolic compounds and raw lignin oil. This work highlights the critical role of electronic effects in modulating adsorption properties and HDO activity.

The synergistic effect of bimetallic combinations can enable transition metals to exhibit catalytic performance comparable to that of noble metals. Zhang et al. [133] prepared a MoO_x-decorated bimetallic Ni-Mo catalyst with a unique hierarchical flower-like micro/nanoarchitecture via a facile dopamine-assisted hydrothermal method (Figure 13a), and applied it to the HDO of guaiacol for cyclohexane production. Structural characterization revealed that, after high temperature reduction, Ni-Mo alloy sites coexisted with surface-defective MoO_x species on the catalyst surface. By tuning the Mo content, the bimetallic Ni-Mo catalyst with a Mo/Ni molar ratio of 0.1 exhibited superior HDO performance compared to the Mo-free catalyst, as well as to Al_2O_3-supported Ni and bimetallic Ni-Mo catalysts prepared by impregnation (Figure 13b). DFT calculations revealed that the surface-defective MoO_x species adjacent to the metal sites promoted the demethoxylation of guaiacol and its reaction intermediates, while the Ni-Mo alloy sites facilitated the dehydroxylation of the cyclohexanol intermediate (Figure 13c). Thus, the cooperative effect between the Ni-Mo alloy sites and the defective MoO_x structures, wherein both metal species participate in the chemical bonding at different steps of the reaction, plays a crucial role in accelerating the demethoxylation and dehydroxylation processes during guaiacol HDO. This surface-defect bimetallic engineering approach provides promising guidance for the construction of highly efficient bimetallic catalysts for the production of lignin-based cycloalkanes.

Selective conversion of lignin to cycloalkanes under mild conditions remains a significant challenge [122], as the cleavage of aromatic C-O bonds requires a bond dissociation energy as high as 468 kJ mol^{-1} [111]. Exerting bimetallic interactions offers a promising avenue to overcome this obstacle. Chen et al. [134] developed a novel two-dimensional NiO nanosheet-supported Pd-Pt alloy catalyst ($Pd_{1.7}$-$Pt_{0.3}$/NiO), which enabled efficient HDO of lignin-derived phenolic compounds (conversion > 95%) under near-ambient pressure (1 atm). Mechanistic studies revealed that the catalyst operated via a dual-active-site

synergistic cascade mechanism: the Pd-Pt alloy nanoparticles served as the primary active sites for hydrogen activation and substrate conversion, while the NiO support synergistically enhanced aromatic ring hydrogenation through hydrogen spillover. The outstanding catalytic performance was attributed to the synergistic contribution of three factors: firstly, the hydrogen spillover synergy between the alloy sites and the NiO support enabled the relay of aromatic ring hydrogenation and C-O bond cleavage across the two types of sites; secondly, the average particle size of the alloy nanoparticles was only 3.35 nm (substantially smaller than the 5.14 nm of Pd_2/NiO), and this reduced particle size significantly increased the number of metal–support interfacial sites; and thirdly, the formation of the Pd-Pt alloy modulated the electronic structure of the active metals, enhancing the Lewis acidity at the metal–support interface, thereby promoting the adsorption of the cyclohexanol intermediate and facilitating C-O bond cleavage. This work provides a new catalyst design strategy for the synthesis of lignin-based jet-fuel-range cycloalkanes under mild conditions.

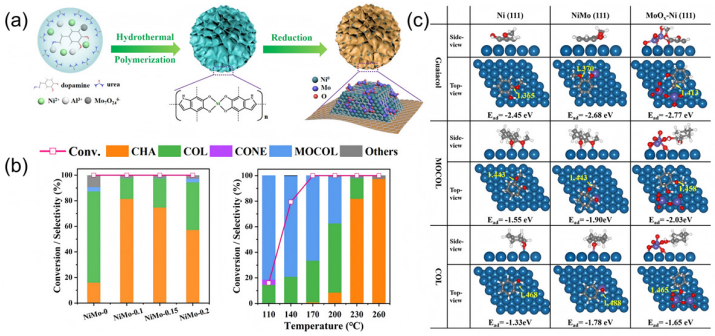


Figure 13. (**a**) Schematic Illustrations of the Synthesis of Surface MoO_x-Decorated Ni-Mo Bimetallic Catalysts via a Facile Dopamine-Assisted Hydrothermal Approach. (**b**) HDO behavior of guaiacol under different catalysts and at different temperatures. (**c**) Optimized geometries for guaiacol, MOCOL, and COL adsorption configurations on Ni (111), Ni-Mo (111), and MoO_x-Ni (111) model surfaces. Reproduced with permission from [133]; published by American Chemical Society, 2021.

In summary, bimetallic systems provide a versatile platform for tuning deoxygenation selectivity through geometric, electronic, stabilization, and synergistic effects [28]. It should be noted that, despite the evident advantages of using bimetallic catalysts, several challenges remain to be addressed. First, carbon deposition on (Co, Ni)- and (Mo, W)-based catalysts [140] constitutes a major issue in HDO: coking increases with catalyst acidity, yet acid sites are inherently required in the conventional HDO mechanism [141]. Second, the interactions between catalysts and impurities are not yet well understood. This problem becomes particularly prominent when real feedstocks containing various impurities are employed. Consequently, more fundamental studies are needed to establish correlations between the structural features of real lignin feedstocks and the corresponding catalytic performance.

2.4. Bifunctional Catalysts

When the second metal does not function as a metal per se, but rather introduces a second type of functionality to the catalyst, a different type of activation effect arises. For example, the presence of metal oxides can introduce acid sites or redox sites. In such cases, the catalyst generally operates through bifunctional synergy, which may alter the reaction selectivity compared to pure metal catalysts. The boundary between bimetallic catalysts and bifunctional catalysts is not always well-defined, because when one of the metals is not fully reduced, metal oxides may form and serve as a support that provides secondary active sites. In such cases, the catalyst should be classified as bifunctional. Whether a catalyst is defined as bimetallic or bifunctional is ultimately determined by the degree of

metal reduction [28]. In recent years, bifunctional catalysts have achieved breakthrough progress among numerous catalytic materials owing to their superior performance, and have become a growing research focus [142,143]. Table 4 summarizes recent studies on the application of bifunctional catalysts in the HDO of lignin and its derivatives.

Table 4. A summary of recent literature on the application of bifunctional catalysts in the catalytic HDO of lignin.

Year	Catalyst	Substrate	Major Product	Catalyst to Biomass Ratio (C:B)	Size (nm)	Reaction Conditions				Conv. (%)	Sel. (%)	Ref.
						T (°C)	P (MPa)	Time (h)	Solvent			
2023	$Ni_{13\%}$/HZ-5(25)	Oxydibenzene	Cyclohexane	1:2	5	160	5	2	*n*-Hexane	79.90	80.80	[144]
2024	Ru/HZSM-5-P	Guaiacol	Cyclohexane	1	11.9	160	2	2	*n*-Hexane	99.9	99.9	[145]
2021	Ru/TiO_2-CeO_2	Guaiacol	Cyclohexane	1:2	n.r.	230	1	4	Octane	99.9	99.9	[146]
2025	Ni/$Ti_{0.5}Zr_{0.5}O_2$	Anisole	Cyclohexane	1:2	n.r.	230	4	3	Decane	100	94.3	[147]
2022	Ru/C-HPW	Guaiacol	Cycloalkanes	1:2	n.r.	200	1	2	Octane	100	98.60	[137]
2020	SiW_{12}-Pt/C	Phenol	Benzene+ Cyclohexane	1:20	n.r.	85	0.064	0.5	Water	100	90.89	[148]
		Guaiacol				95	0.042	0.75	Water	100	83.4	[148]
2024	Ni/NOAC	Guaiacol	Benzene+ Cyclohexane	1	8.6	300	2.5	5	Water and decalin	100	17.1 [a]	[149]
2021	Pt/UiO-66-20def	Anisole	Benzene+ Cyclohexane	N/A	3.5	270	1	3	Decane	86%	84	[150]

N/A: not applicable. [a]: HDO efficiency.

2.4.1. Metal-Zeolite Composite Bifunctional Catalysts

Zeolites have been widely employed in biomass valorization owing to their tunable Brønsted/Lewis acid sites, well-defined pore structures, and shape-selective catalytic capabilities, which render them highly effective in promoting reactions such as cracking, aromatization, and isomerization. In the HDO of lignin derivatives, ZSM-5 stands out for aromatics production due to its moderate pore dimensions and relatively strong acidity; zeolite Y, with its larger pore sizes, facilitates the diffusion and conversion of bulky reactant molecules; and zeolite β, characterized by its three-dimensional intersecting channel systems and medium-strength acidity, also exhibits favorable reaction adaptability. These three zeolite systems are currently the main focuses of research in this field.

However, the practical application of zeolite catalysts alone still faces challenges such as incomplete deoxygenation, unsatisfactory selectivity toward aromatics, and rapid catalyst deactivation due to coke deposition [151]. The HDO of lignin typically involves a tandem process comprising C-O bond cleavage and aromatic ring hydrogenation, which requires the efficient transfer of active hydrogen species [152]. Therefore, by combining metal active sites with the acidic properties of zeolites, the development of metal–zeolite-integrated catalysts enables the construction of a micro-reaction system with a confined adjacency structure at the nanoscale. In this system, the metal component (e.g., Pt, Ni) is primarily responsible for hydrogen activation and selective deoxygenation, while the zeolite governs C-C bond cleavage, isomerization, and aromatization through its acid sites and shape-selective pore channels [153,154]. The synergy between the two functionalities not only optimizes the reaction pathway and lowers the reaction energy barrier, but also enhances the yield and selectivity of target hydrocarbon products such as aromatics, while simultaneously improving coking resistance and extending the catalyst lifetime.

Highly active bifunctional catalysts consisting of metal nanoparticles supported on various zeolites exhibit unique advantages in catalyzing HDO [155]. For inexpensive non-

noble metals, particularly nickel-based bifunctional catalysts, their intrinsic atomic structure features a broader d-electron band and higher energy density, which endow them with strong H_2 activation capability and enhanced catalytic activity under mild conditions [156]. Correspondingly, zeolite supports such as HZSM-5, HY, and Hβ possess three-dimensional channel-type micropores that enhance both thermal and hydrothermal stability, thereby improving the HDO performance of the bifunctional catalysts [157,158]. Furthermore, hydrogenation predominantly occurs on the exposed metal centers, while deoxygenation primarily takes place at the acid sites of the zeolite [158]. Therefore, establishing the relationship between the acid strength and acid amount of zeolite supports and the cleavage of C-O bonds is of great significance for the catalytic HDO of lignin. Lee et al. established a linear correlation between cyclohexane yield and acid amount in Pt/zeolite-HY and Pt/zeolite-Beta catalysts for the HDO of guaiacol [159]. Kang et al. [144] prepared a series of Ni nanoparticle (NP)-loaded HZSM-5 (HZ-5) catalysts with different Si/Al ratios (n = 25, 50, 170, and 200) via a modified deposition–precipitation method, and applied them to the HDO of lignin-related model compounds (LRMCs) containing various C-O bonds and aromatic rings, including oxydibenzene (ODB), oxybis(methylene)dibenzene (OBMDB), benzyloxybenzene (BOB), and oxydinaphthalene (ODN). The catalytic HDO mechanisms of ODB, OBMDB, BOB, and ODN over $Ni_{13\%}$/HZ-5(n) were subsequently investigated. The results revealed that, with the synergy of Ni NPs, Ni/HZ-5(n) could activate H_2 to form diatomic hydrogen (H· · · H) and heterolytically split H· · · H into relatively mobile H^+ and immobile H^-, further inducing C-O bond cleavage to varying extents via active hydrogen transfer. This mechanism clarifies the different roles of metal sites and acid sites in C-O bond cleavage: metal sites govern hydrogen activation and transfer, whereas acid sites promote the activation and dissociation of C-O bonds. This thereby provides a theoretical basis for the rational design of metal–acid sites in bifunctional catalysts and offers valuable guidance for the HDO of lignin to produce jet-fuel-range cycloalkanes and aromatics.

Beyond acid amount and acid strength, it is well established that the morphology and particle size of zeolites also significantly influence catalytic performance [160–162]. Tian et al. [145] conducted a comparative study on the effect of Ru/HZSM-5 catalysts with different morphologies on the selective HDO of guaiacol to cyclohexane. Among them, the Ru/HZSM-5-P catalyst with a two-dimensional nanosheet structure (Figure 14a) exhibited the best accessibility, smaller metal particle size (Figure 14b), favorable metal–support interaction, and appropriate B/L ratio (Figure 14c), which facilitated the activation of C-C and C-O bonds, thereby delivering the optimal conversion and cyclohexane selectivity. Mechanistic studies revealed that the metal and zeolite functioned synergistically in catalysis (Figure 14d): guaiacol diffused to the surface of the Ru/HZSM-5-P catalyst, where HZSM-5 provided interacting acid sites (both Brønsted and Lewis acid sites). Under a hydrogen atmosphere, the Ru active component dissociated H_2 to generate active hydrogen species (H^+), which attacked guaiacol, and cleaved the methoxy group to form phenol. Subsequently, Ru and H^+ together facilitated the hydrogenation of the aromatic ring to yield cyclohexane [163,164].

In summary, metal–zeolite composite catalysts establish an efficient confined adjacency synergistic catalytic system in lignin HDO by integrating the hydrogen activation and hydrogenation capability of metal sites with the acid-site shape-selective catalytic function of zeolites. The advantages of this system are mainly manifested in three aspects: 1. Acid–metal bifunctional synergy. Metal sites are responsible for H_2 dissociation and aromatic ring hydrogenation, while the Brønsted/Lewis acid sites of zeolites promote C-O bond cleavage and C-C bond isomerization/aromatization; the proximity effect between the two functionalities can significantly lower the reaction energy barrier. 2. Shape-selective catalysis and pore confinement. The well-defined pore structures facilitate the selective

conversion of intermediates of specific molecular dimensions. 3. Tunable acidity. The acid amount and acid strength can be systematically modulated by adjusting the Si/Al ratio, enabling the establishment of a linear correlation between acidity and HDO activity of lignin, thereby providing a basis for the rational design of catalysts. Nevertheless, this system still faces several limitations: 1. Diffusion constraints. The microporous channels of zeolites pose mass-transfer limitations for macromolecular lignin and its oligomers, and are prone to coke deposition, leading to rapid catalyst deactivation [165]. 2. Insufficient hydrothermal stability. Under the hydrothermal conditions generated during the HDO reaction, the zeolite framework may undergo dealumination or collapse, compromising long-term operational stability [166]. Therefore, the development of hierarchical zeolites to improve mass transfer, along with the enhancement of hydrothermal stability, represents a crucial direction for advancing the practical application of metal–zeolite composite catalysts in the field of lignin-based aviation kerosene.

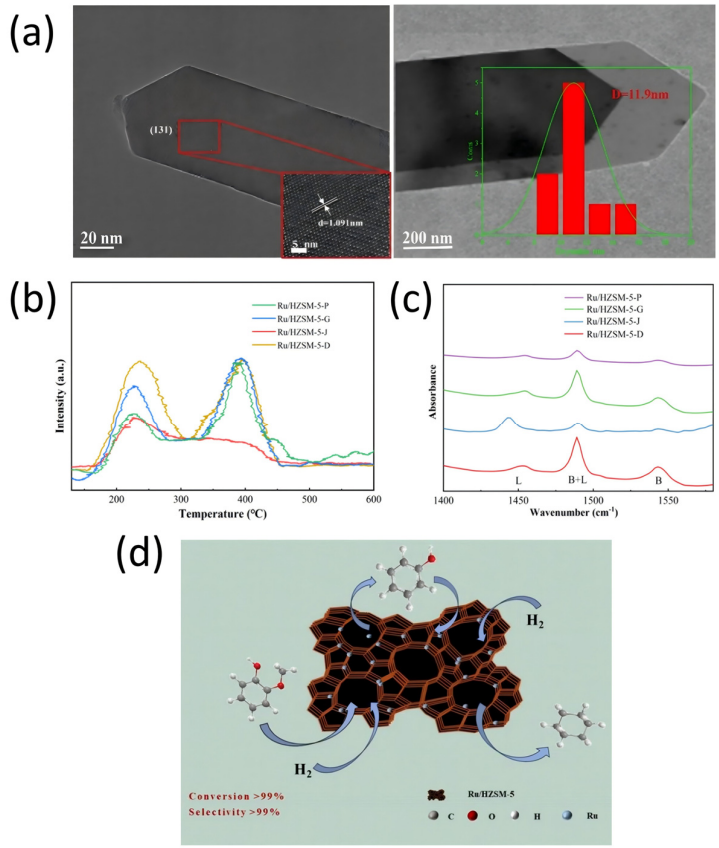


Figure 14. (**a**) TEM and TEM-mapping elemental spectra of Ru catalysts Ru/HZSM-5-P. Acidity analysis patterns of the four catalysts, Ru/HZSM-5-D, Ru/HZSM-5-J, Ru/HZSM-5-G, and Ru/HZSM-5-P: (**b**) NH_3-TPD and (**c**) pyridine infrared. (**d**) Possible reaction mechanism of guaiacol degradation in the (Ru/HZSM-5-P)/*n*-hexane system. Reproduced with permission from [145]; published by American Chemical Society, 2024.

2.4.2. Metal–Metal Oxide Composite Bifunctional Catalysts

In contrast to carbon materials or inert oxides (e.g., SiO_2), which mainly rely on their specific surface area and pore structure to provide physical dispersion, metal oxides possess unique surface physicochemical properties, particularly oxygen vacancies and tunable SMSI, that enable deep synergy with the supported metal active sites. Consequently, metal oxides can actively participate in the reaction, modulating selectivity and stability during the HDO of lignin. Owing to these distinctive advantages, metal–metal oxide composite catalysts have become a research hotspot in the field of lignin HDO.

Studies have revealed that acidic supports such as Al_2O_3 and zeolite β, when used as catalyst carriers, are prone to rapid deactivation during HDO reactions due to coke formation [167]. In contrast, metal oxides, by virtue of the oxygen vacancies present in their bulk or on their surface, can lower the oxidation state of the corresponding metal, facilitating the adsorption of phenolic compounds and promoting C-O bond cleavage, thereby effectively enhancing catalytic activity [168–170]. Shu et al. [146] prepared three catalysts via a photochemical reduction method at room temperature, designated as Ru/TiO_2, Ru/CeO_2, and Ru/TiO_2-CeO_2. This approach utilized UV light to drive the in situ reduction of Ru^{3+} on the support surface, avoiding metal agglomeration typically caused by high-temperature calcination and achieving highly dispersed loading of Ru nanoparticles. HDO performance evaluation showed that Ru/TiO_2-CeO_2 could completely convert guaiacol to cyclohexane (with a selectivity of nearly 100%) at 230 °C and 1 MPa H_2, significantly outperforming Ru/TiO_2 (cyclohexane selectivity of 70.9%) and Ru/CeO_2 (no deoxygenated products). This superior performance was attributed to the integration of the complementary advantages of TiO_2 and CeO_2 within the composite oxide support. The high specific surface area of TiO_2 (203.77 m^2/g) promoted the high dispersion of Ru, and H_2-TPD along with TEM confirmed that Ru/TiO_2-CeO_2 possessed excellent hydrogen adsorption capacity, providing abundant active sites for aromatic ring hydrogenation. XPS analysis revealed that the introduction of CeO_2 substantially increased the oxygen vacancy concentration, enhancing the adsorption of oxygenated substrates and the C-O bond activation capability of the catalyst. Adsorption experiments confirmed that Ru/TiO_2-CeO_2 exhibited significantly better adsorption of guaiacol compared to catalysts supported on single oxides. Meanwhile, NH_3-TPD indicated that Ru/TiO_2-CeO_2 also contained abundant acid sites, providing sufficient acidic centers for C-O bond cleavage. The synergy among these three factors enables Ru/TiO_2-CeO_2 to achieve deep HDO of lignin under mild conditions, with a significant increase in the content of alkylphenols and hydrocarbons in the product.

Building upon the complementary advantages of composite oxide supports, Ali et al. [147] designed a series of Ni-doped $Ti_{1-x}Zr_xO_2$ mixed oxide supports for the HDO of lignin model compounds. It was found that the incorporation of Zr into the TiO_2 lattice induced the formation of abundant oxygen vacancies and Lewis acid sites, significantly enhancing the SMSI between Ni and the support (Figure 15a). Among them, the $Ni/Ti_{0.50}Zr_{0.50}O_2$ catalyst achieved complete conversion of anisole with a cyclohexane yield of 94% at 230 °C and 4 MPa H_2, whereas Ni/ZrO_2 and Ni/TiO_2 afforded cyclohexane yields of only 29% and 49%, respectively (Figure 15b). Multiple characterization techniques, including XPS, O_2-TPD, NH_3-DRIFTS, and H_2-TPR, collectively elucidated the reaction mechanism (Figure 15c): the abundant oxygen vacancies in the mixed oxide support provided extensive adsorption sites for the activation of C-O bonds; the significant increase in both the number and strength of Lewis acid sites facilitated the adsorption of reactants onto oxygen vacancies via the oxygen atom of the methoxy group, thereby weakening the C-O bond; meanwhile, the SMSI promoted the generation of active hydrogen species at the metal–support interface. This synergy enables the efficient HDO of lignin-derived phenolics over low-loaded Ni catalysts under mild conditions, offering a catalyst design strategy for the synthesis of lignin-based jet-fuel-range cycloalkanes.

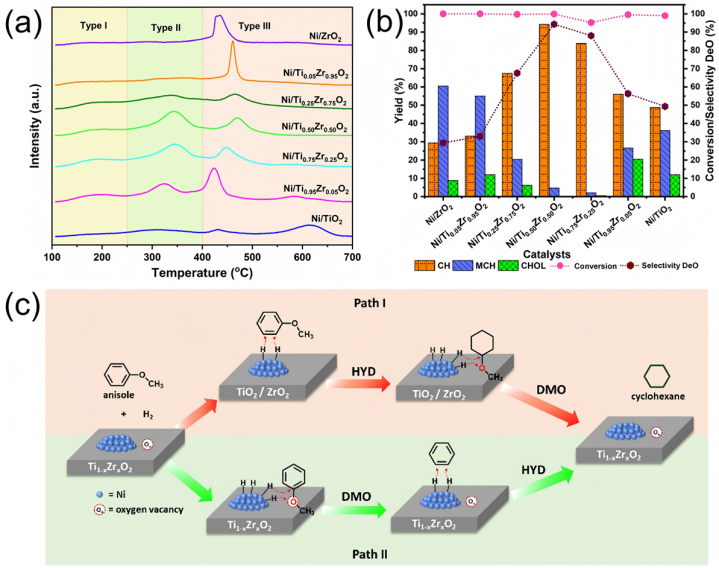


Figure 15. (**a**) O_2-TPD profiles of Ni-supported mono and mixed oxide catalysts. (**b**) HDO of anisole with 3wt% Ni supported mono and mixed oxide catalysts. (**c**) A plausible mechanism for HDO of anisole cyclohexane with $Ni/Ti_{1-x}Zr_xO_2$. Reproduced with permission from [147]; published by Royal Society of Chemistry, 2025.

2.4.3. Metal-Polyoxometalate (POM) Nanoclusters Composite Bifunctional Catalysts

Polyoxometalates (POMs) are a unique class of anionic polynuclear metal–oxygen clusters, exhibiting structural diversity at the atomic level. Countercations balance the negative charge on the framework; these cations may include protons serving as Brønsted acid sites, substituted metal cations, or metal ions with redox properties serving as Lewis acid sites. POMs with protons as the sole countercations are generally referred to as heteropoly acids (HPA) [171]. Owing to their tunable Brønsted/Lewis acidity and redox properties, POMs and POM-based composite materials have long been applied in heterogeneous catalysis [171–173]. Currently, most research has focused on Keggin-type POMs. The Keggin anion family has the general formula $[XM_{12}O_{40}]^{n-}$ (where X = Si, P, etc.; M = Mo, W, etc.) [172]. Keggin-type polyoxometalates possess strong and stable acid sites, excellent redox properties, and remarkable stability [174], and have been employed in a wide range of biomass conversion processes [175] as well as in the HDO of various oxygenated compounds [176–179].

Metal NP-POM composites refer to either metal nanoparticles (NPs) supported on heterogeneous POMs, or metal NPs and POMs immobilized on an additional support. The intimate contact between the metal NPs and POMs facilitates the migration of substrates and intermediates over nanometer-scale distances between the metal sites and acid sites [180,181], thereby enabling synergistic effects in the catalytic HDO of lignin.

Kozhevnikov et al. reported that Pt catalysts supported on cesium salts of phosphotungstic acid could effectively catalyze the HDO of ethers [176] and ketones [182] under mild reaction conditions (<100 °C, <1 bar H_2). Sautet and Yan demonstrated that polyoxometalate-stabilized Pt single-atom catalysts, owing to the effect of metal loading, could suppress the aggregation of Pt single atoms and weaken H_2 adsorption energy, thereby exhibiting a lower apparent reaction energy barrier in hydrogenation reactions [178]. Recently, Liu and co-workers found that the combination of Pt/C and polyoxometallic acids enabled the upgrading of lignin bio-oil to hydrocarbons under mild aqueous conditions, wherein the polyoxometallic acid acted as both an H_2 buffer and a support. However, the good water solubility of polyoxometallic acids may hinder their recovery process [148].

To maximize the synergistic effect, Yang et al. [137] designed a bifunctional catalyst system composed of Ru/C and phosphotungstic acid (HPW), designated as Ru/C-HPW, for the HDO of lignin-derived phenolic compounds. This system cleverly exploited the temperature-controlled phase-transfer behavior of HPW, which is solid at room temperature and melts into a liquid phase upon heating to the reaction temperature (200 °C), thereby enabling uniform dispersion and adsorption onto the Ru/C surface and achieving intimate contact between the metal sites (Ru) and acid sites (HPW) in the liquid phase. This "in-situ assembly" strategy integrated catalyst preparation with the HDO reaction in a single step, avoiding the issue of poor dispersion between metal and acid components typically encountered in conventional methods such as wet impregnation and co-precipitation. The intimate metal–acid contact significantly enhanced the synergistic effect: guaiacol first underwent aromatic ring hydrogenation at Ru sites to form methoxycyclohexanol, followed by efficient C-O bond cleavage catalyzed by the Lewis acid sites of HPW; the deoxygenated product then underwent a second hydrogenation at Ru sites to yield cyclohexane (Figure 16a,b). Benefiting from the efficient mass transfer of substrates between the two types of sites, guaiacol achieved complete conversion within 4 h at 200 °C and 1 MPa H_2, with a cyclohexane selectivity as high as 98.6%. Moreover, the reaction rate far surpassed that of solid acid systems such as Ru/C-Al_2O_3, which suffered from limited mass transfer across the solid–solid interface and afforded a cyclohexane selectivity of only 46.4% (Figure 16c,d). The catalyst showed no significant loss of activity after five cycles, and the use of HPW avoided the risk of water pollution associated with liquid acids such as H_3PO_4. In addition to guaiacol, this system also exhibited excellent HDO performance toward real lignin oil, increasing the hydrocarbon content from 5.5% to 78.9%. This work demonstrates the unique advantages of the temperature-controlled phase-transfer strategy in constructing efficient metal–acid bifunctional catalytic systems, and provides a feasible route for the mild synthesis of lignin-based cycloalkanes.

As mentioned above, the HDO of lignin under low temperature and low pressure is constrained by the high activation energy required for C-O bond cleavage and the extremely low solubility of hydrogen in the aqueous phase. Liu et al. [148] constructed a synergistic bifunctional three-phase hydrogen transfer catalytic system (SiW_{12}-Pt/C) composed of the Keggin-type polyoxometallic acid $H_4SiW_{12}O_{40}$ and suspended Pt/C particles, which effectively avoided the aforementioned issues. By exploiting the low redox potential of $H_4SiW_{12}O_{40}$ (E° = –0.05 V vs. NHE), the authors achieved a reversible redox reaction with H_2 in the presence of Pt/C, enabling the rapid transfer of H_2 from the gas phase to the liquid phase and its release as H^+. This effectively raised the concentration of active hydrogen species in the solution to a level equivalent to that of dissolved hydrogen under 10 atm of H_2 pressure. Meanwhile, $H_4SiW_{12}O_{40}$, acting as a superacid, could protonate partially hydrogenated phenolic intermediates to form oxonium ions, substantially reducing the activation energy for C-O bond cleavage. Under this bifunctional synergy, the SiW_{12}-Pt/C catalyst achieved HDO of phenol at 85 °C with an H_2 partial pressure of only 0.64 atm, affording a total hydrocarbon (benzene and cyclohexane) yield of 90.8%. Other lignin-derived phenolics and dimeric model compounds, such as guaiacol, also underwent efficient HDO under temperatures below 100 °C and atmospheric H_2, with hydrocarbon yields in the range of 60–90%. This work, through the "hydrogen buffer-superacid" bifunctional design of polyoxometalates, overcomes the reliance on high temperature and high pressure in traditional HDO, and offers a new strategy for the mild synthesis of lignin-based aromatics and cycloalkanes.

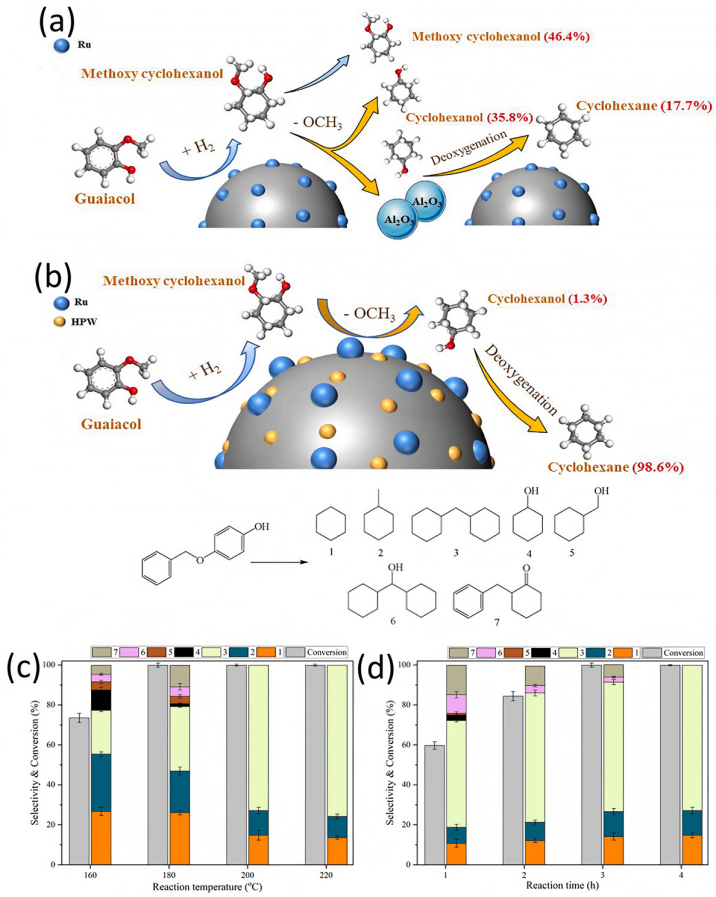


Figure 16. The synergistic effect of active metal–acid sites and the guaiacol HDO reaction pathway (**a**) Ru/C-Al_2O_3 (**b**) Ru/C-HPW. Effects of (**c**) reaction temperature and (**d**) reaction time on the 4-benzyloxy phenol HDO. Reproduced with permission from [137]; published by Elsevier, 2022.

However, the use of metal NP-POM catalysts for biomass valorization still faces considerable challenges. First, the leaching of active components remains a common issue that compromises catalyst stability. In addition, most of the reported POMs for biomass utilization have focused on Keggin-type structures, while the application potential of other architectures, such as Wells–Dawson- and Lindqvist-type POMs, remains largely unexplored. Future research should aim to gain a deeper understanding of the relationships between the catalytic performance and the chemical/electronic/structural properties of metal NP-POMs-based catalysts, which is of great significance for the efficient HDO of lignin [175].

2.4.4. Metal–Other Support Composite Bifunctional Catalysts

Beyond the mainstream composite catalyst systems, including metal–zeolite, metal–oxide, and metal–POM combinations, other supports, exemplified by carbon-based materials and metal–organic frameworks (MOFs), have also demonstrated significant potential in the field of lignin HDO, owing to their unique physicochemical properties.

Activated carbon is frequently employed as a catalyst support owing to its unique physicochemical properties, such as the presence of oxygen-containing functional groups on its surface, a high micropore or mesopore surface area, and structural and morphological stability at elevated temperatures and in various liquid media [183,184]. Consequently, compared to acidic supports with poor water resistance, such as Al_2O_3 and zeolites [185–187], which are widely used in the HDO of lignin and its derivatives [188,189], activated carbon is more suitable for the HDO of lignin derivatives in alkaline solutions. Xu et al. [149]

investigated three nickel catalysts supported on coconut-shell-derived activated carbon for the HDO of guaiacol under alkaline conditions. To enhance the surface acidity of the catalyst, the authors pretreated the activated carbon with HNO_3 and H_2SO_4 to obtain Ni/NOAC and Ni/SOAC, respectively, while the catalyst without acid pretreatment was designated as Ni/CAC. Boehm titration, FT-IR, and XPS characterization revealed that acid pretreatment significantly increased the content of acidic oxygen-containing functional groups on the support surface. These acidic groups played a dual role: on one hand, they directly promoted the cleavage of C-O bonds in guaiacol as Brønsted acid sites; on the other hand, they enhanced the electrostatic adsorption of Ni^{2+} precursors, reducing the average particle size of the resulting Ni nanoparticles from 13.1 nm in Ni/CAC to 8.6 nm in Ni/NOAC and 6.1 nm in Ni/SOAC (Figure 17a–c). Under alkaline conditions at 300 °C and 4 MPa H_2, the HDO efficiency of Ni/NOAC (17.1%) was approximately twice that of Ni/CAC (8.8%), with significantly improved yields of benzene and cyclohexene. In contrast, the cyclohexene yield over Ni/SOAC was nearly double that over Ni/CAC, while the yields of benzene and toluene were lower, which was attributed to the rapid hydrogenation saturation of the aromatic ring catalyzed by Ni/SOAC (Figure 17d). Based on these results, the reaction pathways were elucidated: following acid pretreatment, the smaller Ni particle size provided more metal active sites for aromatic ring hydrogenation, while the abundant acid sites accelerated C-O bond cleavage, thus promoting both the direct deoxygenation (DDO) and hydrogenation–deoxygenation (HYD) routes simultaneously (Figure 17e,f). This work reveals the structure–activity mechanism by which the surface chemistry of carbon supports synergistically enhances HDO performance through the modulation of metal dispersion and acid site density, providing a catalyst design strategy for the efficient valorization of lignin components under strongly alkaline conditions.

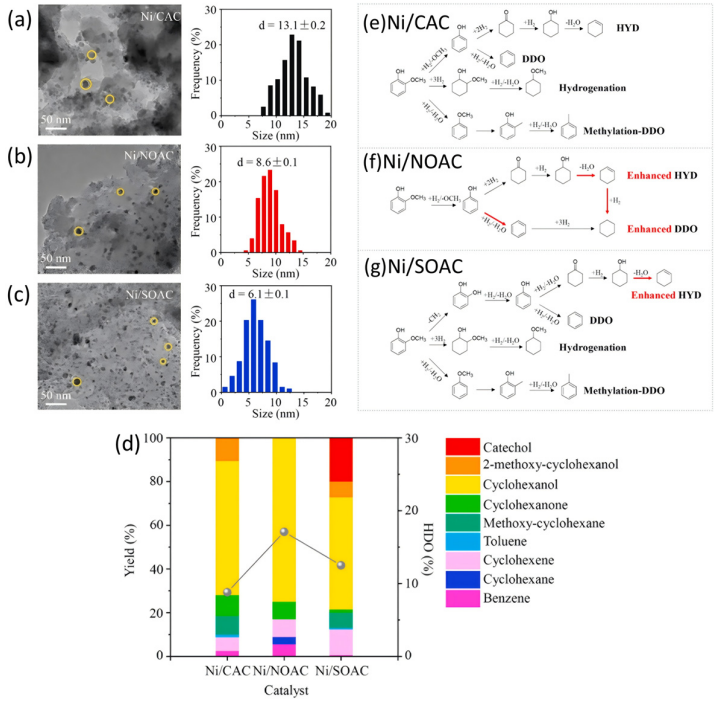


Figure 17. HRTEM images of (**a**) Ni/CAC; (**b**) Ni/NOAC; (**c**) Ni/SOAC and the corresponding Ni particle size normal distribution. (**d**) Guaiacol HDO result over Ni/CAC, Ni/NOAC and Ni/SOAC catalysts. Proposed reaction routes of guaiacol on Ni/CAC (**e**), Ni/NOAC (**f**) and Ni/SOAC (**g**) catalysts. Note: The thick red line represents that the reaction route is promoted by the modified surface chemistry. Reproduced with permission from [149]; published by Elsevier, 2022.

As mentioned above, the key challenge in the catalytic HDO of lignin is to achieve rapid and selective cleavage of aromatic C-O bonds by hydrogen, while avoiding the hydrogenation of aromatic C=C bonds [190]. Therefore, the selective cleavage of aromatic C-O bonds requires the combination of metal sites for H_2 activation and Lewis acid sites of bifunctional catalysts for substrate adsorption. Among the various acidic supports employed for biomass upgrading, MOF materials have been utilized for the selective catalytic cleavage of C-O bonds, owing to their exceptional structural properties [191–193]. Specifically, the unsaturated metal ions within the MOF framework exhibit Lewis acidity, which can be exploited for the adsorption of lignin-derived phenolic compounds [192,194,195]. UiO-66, a MOF characterized by a high specific surface area, tunable pore structures, ease of scale-up, and thermal stability [196,197], has been applied in heterogeneous catalysis [194,195]. Typically, two types of defects exist in the UiO-66 framework, namely missing-cluster defects and missing-linker defects [197,198]. Both types serve as open Lewis acid sites within the UiO-66 structure, which are crucial for catalytic biomass upgrading [197,199]. Accordingly, Phan et al. [150] synthesized a series of UiO-66 supports with varying linker defects (UiO-66-ydef) via a microwave-assisted solvothermal method, and subsequently loaded Pt by impregnation to obtain Pt/defective UiO-66 catalysts. By introducing isophthalic acid (IPA) as a mixed linker, the partial absence of IPA exposed more open Lewis acid sites on the $Zr_6O_4(OH)_4$ clusters, while the linker defects also introduced additional hydroxyl groups, which meant an increase in Brønsted acid sites. NH_3-TPD and XPS characterization revealed that the defective UiO-66 samples exhibited a total acid amount 1.5–2.5 times higher than that of pristine UiO-66, with the number of linker defects increasing with IPA content. CO chemisorption and TEM confirmed that the introduction of defects did not significantly alter the Pt dispersion (~22%) or particle size (3.5 nm); hence, the enhanced catalytic performance was primarily attributable to the increased acidity of the support rather than geometric changes of the metal sites. Under continuous fixed-bed reaction conditions at 270 °C and 1 MPa, the 3Pt/UiO-66-20def catalyst achieved an anisole HDO conversion of 86%, with a TOF 2–3 times higher than that of pristine 3Pt/UiO-66. In terms of selectivity, the selectivity toward benzene increased substantially as the defect content rose from 0 to 20%, with the TOF based on benzene yield increasing by more than 10-fold. This indicated a significant shift in the reaction pathway: the pristine catalyst, owing to the strong hydrogenation capability of Pt sites, tended to convert anisole to cyclohexane through aromatic ring hydrogenation, whereas the abundant Lewis acid sites on defective UiO-66 preferentially adsorbed and activated the oxygen atom of the methoxy group, steering the reaction toward the demethoxylation pathway and thereby converting the oxygenated aromatic ring to benzene. However, 3Pt/UiO-66-30def exhibited decreased activity due to coke formation caused by excessively strong acid sites, indicating that an appropriate defect concentration is key to achieving a balance between high activity and stability. This work reveals the design strategy of defect engineering in MOF supports to steer HDO reaction pathways by modulating the type and density of acid sites, offering a new approach for the selective synthesis of lignin-based aromatics.

Beyond conventional supports such as zeolites and metal oxides, other supports, including carbon-based materials and MOFs, have opened up new avenues for the design of catalytic systems for lignin HDO, owing to their highly tunable physicochemical properties. Nevertheless, both types of supports face common challenges: the surface functional groups of carbon-based materials are susceptible to loss under high-temperature reduction conditions [200], while the microporous structures of MOFs impose significant mass-transfer limitations for macromolecular substrates [201].

In bifunctional catalysts, cascade deoxygenation proceeds through the cooperation of metal sites for H_2 activation with acid, redox, or defect sites for C-O cleavage. The

proximity and ratio between these two functions prove decisive: too few acid sites limit deoxygenation, while excessive acidity promotes coke formation and over-hydrogenation. Metal–zeolite systems benefit from tunable Brønsted/Lewis acidity and shape selectivity [144,145], while metal–oxide systems exploit oxygen vacancies and SMSI to activate C-O bonds and stabilize intermediates [146,147]. Metal–POM systems demonstrate that temperature-controlled phase transfer can maximize metal-acid contact and mass transfer [137], and carbon- or MOF-supported systems show that surface chemistry and defect engineering can steer reaction pathways [149,150]. Future research should focus on the construction of hierarchical pore structures to improve mass transfer, the rational regulation of synthesis conditions to enhance support–metal synergistic stability, and the development of adaptive catalytic systems with high selectivity toward target products by exploiting the structural tunability of these materials, thereby advancing the directed synthesis of lignin-based jet fuel components toward practical application.

2.5. Single-Atom Catalysts

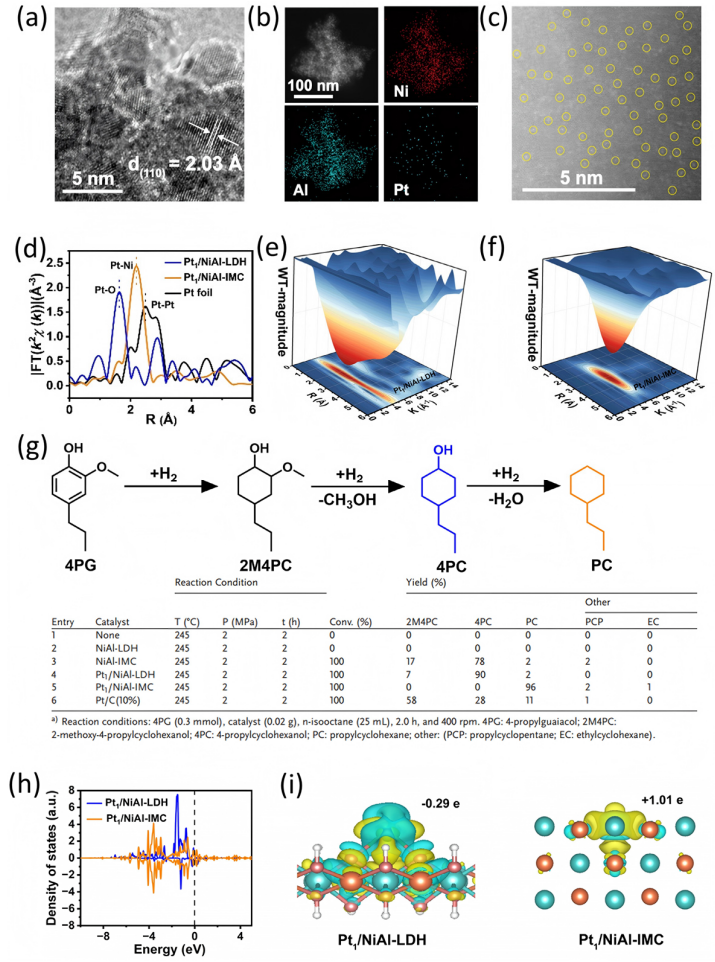
Compared with traditional nanoparticle and nanocluster catalysts, single-atom catalysts (SACs) have attracted widespread attention in energy- and environment-related applications, owing to their high atom utilization efficiency, unique electronic states, and well-defined active sites [202–204]. More importantly, by virtue of their uniform active sites and well-defined coordination structures, SACs tend to steer the lignin conversion pathway toward a single route, thereby affording high selectivity. For example, single-atom catalysts such as Ru/CeO_2 [205], $Pt\text{-}Fe/CeO_2$ [206], and Au_1/Nb_2O_5 [207] have been shown to effectively catalyze the cleavage of C-O bonds in lignin models or lignin itself, yielding cycloalkanes in high yields. Table 5 summarizes recent studies on the application of single-atom catalysts in the HDO of lignin and its derivatives.

Table 5. A summary of recent literature on the application of single-atom catalysts in the catalytic HDO of lignin.

Year	Catalyst	Substrate	Major Product	Catalyst to Biomass Ratio (C:B)	Reaction Conditions				Conv. (%)	Sel. (%)	Ref.
					T (°C)	P (MPa)	Time (h)	Solvent			
2025	$Pt_1/NiAl\text{-}IMC$	4-Propyl guaiacol	Propyl cyclohexane	1:2.5	245	2	2	*n*-Isooctane	100	96	[208]
2024	$Pt_{0.4}/CsPW\text{-}H_2$	4-Propyl guaiacol	Propyl cyclohexane	1:3.3	150	2	4	*n*-Dodecane	98	91.60	[209]
2024	$Ni_1/\beta\text{-}Mo_2C$	Dihydroeugenol	Propyl cyclohexane	1:1.66	250	4	2	*n*-Undecane	100	100	[111]
2025	$Mo/NiFe_{71}\text{-}V$	Guaiacol	Cyclohexane	1:2	240	4	3	*n*-Hexane	100	99.5	[210]

However, the coordination structures of SACs are typically "locked" under specific synthesis conditions, making it difficult to achieve selective switching between different products at the same metal center once the structure is formed. Charge density, as a key electronic parameter governing catalytic behavior, has been recognized as an effective means to overcome this limitation through its precise regulation. Nevertheless, how to achieve controllable modulation of charge density at single-atom sites and establish a quantitative correlation with product selectivity remains a formidable challenge. Dai et al. [208] employed a topotactic transformation strategy using NiAl layered double hydroxide (LDH) precursors to construct two Pt single-atom catalysts with distinct local electronic structures by tuning the reduction temperature (Figure 18a–c). In $Pt_1/NiAl\text{-}LDH$, obtained by reduction at 200 °C, Pt was anchored on the LDH surface with $Pt\text{-}O_x$ coordination, exhibiting an electron-deficient state. In contrast, in $Pt_1/NiAl\text{-}IMC$, obtained by reduction at 400 °C, the

interlayer species of LDH were removed and converted into NiAl intermetallic compounds, with Pt existing in a Pt-Ni_x coordination configuration. Electron transfer between Pt and the NiAl substrate rendered Pt in an electron-rich state (Figure 18d–f). XANES, XPS, and DFT calculations collectively confirmed the completely opposite charge density characteristics of the two Pt sites. In the HDO of 4-propylguaiacol, Pt_1/NiAl-LDH selectively catalyzed aromatic ring hydrogenation and demethoxylation, affording 4-propylcyclohexanol with >90% selectivity. In contrast, Pt_1/NiAl-IMC further enabled complete cleavage of the C-OH bond, yielding propylcyclohexane with 96% selectivity (Figure 18g). Mechanistic studies revealed that the electron-deficient Pt sites on Pt_1/NiAl-LDH exhibited excessively strong adsorption toward 4-propylcyclohexanol, causing the reaction to stall at the alcohol product, whereas the electron-rich Pt sites on Pt_1/NiAl-IMC, through d-electron back-donation into the π* antibonding orbital of the C-O bond, weakened the C-O bond energy and thereby drove complete deoxygenation (Figure 18h,i). This strategy proved equally effective with real lignin feedstocks, achieving a cycloalkane yield of 25.5 wt%. This work demonstrates the precise switching of product selectivity at the same metal center through charge density modulation of single-atom sites via different support structures, providing an atomic-scale catalyst design paradigm for the directed synthesis of lignin-based jet fuel components.



Entry	Catalyst	T (°C)	P (MPa)	t (h)	Conv. (%)	2M4PC	4PC	PC	Other: PCP	Other: EC
1	None	245	2	2	0	0	0	0	0	0
2	NiAl-LDH	245	2	2	0	0	0	0	0	0
3	NiAl-IMC	245	2	2	100	17	78	2	2	0
4	Pt_1/NiAl-LDH	245	2	2	100	7	90	2	0	0
5	Pt_1/NiAl-IMC	245	2	2	100	0	0	96	2	1
6	Pt/C(10%)	245	2	2	100	58	28	11	1	0

Reaction Condition | Yield (%)

[a] Reaction conditions: 4PG (0.3 mmol), catalyst (0.02 g), n-isooctane (25 mL), 2.0 h, and 400 rpm. 4PG: 4-propylguaiacol; 2M4PC: 2-methoxy-4-propylcyclohexanol; 4PC: 4-propylcyclohexanol; PC: propylcyclohexane; other: (PCP: propylcyclopentane; EC: ethylcyclohexane).

Figure 18. Synthesis, characterization and performance testing of Pt SAC. (**a**) HRTEM image, (**b**) EDX spectrum analysis and (**c**) AC-HAADF-STEM image of Pt_1/NiAl-IMC. (**d**) FT-EXAFS spectra of Pt_1/NiAl-LDH, Pt_1/NiAl-IMC, and Pt foil at the Pt K-edge samples. WT-EXAFS of (**e**) Pt_1/NiAl-LDH and (**f**) Pt_1/NiAl-IMC samples. (**g**) Reaction of 4-Propylguaiacol over different catalyst. (**h**) PDOS of Pt d orbital in Pt_1/NiAl-LDH and Pt_1/NiAl-IMC samples. The gray dotted line denotes the Fermi level. (**i**) Calculated charge density difference distribution of Pt_1/NiAl-LDH and Pt_1/NiAl-IMC samples. Reproduced with permission from [208]; published by John Wiley and Sons, 2025.

As mentioned above, Keggin-type polyoxometalates possess abundant and strong acid sites, and have therefore been frequently employed to stabilize and disperse metal atoms [176,178,182]. However, the high water solubility of polyoxometalates renders them susceptible to leaching in aqueous phases [175]. To address this issue, Gao et al. [209] introduced Cs^+ and employed cesium salts of Keggin-type polyoxometalates as supports, constructing an atomically dispersed Pt catalyst ($Pt_{0.4}$/CsPW-H_2) via impregnation followed by hydrogen reduction. This approach converted the heteropoly acid into an insoluble cesium salt while retaining the strong acidity of the Keggin structure. XAS and HAADF-STEM confirmed that Pt atoms were anchored as single atoms at the bridging oxygen sites of the $[PW_{12}O_{40}]^{3-}$ framework, with a Pt-O coordination number of approximately 2. NH_3-TPD and H_2-TPD characterization revealed that the catalyst possessed both strong acidity and high hydrogen storage capacity, and DFT calculations further confirmed the correlation between its structure and catalytic activity. Benefiting from these structural advantages, $Pt_{0.4}$/CsPW-H_2 achieved efficient HDO of various lignin-derived phenolic monomers and β-O-4 dimers under mild conditions at 150 °C and 0.1–2 MPa H_2, with a substrate/Pt molar ratio as high as 909 and a propylcyclohexane yield of up to 97%. Over 20 consecutive cycles, the total turnover number reached 15,095 $mol_{propylcyclohexane}$ $mol_{Pt}{}^{-1}$. When applied to the direct conversion of eucalyptus reductive catalytic fractionation (RCF) lignin oil under solvent-free conditions, the catalyst afforded 32.7wt% of C6-C10 cycloalkanes with a degree of deoxygenation of 95%. This work demonstrates a design strategy combining single-atom dispersed Pt sites with polyoxometalate synergy, offering a new route for the mild synthesis of lignin-based cycloalkanes.

Although single-atom catalysts can achieve high selectivity through atomically dispersed metal sites, how to realize efficient C-O bond cleavage on non-noble metal single atoms remains a significant challenge in this field. Transition metal carbides, such as β-Mo_2C, are considered promising supports for single atoms owing to their noble-metal-like electronic properties and oxygen affinity, which enable the modulation of charge density and adsorption behavior of single atoms through metal–support interactions [211–213]. Guo et al. [111] employed a co-precipitation method combined with temperature-programmed carburization to prepare a catalyst (Ni_1/β-Mo_2C) featuring Ni single atoms dispersed on a β-Mo_2C support, and applied it to the HDO of dihydroeugenol (DHE) to produce propylcyclohexane. Under conditions of 260 °C and 4 MPa H_2, this catalyst achieved nearly 100% conversion of DHE and nearly 100% selectivity toward propylcyclohexane. HAADF-STEM and XAFS confirmed that Ni atoms were anchored as single atoms on the support surface via Ni-C3 coordination. XPS and charge density analysis revealed electron transfer from Mo to Ni, rendering the Ni sites electron-rich and optimizing the adsorption behavior of reactants. DFT calculations further disclosed that the Ni single-atom sites altered the adsorption geometry of intermediates from perpendicular to parallel orientation, thereby lowering the energy barrier for aromatic ring hydrogenation and shifting the reaction pathway from preferential deoxygenation to a synergistic hydrogenation-deoxygenation mode, ultimately affording propylcyclohexane with high selectivity. In addition, the catalyst exhibited good substrate generality toward various lignin-derived phenolics and maintained high activity after recycling. This work provides an atomic-scale design strategy for the selective conversion of lignin derivatives into jet-fuel-range cycloalkanes using non-noble metal single-atom catalysts.

In addition, cationic vacancies also serve as effective anchoring sites for stabilizing single atoms, owing to their unique electronic effects at the microscopic scale [214,215]. Meanwhile, LDHs with their distinctive lattice effects that enable ordered dispersion of metals, are ideal precursors for constructing cationic vacancies [216,217]. Hu et al. [210] employed a topotactic transformation strategy based on LDH precursors to construct

NiFe-LDH cationic vacancies via alkaline etching, followed by impregnation and reduction to anchor Mo single atoms within the vacancies, yielding the Mo/$NiFe_{71}$-V single-atom catalyst. AC-HAADF-STEM and EXAFS confirmed that Mo atoms occupied the cationic vacancies of the NiFe matrix as isolated single atoms, forming a Mo-Ni coordination structure. XPS, XANES, and charge density difference analyses further revealed that electron transfer occurred from the anchored Mo to the adjacent Ni, rendering the Mo sites electron-deficient. DFT calculations showed that the adsorption energy of cyclohexanol on the vacancy-anchored Mo sites was as low as −1.16 eV, indicating that the vacancy-induced metal–metal interaction significantly enhanced the catalyst's adsorption capacity toward oxygenated intermediates. Benefiting from this, the catalyst achieved nearly 100% conversion and a cyclohexane yield of 99.5% in the HDO of guaiacol at 240 °C and 4 MPa H_2. Moreover, as the regeneration of active sites required overcoming an energy barrier of only 0.10 eV, the catalyst maintained a yield of 92.1% after six cycles, showcasing superior high-temperature stability compared to most reported single-atom systems. In addition, the catalyst exhibited excellent selectivity toward cycloalkanes for various real lignin feedstocks. To sum up, by utilizing cationic vacancies to stabilize non-noble metal single-atom catalysts, this work provides a new strategy for the efficient and stable production of lignin-based cycloalkanes.

Over the past few decades, SACs have been widely employed in catalytic reactions owing to their uniform active sites and near-100% atom utilization efficiency [218–220]. Moreover, their catalytic behavior is governed by the coordination environment, charge density, and anchoring site rather than by size alone [208]. However, the weak adsorption capability of isolated metal atoms toward hydrogen donor molecules, coupled with their inability to effectively stabilize intermediates after dehydrogenation, limits the generation of active hydrogen species. Consequently, non-noble metal SACs often fail to achieve satisfactory catalytic performance in C-O bond cleavage reactions [221,222]. Furthermore, SACs typically possess relatively stable coordination structures under specific synthesis conditions, making the modulation of catalytic selectivity through atomic microenvironment regulation a challenging goal, thereby restricting their potential for efficient lignin conversion [223–225]. Therefore, metal nanoparticles remain the mainstream catalysts in lignin HDO reactions [226].

The nanocatalysts discussed above have already demonstrated the ability to achieve highly selective C-O bond cleavage and controlled aromatic ring hydrogenation in the HDO of lignin model compounds. Although the foregoing discussion has centered on well-defined model compounds, several of the catalysts surveyed above have also been extended to lignin-derived oils and even to raw lignin. For instance, Mo-Co_9S_8/Al_2O_3 converted not only model substrates but also lignin bio-oil and raw lignin into aromatic hydrocarbons [69]; Ni_2P-Al_2O_3 proved effective for the conversion of lignin oil and poplar lignin [113]; and Ru/C-HPW increased the hydrocarbon content of a real lignin oil from 5.5% to 78.9% [137]. Likewise, among single-atom systems, Pt_1/NiAl-IMC afforded a 25.5wt% cycloalkane yield from real lignin feedstocks [208], and $Pt_{0.4}$/CsPW-H_2 converted eucalyptus RCF lignin oil into 32.7wt% of C6-C10 cycloalkanes with a deoxygenation degree of 95% [209]. These studies confirm that the catalytic principles established on model substrates are, in a qualitative sense, transferable to real lignin: the same active sites that mediate selective C-O bond cleavage and controlled aromatic-ring hydrogenation remain operative.

Nevertheless, the results obtained on real lignin are not fully comparable to those on model compounds, which generally deliver higher hydrocarbon yields and selectivities than those achieved on genuine substrates. The principal reason is that real lignin possesses a highly cross-linked macromolecular structure, complex functional group compositions,

and significant feedstock heterogeneity [1,29,227]. Its conversion to jet-fuel-range hydrocarbons is not a single HDO process, but rather involves multiple consecutive steps, including lignin depolymerization, stabilization of reactive intermediates, deoxygenation, and selective aromatic ring hydrogenation [227,228]. Different steps impose distinct requirements on catalytic function and reaction conditions: lignin depolymerization generally demands strong bond activation capability and relatively high temperatures, whereas the subsequent HDO requires efficient hydrogen activation and transfer, along with a precise balance between C-O bond cleavage and aromatic ring saturation. Meanwhile, if the reactive intermediates generated during depolymerization cannot be stabilized in a timely manner, they are prone to repolymerization, condensation, and coke deposition, leading to carbon loss and catalyst deactivation [203,227]. Therefore, the core issue in the cascade conversion of real lignin is not simply the addition of more reaction steps, but rather how to coordinate the functions of depolymerization, stabilization, and HDO through the composition, active sites, and spatial organization of the catalyst.

3. Catalyst Design in Cascade Conversion Processes

On the basis of the multifunctional catalytic requirements for the cascade conversion of real lignin identified above, the existing cascade systems have mainly developed two catalyst design paradigms. The first is a two-stage cascade configuration, in which depolymerization and HDO are separately assigned to different reaction units, with catalysts tailored to each step, thereby achieving macroscopic decoupling of catalytic functions and reaction conditions. The second is simultaneous depolymerization and HDO (one-pot synthesis), which involves constructing bifunctional or multicomponent nanocatalysts within a single reactor, enabling in situ stabilization of depolymerization intermediates and continuous deoxygenation through the proximity synergy between acid sites and metal sites, as well as hydrogen spillover. In the following sections, these two types of cascade systems will be discussed from the perspectives of catalyst functional design and structure-activity relationships.

Fang et al. [229] constructed a two-stage cascade system by synthesizing a dual-catalyst combination comprising W_xC@CS and Ni/CNT, which allocated C-O bond cleavage and aromatic ring hydrogenation to different active components. W_xC@CS, with a surface C/W ratio of approximately 7–8, primarily promoted the cleavage of aryl C-O bonds, converting guaiacol into phenolic intermediates, while Ni/CNT was responsible for H_2 activation and aromatic ring hydrogenation. The resulting cyclohexanol was then further deoxygenated at either W_xC or Ni sites. The intimate contact between the two catalysts shortened the intermediate transfer distance and reduced the apparent activation energy of the system to 56.7 kJ mol^{-1}. The Ni particle size also influenced product selectivity: smaller Ni particles favored deep deoxygenation to cyclohexane, whereas larger particles were more conducive to the retention of cyclohexanol. This system achieved a guaiacol conversion of nearly 100% and a cyclohexane selectivity of 92.4%, underscoring the critical roles of active-site functional separation, particle size regulation, and spatial synergy in the design of cascade catalysts.

In contrast, the one-pot approach simplifies the process flow and improves the yield of target products by optimizing the cascade reactions while minimizing side reactions, thereby enhancing both cost-effectiveness and energy efficiency [110,230]. The integration of direct catalytic depolymerization of lignin with HDO in a single reactor represents a viable route for producing stable cycloalkanes. Mao et al. [231] constructed a hydrotalcite-derived bimetallic Ru/$NiAlO_x$ catalyst for the one-pot conversion of lignin to cycloalkane-rich SAF precursors (Figure 19a). This catalyst promoted the cleavage and HDO of phenolic oligomers in lignin through metal–metal and metal–support synergy: electron transfer from

Ru to Ni nanoparticles increased the electron density of Ni sites, enhancing H_2 adsorption and activation; the generated active hydrogen species further migrated to the oxygen vacancies at the metal-oxide interface, promoting the adsorption of oxygenated oligomers and C-O bond cleavage (Figure 19b). Meanwhile, the incorporation of Ru suppressed the agglomeration of Ni particles, and the smaller particle size (4.2 nm, Figure 19c,d) along with a high specific surface area (197.53 m^2/g) provided abundant active centers and sufficient reaction space for the efficient HDO of oxygenated intermediates. Compared with monometallic catalysts and physically mixed systems, Ru/NiAlO$_x$ exhibited a higher cycloalkane yield, indicating that the electronic coupling at the Ru-Ni interface and oxygen vacancy regulation were key factors for enhancing the cascade reaction efficiency. Over five consecutive cycles, this catalyst achieved a lignin deoxygenation degree of 78.5% and maintained a cycloalkane yield of 31.9–36.6 C% (Figure 19e,f). The results further demonstrated that the resulting cycloalkanes possessed fuel properties comparable to those of conventional jet fuel, including a high heating value (49.4 MJ/kg), an optimal H/C ratio (2.3 mol/mol), suitable kinematic viscosity (4.3 mm^2/s @ 20 °C), and appropriate density (0.865 g/cm^3 @ 15 °C). This work demonstrates that rational bifunctional catalyst design, through multi-active-site synergy, enables the efficient one-pot conversion of waste lignin into cycloalkane-type SAF components.

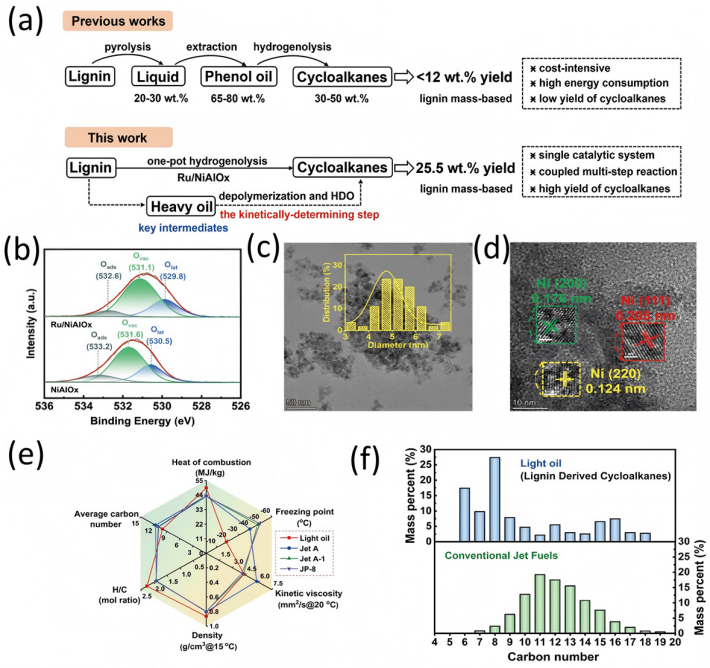


Figure 19. (**a**) Comparative evaluation of procedures and critical analysis of relative merits and limitations between the previous works and this work. (**b**) O 1s XPS spectrum of Ru/NiAlO$_x$. (**c**,**d**) HRTEM image of Ru/NiAlO$_x$. (**e**) Comparison of fuel properties in lignin-derived light oil and commercial/military jet fuels. (**f**) Carbon distributions of light oil and CJFs. Reproduced with permission from [231]; published by American Chemical Society, 2025.

However, the sources and extraction processes of industrial lignin vary significantly, leading to considerable fluctuations in molecular weight, solubility, and impurity content. Such variability may give rise to issues including limited mass transfer of substrates, catalyst surface coking, and even reactor blockage during the actual cascade conversion process [232]. Therefore, when designing nanocatalysts for cascade conversion, it is essential to take full account of the complex composition of industrial lignin and its compatibility with the reaction medium, and to improve the accessibility of macromolecular substrates through strategies such as pore structure optimization and surface polarity modulation [233,234].

Meanwhile, a rational balance between acid and metal functionalities is critical for achieving in situ synergy between depolymerization and HDO while suppressing intermediate repolymerization and condensation; otherwise, coking, carbon loss, and rapid catalyst deactivation may occur [235].

4. Conclusions

This review systematically summarizes recent research progress on a series of nanocatalysts for the HDO of lignin to produce jet-fuel-range cycloalkanes and aromatics. Focusing on catalyst composition, structural design, and reaction pathway regulation, the review highlights the performance characteristics and mechanistic roles of molybdenum-based catalysts, nickel-based catalysts, bimetallic catalysts, bifunctional catalysts, and single-atom catalysts. The core scientific challenge in HDO lies in how to achieve selective cleavage of C-O bonds while precisely controlling the degree of aromatic ring hydrogenation, so as to meet the dual requirements of jet fuel for both aromatics (8–25%) and cycloalkanes. Addressing this challenge, existing studies have developed distinctive design strategies based on different catalyst types: molybdenum-based catalysts leverage MoS_2 edge-site engineering and oxygen vacancy regulation, utilizing the tunability of layered structures to achieve targeted deoxygenation under mild conditions; nickel-based catalysts focus on particle size control and hydrogen spillover/transfer strategies to enhance low-temperature activity and C-C/C-O cleavage capability; bimetallic catalysts achieve optimized deoxygenation selectivity through geometric, electronic, and synergistic effects; bifunctional catalysts realize cascade synergy through the proximity effect between acid and metal sites; and single-atom catalysts enable precise manipulation of product selectivity through fine-tuning of coordination environment and charge density. These strategies, operating at the three levels of geometric structure, electronic density, and spatial organization of active sites, collectively provide a systematic catalyst design framework for resolving the trade-off between selective C-O bond cleavage and competing aromatic ring hydrogenation.

In summary, the precise design of nanocatalysts has become a core driving force for promoting the targeted conversion of lignin into jet fuel components (aromatics and cycloalkanes). Current research has extended from model compounds to real lignin feedstocks, and substantial progress has been made in terms of mild reaction conditions, high selectivity, and catalyst stability. Nevertheless, several challenges remain for practical applications: 1. The poisoning mechanisms of impurities (sulfur, water, inorganic salts) in real lignin toward the structure and long-term stability of catalyst active sites remain unclear, lacking support from in situ dynamic characterization. 2. Catalyst performance evaluation still relies heavily on model compounds [86,236,237]; the complex structure of lignin itself and the structural changes introduced during extraction make it difficult to accurately establish structure–activity relationships on actual substrates. 3. Simultaneously meeting the strict specifications of jet fuel regarding carbon number distribution, aromatics content, and cycloalkane proportion imposes differentiated and even competing demands on the geometric configuration and electronic density of catalyst active sites; how to achieve coordinated regulation of multiple selectivities within a single catalytic system remains a major challenge. 4. The catalyst-to-lignin ratio remains relatively high, resulting in low reaction efficiency, and there is an urgent need for breakthroughs in controllable synthesis and regenerating technologies, from laboratory scale to industrial-scale production. 5. The efficiency of hydrogen activation and transfer directly influences deoxygenation pathway selectivity and hydrogen consumption costs; the balance between hydrogen spillover capability and hydrogen dissociation/hydrogenation activity of the catalyst still needs further optimization. These metrics will ultimately be necessary to compare laboratory-scale catalyst performance on a consistent industrial SAF basis. In view of these challenges, the

authors believe that future research at the catalyst level should focus on the following aspects: 1. combining in situ/operando characterization techniques (e.g., XPS, XAFS, electron microscopy) to reveal impurity-induced deactivation mechanisms, and designing poisoning-resistant catalytic systems accordingly; 2. establishing a stepwise catalyst evaluation system from model molecules to real lignin oil, and developing structure–activity correlation models through machine learning; 3. achieving synergistic optimization of aromatic ring hydrogenation and C-O bond cleavage, thereby meeting jet fuel composition specifications, through strategies such as spatial separation of active sites (e.g., the proximity effect in bifunctional catalysts), charge density modulation (e.g., single-atom coordination environment design), or kinetic partitioning of reaction pathways (e.g., cascade catalysis); 4. developing scalable catalyst synthesis routes (e.g., continuous flow synthesis, template-free green synthesis) and mild regeneration processes; 5. exploring alternative hydrogen source strategies such as catalytic transfer hydrogenation and photo/electrocatalytic in situ hydrogen production, while optimizing hydrogen spillover performance to reduce the hydrogen-to-oil ratio and thereby lower hydrogen source costs; 6. in addition, to enable meaningful comparison of laboratory-scale catalysts from an industrial SAF perspective, future studies should systematically report long-term continuous-flow testing, catalyst productivity, regeneration efficiency, and hydrogen consumption, as these metrics are currently scarce but ultimately indispensable. Techno-economic analysis (TEA) is therefore essential to determine whether catalyst-level gains in the comprehensive metrics above can be translated into cost-competitive, industrially viable lignin-derived SAF production [20]. Achieving these breakthroughs will rely on the synergistic application of multi-scale research methodologies and interdisciplinary approaches such as artificial intelligence, so as to advance the industrialization of lignin-based sustainable aviation fuel.

Author Contributions: Conceptualization, Y.G. and K.G.; writing—original draft preparation, K.G.; writing—review and editing, K.G. and M.Y.; visualization, K.G.; supervision, D.Z., S.Y. and Y.G.; funding acquisition, Y.G. and W.F. All authors have read and agreed to the published version of the manuscript.

Funding: This research was funded by National Natural Science Foundation of China [grant numbers 22573091], Zhejiang Key Laboratory of Low-Carbon Synthesis of Value-Added Chemicals (2025E10097).

Institutional Review Board Statement: Not applicable.

Informed Consent Statement: Not applicable.

Data Availability Statement: No new data were created or analyzed in this study. Data sharing is not applicable to this article.

Acknowledgments: We acknowledge the support from Center of Chemistry for Frontier Technologies of Zhejiang University.

Conflicts of Interest: The authors declare no conflicts of interest.

References

1. Li, C.; Zhao, X.; Wang, A.; Huber, G.W.; Zhang, T. Catalytic transformation of lignin for the production of chemicals and fuels. *Chem. Rev.* **2015**, *115*, 11559–11624. [CrossRef] [PubMed]
2. Millinger, M.; Hedenus, F.; Zeyen, E.; Neumann, F.; Reichenberg, L.; Berndes, G. Diversity of biomass usage pathways to achieve emissions targets in the European energy system. *Nat. Energy* **2025**, *10*, 226–242. [CrossRef]
3. Ji, J.; Zhu, W.; Zhang, B.; Skagfjörd Reinhold, J.; Wang, A.; Zhang, T. Synthesis of bio-based N-containing compounds from biomass. *Natl. Sci. Rev.* **2025**, *12*, nwaf450. [CrossRef] [PubMed]
4. Huber, G.W.; Iborra, S.; Corma, A. Synthesis of transportation fuels from biomass: Chemistry, catalysts, and engineering. *Chem. Rev.* **2006**, *106*, 4044–4098. [CrossRef] [PubMed]

5. Pierozzi, N. Alternative fuels: From niche solutions to pillars of the Energy Transition. In Proceedings of the RINA Energy Transition Conference, Genoa, Italy, 17 February 2026.
6. FICCI; KPMG in India. Sustainable skies: Positioning India as a global SAF hub. In Proceedings of the India Sustainable Aviation Fuel Summit, New Delhi, India, 6 November 2025.
7. World Economic Forum. Global Aviation Sustainability Outlook 2025. In Proceedings of the World Economic Forum Aviation Sustainability Summit, Geneva, Switzerland, 12 March 2025.
8. Cheng, F.; Brewer, C.E. Producing jet fuel from biomass lignin: Potential pathways to alkyl benzenes and cycloalkanes. *Renew. Sustain. Energy Rev.* **2017**, *72*, 673–722. [CrossRef]
9. Hileman, J.I.; Stratton, R.W. Alternative jet fuel feasibility. *Transp. Policy* **2014**, *34*, 52–62. [CrossRef]
10. University of Sheffield. *Investigating the Impact of Reducing the Aromatic Content of Kerosene*; Energy Innovation Centre, University of Sheffield: Sheffield, UK, 2025. Available online: https://eic.sheffield.ac.uk/wp-content/uploads/2025/03/executive-summary-investigating-the-impact-of-reducing-the-aromatic-content-of-kerosene.pdf (accessed on 14 October 2026).
11. Petrukhina, N.N.; Maksimov, A.A. Physicochemical properties and performance characteristics of naphthenoaromatic jet and diesel fuels obtained by hydrotreating of highly aromatic fractions. *Pet. Chem.* **2018**, *58*, 347–374. [CrossRef]
12. Zhang, X.S.; Lei, H.W.; Zhu, L.; Qian, M.; Chan, J.C.; Zhu, X.L.; Liu, Y.P.; Yadavalli, G.; Yan, D.; Wang, L.; et al. Development of a catalytically green route from diverse lignocellulosic biomasses to high-density cycloalkanes for jet fuels. *Catal. Sci. Technol.* **2016**, *6*, 4210–4220. [CrossRef]
13. Munzar, J.D.; Akih-Kumgeh, B.; Denman, B.M.; Zia, A.; Bergthorson, J.M. An experimental and reduced modeling study of the laminar flame speed of jet fuel surrogate components. *Fuel* **2013**, *113*, 586–597. [CrossRef]
14. Natelson, R.H.; Kurman, M.S.; Cernansky, N.P.; Miller, D.L. Low temperature oxidation of *n*-butylcyclohexane. *Combust. Flame* **2011**, *158*, 2325–2337. [CrossRef]
15. Graham, J.L.; Striebich, R.C.; Myers, K.J.; Minus, D.K.; Harrison, W.E. Swelling of nitrile rubber by selected aromatics blended in a synthetic jet fuel. *Energy Fuels* **2006**, *20*, 759–765. [CrossRef]
16. Dewitt, M.J.; West, Z.; Zabarnick, S.; Shafer, L.; Striebich, R.; Higgins, A.; Edwards, T. Effect of aromatics on the thermal-oxidative stability of synthetic paraffinic kerosene. *Energy Fuels* **2014**, *28*, 3696–3703. [CrossRef]
17. Sharma, S.; Singh, P.; Bhardwaj, C.; Khandelwal, B.; Kumar, S. Investigations on combustion and emissions characteristics of aromatic fuel blends in a distributed combustor. *Energy Fuels* **2021**, *35*, 3150–3163. [CrossRef]
18. Gopalakrishnan, V.; Patel, P.; Gupta, S.; Gupta, G.K. Advancement of FT-SPK pathway for sustainable aviation fuel (SAF) production through catalyst-assisted co-gasification integrated fischer tropsch synthesis: A review. *Bioenergy Res.* **2026**, *19*, 70. [CrossRef]
19. Liow, M.Y.; Ng, W.Z.; Song, C.P.; Chang, M.Y.; Adiiba, S.H.; Chien, C.S.; Borhan, N.; Japar, A.S.; Shukor, M.S.M.; Mat, T.; et al. Lipid feedstocks for sustainable aviation fuel (SAF) production via hydroprocessed esters and fatty acids (HEFA) pathway: Current status and challenges in quality, sustainability, availability and cost. *Renew. Sustain. Energy Rev.* **2026**, *236*, 117006. [CrossRef]
20. Gyandoh, E.; Gomez, J. Techno-Economic Analysis (TEA) of Civilian Sustainable Aviation Fuel (SAF)—A systematic review of Hydrotreated Esters and Fatty Acids (HEFA) and Lignocellulosic Biomass Conversion (LCBC) Strategies. *Appl. Energy* **2025**, *399*, 126421. [CrossRef]
21. Klimczyk, W.; Jasinski, R.; Niklas, J.; Siedlecki, M.; Ziólkowski, A. Sustainable aviation fuels: A comprehensive review of production pathways, environmental impacts, lifecycle assessment, and certification frameworks. *Energies* **2025**, *18*, 3705. [CrossRef]
22. Uddin, M.N.; Wang, F. Sustainable aviation fuels: A review of current techno economic viability and life cycle impacts. *Energies* **2025**, *18*, 5510. [CrossRef]
23. Rojas-Michaga, M.F.; Michailos, S.; Cardozo, E.; Akram, M.; Hughes, K.J.; Ingham, D.; Pourkashanian, M. Sustainable aviation fuel (SAF) production through power-to-liquid (PtL): A combined techno-economic and life cycle assessment. *Energy Convers. Manag.* **2023**, *292*, 117427. [CrossRef]
24. Stone, M.L.; Webber, M.S.; Mounfield, W.P.; Bell, D.C.; Christensen, E.; Morais, A.R.C.; Li, Y.; Anderson, E.M.; Heyne, J.S.; Beckham, G.T.; et al. Continuous hydrodeoxygenation of lignin to jet-range aromatic hydrocarbons. *Joule* **2022**, *6*, 2324–2337. [CrossRef]
25. Liu, G.R.; Yan, B.B.; Chen, G.Y. Technical review on jet fuel production. *Renew. Sustain. Energy Rev.* **2013**, *25*, 59–70. [CrossRef]
26. Bi, P.Y.; Wang, J.C.; Zhang, Y.J.; Jiang, P.W.; Wu, X.P.; Liu, J.X.; Xue, H.; Wang, T.J.; Li, Q.X. From lignin to cycloparaffins and aromatics: Directional synthesis of jet and diesel fuel range biofuels using biomass. *Bioresour. Technol.* **2015**, *183*, 10–17. [CrossRef] [PubMed]
27. Abo, B.O.; Gao, M.; Wang, Y.L.; Wu, C.F.; Ma, H.Z.; Wang, Q.H. Lignocellulosic biomass for bioethanol: An overview on pretreatment, hydrolysis and fermentation processes. *Rev. Environ. Health* **2019**, *34*, 57–68. [CrossRef] [PubMed]

28. Alonso, D.M.; Wettstein, S.G.; Dumesic, J.A. Bimetallic catalysts for upgrading of biomass to fuels and chemicals. *Chem. Soc. Rev.* **2012**, *41*, 8075–8098. [CrossRef] [PubMed]
29. Palumbo, C.T.; Ouellette, E.T.; Zhu, J.; Román-Leshkov, Y.; Stahl, S.S.; Beckham, G.T. Accessing monomers from lignin through carbon-carbon bond cleavage. *Nat. Rev. Chem.* **2024**, *8*, 799–816. [CrossRef] [PubMed]
30. Fan, Y.Y.; Liu, C.; Kong, X.C.; Han, Y.; Lei, M.; Xiao, R. A new perspective on polyethylene-promoted lignin pyrolysis with mass transfer and radical explanation. *Green Energy Environ.* **2022**, *7*, 1318–1326. [CrossRef]
31. Kang, S.M.; Li, X.L.; Fan, J.; Chang, J. Hydrothermal conversion of lignin: A review. *Renew. Sustain. Energy Rev.* **2013**, *27*, 546–558. [CrossRef]
32. Ren, J.; Cao, J.P.; Zhao, X.Y.; Yang, F.L.; Wei, X.Y. Recent advances in syngas production from biomass catalytic gasification: A critical review on reactors, catalysts, catalytic mechanisms and mathematical models. *Renew. Sustain. Energy Rev.* **2019**, *116*, 109426. [CrossRef]
33. Yu, H.M.; Wu, Z.L.; Chen, G. Catalytic gasification characteristics of cellulose, hemicellulose and lignin. *Renew. Energy* **2018**, *121*, 559–567. [CrossRef]
34. Liu, Z.Z.; Li, H.L.; Gao, X.Y.; Guo, X.; Wang, S.Z.; Fang, Y.M.; Song, G.Y. Rational highly dispersed ruthenium for reductive catalytic fractionation of lignocellulose. *Nat. Commun.* **2022**, *13*, 4716. [CrossRef] [PubMed]
35. Meng, Q.L.; Yan, J.; Wu, R.Z.; Liu, H.Z.; Sun, Y.; Wu, N.N.; Xiang, J.F.; Zheng, L.R.; Zhang, J.; Han, B.X. Sustainable production of benzene from lignin. *Nat. Commun.* **2021**, *12*, 4534. [CrossRef] [PubMed]
36. Yan, J.; Meng, Q.L.; Shen, X.J.; Chen, B.F.; Sun, Y.; Xiang, J.F.; Liu, H.Z.; Han, B.X. Selective valorization of lignin to phenol by direct transformation of C_{sp2}–C_{sp3} and C-O bonds. *Sci. Adv.* **2020**, *6*, eabd1951. [CrossRef] [PubMed]
37. Guo, H.W.; Chen, Z.; Yin, Q.Q.; Sun, T.; Liu, Y.X.; Ren, G.B.; Li, C.Z. Waste to wealth: H_2S-free fabrication of Fe-ZnS/NC by industrial lignin self S-doping for efficient lignin aerobic oxidation. *Appl. Catal. B Environ.* **2023**, *339*, 123129. [CrossRef]
38. Ouyang, D.H.; Gao, D.H.; Qiang, Y.; Zhao, X.B. Highly-efficient conversion of lignin to electricity by nickel foam anode loaded with solid electrocatalysts. *Appl. Catal. B Environ.* **2023**, *328*, 122491. [CrossRef]
39. Wang, H.; Qiu, X.Q.; Liu, W.F.; Yang, D.J. Facile preparation of well-combined lignin-based carbon/ZnO hybrid composite with excellent photocatalytic activity. *Appl. Surf. Sci.* **2017**, *426*, 206–216. [CrossRef]
40. Wu, X.J.; Fan, X.T.; Xie, S.J.; Lin, J.C.; Cheng, J.; Zhang, Q.H.; Chen, L.Y.; Wang, Y. Solar energy-driven lignin-first approach to full utilization of lignocellulosic biomass under mild conditions. *Nat. Catal.* **2018**, *1*, 772–780. [CrossRef]
41. Qu, C.; Ito, K.; Katsuyama, I.; Mitani, T.; Kashimura, K.; Watanabe, T. Directly microwave-accelerated cleavage of C-C and C-O bonds of lignin by copper oxide and H_2O_2. *ChemSusChem* **2020**, *13*, 4510–4518. [CrossRef] [PubMed]
42. Zhao, Z.Y.; Jiang, Z.W.; Lin, L.; Qiu, R.L.; Yan, K. Synthesis of alkoxyphenols-rich bio-oil by microwave-assisted catalytic pyrolysis of wood over MoS_2 catalyst. *Renew. Energy* **2023**, *219*, 122491. [CrossRef]
43. Zhao, Z.Y.; Jiang, Z.W.; Xu, H.; Yan, K. Selective Production of phenol-rich bio-oil from corn straw waste by direct microwave pyrolysis without extra catalyst. *Front. Chem.* **2021**, *9*, 700887. [CrossRef] [PubMed]
44. Liu, H.; Liu, Z.H.; Zhang, R.K.; Yuan, J.S.; Li, B.Z.; Yuan, Y.J. Bacterial conversion routes for lignin valorization. *Biotechnol. Adv.* **2022**, *60*, 108000. [CrossRef] [PubMed]
45. Ren, N.Q.; Wang, A.J.; Cao, G.L.; Xu, J.F.; Gao, L.F. Bioconversion of lignocellulosic biomass to hydrogen: Potential and challenges. *Biotechnol. Adv.* **2009**, *27*, 1051–1060. [CrossRef] [PubMed]
46. Yu, J.; Gao, Y.; Zhang, H.; Xiao, R. Hydrodeoxygenation of lignin derivatives on heterogeneous catalysts. *Energy Environ. Nexus* **2025**, *1*, e002. [CrossRef]
47. Diao, X.Y.; Ji, N. Rational design of MoS_2-based catalysts toward lignin hydrodeoxygenation: Interplay of structure, catalysis, and stability. *J. Energy Chem.* **2023**, *77*, 601–631. [CrossRef]
48. Lv, X.Q.; Zhao, C.K.; Yan, N.; Ma, X.B.; Feng, S.X.; Shuai, L. Sustainable aviation fuel (SAF) from lignin: Pathways, catalysts, and challenges. *Bioresour. Technol.* **2025**, *419*, 132039, Correction in *Bioresour. Technol.* **2026**, *461*, 135839. [CrossRef] [PubMed]
49. Hart, A.; Onwudili, J.A.; Yildirir, E.; Hashemnezhad, S.E. Energy-dense sustainable aviation fuel-range hydrocarbons from cyclohexanone as a biomass-derived feedstock via sequential catalytic aldol condensation and hydrodeoxygenation. *Chem. Eng. J.* **2025**, *509*, 161494. [CrossRef]
50. Wu, X.; Zhang, H.; Hu, C.; Bao, X.; Yuan, P. Advances in enhancing hydrodeoxygenation selectivity of lignin-derived oxygenates: From synthetic strategies to fundamental techniques. *Green Energy Environ.* **2025**, *10*, 292–321. [CrossRef]
51. Ganesan, M.; Hughes, K.J.; Tenchov, R.; Iyer, K.A.; Ralhan, K.; Diaz, L.M.L.; Bird, R.E.; Ivanov, J.M.; Zhou, Q.A. Leveraging nanoscience for advancing heterogeneous catalysis: An analysis of the influence of nanocatalyst dimensions. *ACS Appl. Energy Mater.* **2025**, *8*, 8656–8679. [CrossRef]
52. Mondelli, C.; Gözaydın, G.; Yan, N.; Pérez-Ramírez, J. Biomass valorisation over metal-based solid catalysts from nanoparticles to single atoms. *Chem. Soc. Rev.* **2020**, *49*, 3764–3782. [CrossRef] [PubMed]
53. Marlowe, J.; Ford, P.C.; Abu-Omar, M.M.; Christopher, P. Structure sensitivity in Pt-catalyzed hydrodeoxygenation of multi-oxygenated lignol model compounds. *Catal. Sci. Technol.* **2023**, *13*, 5662–5678. [CrossRef]

54. Tan, X.; Wu, H.G.; Zhang, H.; Li, H.; Yang, S. Relay catalysis of Pt single atoms and nanoclusters enables alkyl/aryl C-O bond scission for oriented lignin upgrading and N-functionalization. *Chem. Eng. J.* **2023**, *462*, 142225. [CrossRef]
55. Van Deelen, T.W.; Mejía, C.H.; De Jong, K.P. Control of metal-support interactions in heterogeneous catalysts to enhance activity and selectivity. *Nat. Catal.* **2019**, *2*, 955–970. [CrossRef]
56. Wang, H.; Lu, J. A review on particle size effect in metal-catalyzed heterogeneous reactions. *Chin. J. Chem.* **2020**, *38*, 1422–1444. [CrossRef]
57. Li, Z.; Ji, S.F.; Liu, Y.W.; Cao, X.; Tian, S.B.; Chen, Y.J.; Niu, Z.G.; Li, Y.D. Well-defined materials for heterogeneous catalysis: From nanoparticles to isolated single-atom sites. *Chem. Rev.* **2020**, *120*, 623–682. [CrossRef] [PubMed]
58. Begum, G.; Chilivery, R.; Gudimella, K.K.; Mohanapriya, S.; Baithy, M. Recent advancements in the hydrodeoxygenation of lignin-derived phenols to cyclohexane-based products over supported ruthenium catalysts. *ChemCatChem* **2025**, *17*, e01116. [CrossRef]
59. Qu, L.; Jiang, X.; Zhang, Z.H.; Zhang, X.G.; Song, G.Y.; Wang, H.L.; Yuan, Y.P.; Chang, Y.L. A review of hydrodeoxygenation of bio-oil: Model compounds, catalysts, and equipment. *Green Chem.* **2021**, *23*, 9348–9376. [CrossRef]
60. Lang, M.; Li, H. Toward value-added arenes from lignin-derived phenolic compounds via catalytic hydrodeoxygenation. *ACS Sustain. Chem. Eng.* **2022**, *10*, 13208–13243. [CrossRef]
61. Renom-Carrasco, M.; Lefort, L. Ligand libraries for high throughput screening of homogeneous catalysts. *Chem. Soc. Rev.* **2018**, *47*, 5038–5060. [CrossRef] [PubMed]
62. Jiang, L.; Xu, G.Y.; Fu, Y. Catalytic cleavage of the C-O bond in lignin and lignin-derived aryl ethers over Ni/AlP_yO_x catalysts. *ACS Catal.* **2022**, *12*, 9473–9485. [CrossRef]
63. Nimmanwudipong, T.; Runnebaum, R.C.; Block, D.E.; Gates, B.C. Catalytic conversion of guaiacol catalyzed by platinum supported on alumina: Reaction network including hydrodeoxygenation reactions. *Energy Fuels* **2011**, *25*, 3417–3427. [CrossRef]
64. Lin, Y.C.; Li, C.L.; Wan, H.P.; Lee, H.T.; Liu, C.F. Catalytic hydrodeoxygenation of guaiacol on Rh-based and sulfided CoMo and NiMo catalysts. *Energy Fuels* **2011**, *25*, 890–896. [CrossRef]
65. Ardiyanti, A.R.; Gutierrez, A.; Honkela, M.L.; Krause, A.O.I.; Heeres, H.J. Hydrotreatment of wood-based pyrolysis oil using zirconia-supported mono- and bimetallic (Pt, Pd, Rh) catalysts. *Appl. Catal. A-Gen.* **2011**, *407*, 56–66. [CrossRef]
66. National Renewable Energy Laboratory. Liquid fuels from lignins: Annual Report. In Proceedings of the NREL Biofuels Symposium, Golden, CO, USA, 13–16 May 1986.
67. Zhang, S.Q.; Cheng, Y.; Wang, P.; Lei, X.F.; You, J.H.; Guo, R.; Zhang, H.Z. Research progress on surface reconstruction of transition metal sulfides (TMS, M=Fe, Co, Ni) as precatalysts for oxygen evolution reaction. *Int. J. Hydrogen Energy* **2024**, *51*, 545–560. [CrossRef]
68. Ambrosi, A.; Pumera, M. Exfoliation of layered materials using electrochemistry. *Chem. Soc. Rev.* **2018**, *47*, 7213–7224. [CrossRef] [PubMed]
69. Yu, Z.H.; Pan, Y.M.; Shen, Y.T.; Wang, Z.L.; Ong, Z.Y.; Xu, T.; Xin, R.; Pan, L.J.; Wang, B.G.; Sun, L.T.; et al. Towards intrinsic charge transport in monolayer molybdenum disulfide by defect and interface engineering. *Nat. Commun.* **2014**, *5*, 5290. [CrossRef] [PubMed]
70. Lei, L.; Huang, D.L.; Zeng, G.M.; Cheng, M.; Jiang, D.N.; Zhou, C.Y.; Chen, S.; Wang, W.J. A fantastic two-dimensional MoS_2 material based on the inert basal planes activation: Electronic structure, synthesis strategies, catalytic active sites, catalytic and electronics properties. *Coord. Chem. Rev.* **2019**, *399*, 213020. [CrossRef]
71. Wang, W.; Xiao, T.; Wang, D.; Yang, H.; Qiang, Q.; Shen, Z.; Yang, Y.; Wu, K.; Li, C. Scale-up foreseeable fabrication of CoS-MoS_2 for efficient deoxygenation of lignin-derived phenolics to arenes. *ACS Catal.* **2023**, *13*, 8792–8802. [CrossRef]
72. Wu, K.; Li, X.; Wang, W.; Huang, Y.; Jiang, Q.; Li, W.; Chen, Y.; Yang, Y.; Li, C. Creating edge sites within the basal plane of a MoS_2 catalyst for substantially enhanced hydrodeoxygenation activity. *ACS Catal.* **2022**, *12*, 8–17. [CrossRef]
73. Diao, X.Y.; Shi, Y.W.; Zhang, Z.Y.; Li, H.Y.; Niu, X.Y.; Zhang, S.B.; Ji, N. Confined Co_xS_y cluster on basal nanoporous MoS_2 for mild hydrodeoxygenation of lignin derivatives to arenes. *Adv. Funct. Mater.* **2026**, *36*, e18336. [CrossRef]
74. Diao, X.; Ji, N.; Li, X.; Rong, Y.; Zhao, Y.; Lu, X.; Song, C.; Liu, C.; Chen, G.; Ma, L.; et al. Fabricating high temperature stable Mo-Co_9S_8/Al_2O_3 catalyst for selective hydrodeoxygenation of lignin to arenes. *Appl. Catal. B Environ.* **2022**, *305*, 121067. [CrossRef]
75. Dionizio, D.G.B.; De Souza, P.M.; Henriques, C.A.; Berhault, G. Comparative assessment of Mo/Ti and Mo/C catalysts for phenol hydrodeoxygenation: Influence of support and hydrogen treatment. *Catal. Today* **2025**, *454*, 115291. [CrossRef]
76. Yu, Z.; Yu, Z.; Wang, Y.; Sun, Z.; Liu, Y.; Wang, A. Hydrodeoxygenation of guaiacol to aromatic hydrocarbons over Mo_2C prepared in nonthermal plasma. *Plasma Chem. Plasma Process.* **2022**, *42*, 1069–1083. [CrossRef]
77. Wang, F.; Wen, C.; Lu, M.; Zhang, P.; Zhu, J.; Li, M.; Shan, Y.; Song, C. SBA-15-supported ultrastable Mo_2N@CN catalysts for hydrodeoxygenation of guaiacol. *Biomass Bioenergy* **2023**, *168*, 106680. [CrossRef]
78. Kong, D.S.; Cha, J.J.; Wang, H.T.; Lee, H.R.; Cui, Y. First-row transition metal dichalcogenide catalysts for hydrogen evolution reaction. *Energy Environ. Sci.* **2013**, *6*, 3553–3558. [CrossRef]

79. Xu, X.; Liu, W.; Kim, Y.; Cho, J. Nanostructured transition metal sulfides for lithium ion batteries: Progress and challenges. *Nano Today* **2014**, *9*, 604–630. [CrossRef]
80. Wang, Z.Y.; Mi, B.X. Environmental applications of 2D molybdenum disulfide (MoS_2) nanosheets. *Environ. Sci. Technol.* **2017**, *51*, 8229–8244. [CrossRef] [PubMed]
81. Daudin, A.; Lamic, A.E.; Pérot, G.; Brunet, S.; Raybaud, P.; Bouchy, C. Microkinetic interpretation of HDS/HYDO selectivity of the transformation of a model FCC gasoline over transition metal sulfides. *Catal. Today* **2008**, *130*, 221–230. [CrossRef]
82. Gronborg, S.S.; Saric, M.; Moses, P.G.; Rossmeisl, J.; Lauritsen, J.V. Atomic scale analysis of sterical effects in the adsorption of 4,6-dimethyldibenzothiophene on a CoMoS hydrotreating catalyst. *J. Catal.* **2016**, *344*, 121–128. [CrossRef]
83. Liu, G.L.; Robertson, A.W.; Li, M.M.J.; Kuo, W.C.H.; Darby, M.T.; Muhieddine, M.H.; Lin, Y.C.; Suenaga, K.; Stamatakis, M.; Warner, J.H.; et al. MoS_2 monolayer catalyst doped with isolated Co atoms for the hydrodeoxygenation reaction. *Nat. Chem.* **2017**, *9*, 810–816. [CrossRef] [PubMed]
84. Ji, N.; Diao, X.Y.; Li, X.X.; Jia, Z.C.; Zhao, Y.J.; Lu, X.B.; Song, C.F.; Liu, Q.L.; Li, C.Z. Toward alkylphenols production: Lignin depolymerization coupling with methoxy removal over supported MoS_2 catalyst. *Ind. Eng. Chem. Res.* **2020**, *59*, 17287–17299. [CrossRef]
85. Chen, T.S.; Li, Y.J.; Liu, Y.L.; Du, Z.Y.; Li, W.Y. Elucidating the morphology-performance relationship of molybdenum disulfide catalysts in catalytic hydrodeoxygenation. *Chem. Eng. Sci.* **2026**, *328*, 123717. [CrossRef]
86. Si, Z.; Zhang, X.H.; Wang, C.G.; Ma, L.L.; Dong, R.J. An overview on catalytic hydrodeoxygenation of pyrolysis oil and its model compounds. *Catalysts* **2017**, *7*, 169. [CrossRef]
87. Wang, W.Y.; Yang, Y.Q.; Luo, H.A.; Peng, H.Z.; He, B.; Liu, W.Y. Preparation of Ni(Co)-W-B amorphous catalysts for cyclopentanone hydrodeoxygenation. *Catal. Commun.* **2011**, *12*, 1275–1279. [CrossRef]
88. Ansaloni, S.; Russo, N.; Pirone, R. Hydrodeoxygenation of guaiacol over molybdenum-based catalysts: The effect of support and the nature of the active site. *Can. J. Chem. Eng.* **2017**, *95*, 1730–1744. [CrossRef]
89. Prasomsri, T.; Nimmanwudipong, T.; Román-Leshkov, Y. Effective hydrodeoxygenation of biomass-derived oxygenates into unsaturated hydrocarbons by MoO_3 using low H_2 pressures. *Energy Environ. Sci.* **2013**, *6*, 1732–1738. [CrossRef]
90. Prasomsri, T.; Shetty, M.; Murugappan, K.; Román-Leshkov, Y. Insights into the catalytic activity and surface modification of MoO_3 during the hydrodeoxygenation of lignin-derived model compounds into aromatic hydrocarbons under low hydrogen pressures. *Energy Environ. Sci.* **2014**, *7*, 2660–2669. [CrossRef]
91. Shetty, M.; Murugappan, K.; Prasomsri, T.; Green, W.H.; Román-Leshkov, Y. Reactivity and stability investigation of supported molybdenum oxide catalysts for the hydrodeoxygenation (HDO) of m-cresol. *J. Catal.* **2015**, *331*, 86–97. [CrossRef]
92. Cai, Z.; Wang, F.M.; Zhang, X.B.; Ahishakiye, R.; Xie, Y.; Shen, Y. Selective hydrodeoxygenation of guaiacol to phenolics over activated carbon supported molybdenum catalysts. *Mol. Catal.* **2017**, *441*, 28–34. [CrossRef]
93. Rahzani, B.; Saidi, M.; Rahimpour, H.R.; Gates, B.C.; Rahimpour, M.R. Experimental investigation of upgrading of lignin-derived bio-oil component anisole catalyzed by carbon nanotube-supported molybdenum. *RSC Adv.* **2017**, *7*, 10545–10556. [CrossRef]
94. Thomazeau, C.; Martin, V.; Afanasiev, P. Effect of support on the thermal decomposition of $(NH_4)_6Mo_7O_{24}\bullet 4H_2O$ in the inert gas atmosphere. *Appl. Catal. A-Gen.* **2000**, *199*, 61–72. [CrossRef]
95. Li, X.; Luo, X.Y.; Jin, Y.B.; Li, J.Y.; Zhang, H.D.; Zhang, A.P.; Xie, J. Heterogeneous sulfur-free hydrodeoxygenation catalysts for selectively upgrading the renewable bio-oils to second generation biofuels. *Renew. Sustain. Energy Rev.* **2018**, *82*, 3762–3797. [CrossRef]
96. Ochoa, E.; Torres, D.; Pinilla, J.L.; Suelves, I. On the hydrothermal-enhanced synthesis of highly selective Mo_2C catalysts to fully deoxygenated products in the guaiacol HDO reaction. *J. Environ. Chem. Eng.* **2021**, *9*, 105146. [CrossRef]
97. Cattelan, L.; Yuen, A.K.L.; Lui, M.Y.; Masters, A.F.; Selva, M.; Perosa, A.; Maschmeyer, T. Renewable aromatics from kraft lignin with molybdenum-based Catalysts. *ChemCatChem* **2017**, *9*, 2717–2726. [CrossRef]
98. Wang, Q.; Su, T.; Wang, Y.; Chen, Y.; Lu, X.; Ma, R.; Fu, Y.; Zhu, W. Metal-Organic Framework-mediated synthesis of one-dimensional nitrogen-doped molybdenum carbide for the cleavage of lignin and dimeric lignin model compounds. *ACS Sustain. Chem. Eng.* **2020**, *8*, 17008–17015. [CrossRef]
99. Xiao, T.C.; York, A.P.E.; Williams, V.C.; Al-Megren, H.; Hanif, A.; Zhou, X.Y.; Green, M.L.H. Preparation of molybdenum carbides using butane and their catalytic performance. *Chem. Mater.* **2000**, *12*, 3896–3905. [CrossRef]
100. Zhong, Y.; Xia, X.H.; Shi, F.; Zhan, J.Y.; Tu, J.P.; Fan, H.J. Transition metal carbides and nitrides in energy storage and conversion. *Adv. Sci.* **2016**, *3*, 1500286, Erratum in *Adv. Sci.* **2017**, *4*, 201700047. [CrossRef] [PubMed]
101. Chen, J.G.G. Carbide and nitride overlayers on early transition metal surfaces: Preparation, characterization, and reactivities. *Chem. Rev.* **1996**, *96*, 1477–1498. [CrossRef] [PubMed]
102. Ghampson, I.T.; Sepúlveda, C.; Garcia, R.; Fierro, J.L.; Escalona, N.; Desisto, W.J. Comparison of alumina- and SBA-15-supported molybdenum nitride catalysts for hydrodeoxygenation of guaiacol. *Appl. Catal. A-Gen.* **2012**, *435*, 51–60. [CrossRef]
103. Sepúlveda, C.; Leiva, K.; García, R.; Radovic, L.R.; Ghampson, I.T.; Desisto, W.J.; Fierro, J.L.G.; Escalona, N. Hydrodeoxygenation of 2-methoxyphenol over Mo2N catalysts supported on activated carbons. *Catal. Today* **2011**, *172*, 232–239. [CrossRef]

104. Zhang, J.H.; Sun, J.M.; Wang, Y. Recent advances in the selective catalytic hydrodeoxygenation of lignin-derived oxygenates to arenes. *Green Chem.* **2020**, *22*, 1072–1098. [CrossRef]
105. Ghampson, I.T.; Sepúlveda, C.; Garcia, R.; Radovic, L.R.; Fierro, J.L.G.; Desisto, W.J.; Escalona, N. Hydrodeoxygenation of guaiacol over carbon-supported molybdenum nitride catalysts: Effects of nitriding methods and support properties. *Appl. Catal. A-Gen.* **2012**, *439*, 111–124. [CrossRef]
106. Monnier, J.; Sulimma, H.; Dalai, A.; Caravaggio, G. Hydrodeoxygenation of oleic acid and canola oil over alumina-supported metal nitrides. *Appl. Catal. A-Gen.* **2010**, *382*, 176–180. [CrossRef]
107. Alvarez-Galvan, M.C.; Blanco-Brieva, G.; Capel-Sanchez, M.; Morales-Delarosa, S.; Campos-Martin, J.M.; Fierro, J.L.G. Metal phosphide catalysts for the hydrotreatment of non-edible vegetable oils. *Catal. Today* **2018**, *302*, 242–249. [CrossRef]
108. Tian, S.; Qiang, Q.; Yang, H.; Wu, K.; Wang, W.; Ji, N.; Li, C.; Zhang, T. Directional synthesis of aromatics and cycloalkanes in aviation kerosene from lignin over transition metal sulfides. *Sci. Sin. Chim.* **2024**, *55*, 3–17. [CrossRef]
109. Zhang, X.; Wu, J.F.; Li, T.; Zhang, C.Z.; Zhu, L.J.; Wang, S.R. Selective hydrodeoxygenation of lignin-derived phenolics to cycloalkanes over highly stable $NiAl_2O_4$ spinel-supported bifunctional catalysts. *Chem. Eng. J.* **2022**, *429*, 132181. [CrossRef]
110. Ji, N.; Cheng, S.; Jia, Z.C.; Li, H.Y.; Ri, P.; Wang, S.R.; Diao, X.Y. Fabricating bifunctional Co-Al_2O_3@USY catalyst via in-situ growth method for mild hydrodeoxygenation of lignin to naphthenes. *ChemCatChem* **2022**, *14*, e202200274. [CrossRef]
111. Guo, H.Q.; Zhao, J.W.; Chen, Y.; Lu, X.Y.; Yang, Y.; Ding, C.R.; Wu, L.Z.; Tan, L.; Long, J.L.; Yang, G.H.; et al. Mechanistic insights into hydrodeoxygenation of lignin derivatives over ni single atoms supported on Mo_2C. *ACS Catal.* **2024**, *14*, 703–717. [CrossRef]
112. Diao, X.; Hao, L.; Shi, Y.; Zhang, S.; Ji, N. Boosted hydrodeoxygenation of lignin and its derivatives to cycloalkanes over Ni catalysts with surface decoration of $AlPO_4$ species. *J. Energy Chem.* **2025**, *104*, 360–371. [CrossRef]
113. Jia, Z.; Ji, N.; Diao, X.; Li, X.; Zhao, Y.; Lu, X.; Liu, Q.; Liu, C.; Chen, G.; Ma, L.; et al. Highly Selective Hydrodeoxygenation of lignin to naphthenes over three-dimensional flower-like Ni_2P derived from hydrotalcite. *ACS Catal.* **2022**, *12*, 1338–1356. [CrossRef]
114. Zeng, Q.; Lv, Y.; Shi, M.; Pan, T.; Xie, Y.; Liu, Y.; Liu, M. Synergistic interaction between Ni single atoms and nanoparticles for selective cleavage of C-O bonds in lignin without external hydrogen. *J. Catal.* **2026**, *453*, 116565. [CrossRef]
115. Zhao, H.Y.; Li, D.; Bui, P.; Oyama, S.T. Hydrodeoxygenation of guaiacol as model compound for pyrolysis oil on transition metal phosphide hydroprocessing catalysts. *Appl. Catal. A-Gen.* **2011**, *391*, 305–310. [CrossRef]
116. Li, K.L.; Wang, R.J.; Chen, J.X. Hydrodeoxygenation of anisole over silica-supported Ni_2P, MoP, and NiMoP Catalysts. *Energy Fuels* **2011**, *25*, 854–863. [CrossRef]
117. Oyama, S.T.; Wang, X.; Lee, Y.K.; Chun, W.J. Active phase of Ni_2P/SiO_2 in hydroprocessing reactions. *J. Catal.* **2004**, *221*, 263–273. [CrossRef]
118. Zhao, H.Y.; Oyama, S.T.; Freund, H.J.; Wlndarczyk, R.; Sierka, M. Nature of active sites in Ni_2P hydrotreating catalysts as probed by iron substitution. *Appl. Catal. B Environ.* **2015**, *164*, 204–216. [CrossRef]
119. Oyama, S.T.; Lee, Y.K. The active site of nickel phosphide catalysts for the hydrodesulfurization of 4,6-DMDBT. *J. Catal.* **2008**, *258*, 393–400. [CrossRef]
120. Moon, J.S.; Kim, E.G.; Lee, Y.K. Active sites of Ni_2P/SiO_2 catalyst for hydrodeoxygenation of guaiacol: A joint XAFS and DFT study. *J. Catal.* **2014**, *311*, 144–152. [CrossRef]
121. Hsu, P.J.; Lin, Y.C. Hydrodeoxygenation of 4-methylguaiacol over silica-supported nickel phosphide catalysts: The particle size effect. *J. Taiwan Inst. Chem. Eng.* **2017**, *79*, 80–87. [CrossRef]
122. Cao, X.C.; Zhao, J.P.; Long, F.; Zhang, X.L.; Xu, J.M.; Jiang, J.C. Al-modified Pd@mSiO_2 core-shell catalysts for the selective hydrodeoxygenation of fatty acid esters: Influence of catalyst structure and Al atoms incorporation. *Appl. Catal. B Environ.* **2022**, *305*, 1015–1027. [CrossRef]
123. He, Y.F.; Bie, Y.W.; Lehtonen, J.; Liu, R.H.; Cai, J.M. Hydrodeoxygenation of guaiacol as a model compound of lignin-derived pyrolysis bio-oil over zirconia-supported Rh catalyst: Process optimization and reaction kinetics. *Fuel* **2019**, *239*, 1015–1027. [CrossRef]
124. Godwin, J.A.; Babusci, J.P.; Wonderling, N.M.; Shallenberger, J.R.; Seabright, K.; Harper, D.P.; Chmely, S.C. Catalytic transfer hydrogenolysis of switchgrass lignin with ethanol using spinel-type mixed-metal oxide catalysts affords control of the oxidation state of isolated aromatic products. *ACS Sustain. Chem. Eng.* **2024**, *12*, 2611–2620. [CrossRef]
125. Regmi, Y.N.; Mann, J.K.; Mcbride, J.R.; Tao, J.M.; Barnes, C.E.; Labbé, N.; Chmely, S.C. Catalytic transfer hydrogenolysis of organosolv lignin using B-containing FeNi alloyed catalysts. *Catal. Today* **2018**, *302*, 190–195. [CrossRef]
126. Jiao, H.R.; Xu, G.F.; Sang, Y.S.; Chen, H.; Li, Y.D. Direct conversion of enzymatic hydrolysis lignin to cycloalkane fuel with hydrotalcite-derived Ni catalyst. *Catal. Today* **2024**, *430*, 114542. [CrossRef]
127. Sang, Y.S.; Wu, K.; Liu, Q.F.; Bai, Y.F.; Chen, H.; Li, Y.D. Catalytic Ethanolysis of enzymatic hydrolysis lignin over an unsupported nickel catalyst: The effect of reaction conditions. *Energy Fuels* **2021**, *35*, 519–528. [CrossRef]
128. González-Borja, M.A.; Resasco, D.E. Anisole and guaiacol hydrodeoxygenation over monolithic Pt-Sn catalysts. *Energy Fuels* **2011**, *25*, 4155–4162. [CrossRef]

129. Feng, B.; Kobayashi, H.; Ohta, H.; Fukuoka, A. Aqueous-phase hydrodeoxygenation of 4-propylphenol as a lignin model to n-propylbenzene over Re-Ni/ZrO_2 catalysts. *J. Mol. Catal. A-Chem.* **2014**, *388*, 41–46. [CrossRef]
130. Ohta, H.; Feng, B.; Kobayashi, H.; Hara, K.; Fukuoka, A. Selective hydrodeoxygenation of lignin-related 4-propylphenol into n-propylbenzene in water by Pt-Re/ZrO_2 catalysts. *Catal. Today* **2014**, *234*, 139–144. [CrossRef]
131. Parsell, T.H.; Owen, B.C.; Klein, I.; Jarrell, T.M.; Marcum, C.L.; Haupert, L.J.; Amundson, L.M.; Kenttämaa, H.I.; Ribeiro, F.; Miller, J.T.; et al. Cleavage and hydrodeoxygenation (HDO) of C-O bonds relevant to lignin conversion using Pd/Zn synergistic catalysis. *Chem. Sci.* **2013**, *4*, 806–813. [CrossRef]
132. Li, R.; Qiu, J.; Chen, H.; Shu, R.; Chen, Y.; Liu, Y.; Liu, P.-F. Hydrodeoxygenation of phenolic compounds and raw lignin-oil over bimetallic RuNi catalyst: An experimental and modeling study focusing on adsorption properties. *Fuel* **2020**, *281*, 118758. [CrossRef]
133. Zhang, Y.; Fan, G.; Yang, L.; Zheng, L.; Li, F. Cooperative effects between Ni-Mo alloy sites and defective structures over hierarchical Ni-Mo bimetallic catalysts enable the enhanced hydrodeoxygenation activity. *ACS Sustain. Chem. Eng.* **2021**, *9*, 11604–11615. [CrossRef]
134. Chen, H.; Chen, B.; Wei, X.; Liu, L.; Jin, X.; Huang, H.; Wang, C.; Ge, Y.; Li, Z. Pd-Pt alloy/NiO nanosheets as synergistic catalysts for efficient hydrodeoxygenation of lignin-derived phenolics to cyclic alkanes under near-ambient H_2 pressure. *Int. J. Hydrogen Energy* **2025**, *137*, 526–537. [CrossRef]
135. Dwiatmoko, A.A.; Zhou, L.P.; Kim, I.; Choi, J.W.; Suh, D.J.; Ha, J.M. Hydrodeoxygenation of lignin-derived monomers and lignocellulose pyrolysis oil on the carbon-supported Ru catalysts. *Catal. Today* **2016**, *265*, 192–198. [CrossRef]
136. Chen, M.Y.; Huang, Y.B.; Pang, H.; Liu, X.X.; Fu, Y. Hydrodeoxygenation of lignin-derived phenols into alkanes over carbon nanotube supported Ru catalysts in biphasic systems. *Green Chem.* **2015**, *17*, 1710–1717. [CrossRef]
137. Yang, Z.; Luo, B.W.; Shu, R.Y.; Zhong, Z.J.; Tian, Z.P.; Wang, C.; Chen, Y. Synergistic effect of active metal-acid sites on hydrodeoxygenation of lignin-derived phenolic compounds under mild conditions using Ru/C-HPW catalyst. *Fuel* **2022**, *319*, 123617. [CrossRef]
138. Luo, B.W.; Li, R.X.; Shu, R.Y.; Wang, C.; Zhang, J.T.; Chen, Y. Boric acid as a novel homogeneous catalyst coupled with Ru/C for hydrodeoxygenation of phenolic compounds and raw lignin oil. *Ind. Eng. Chem. Res.* **2020**, *59*, 17192–17199. [CrossRef]
139. Li, C.; Xu, G.Y.; Zhai, Y.X.; Liu, X.H.; Ma, Y.F.; Zhang, Y. Hydrogenation of biomass-derived ethyl levulinate into γ-valerolactone by activated carbon supported bimetallic Ni and Fe catalysts. *Fuel* **2017**, *203*, 23–31. [CrossRef]
140. Furimsky, E.; Massoth, F.E. Deactivation of hydroprocessing catalysts. *Catal. Today* **1999**, *52*, 381–495. [CrossRef]
141. Mortensen, P.M.; Grunwaldt, J.D.; Jensen, P.A.; Knudsen, K.G.; Jensen, A.D. A review of catalytic upgrading of bio-oil to engine fuels. *Appl. Catal. A-Gen.* **2011**, *407*, 1–19. [CrossRef]
142. Robinson, A.M.; Hensley, J.E.; Medlin, J.W. Bifunctional catalysts for upgrading of biomass-derived oxygenates: A review. *ACS Catal.* **2016**, *6*, 5026–5043. [CrossRef]
143. Insyani, R.; Kim, M.K.; Choi, J.W.; Yoo, C.J.; Suh, D.J.; Lee, H.; Kim, C.S.; Kim, K.H.; Kim, K.; Ha, J.M. Selective hydrodeoxygenation of biomass pyrolysis oil and lignin-derived oxygenates to cyclic alcohols using the bimetallic NiFe core-shell supported on TiO_2. *Chem. Eng. J.* **2022**, *446*, 136578. [CrossRef]
144. Kang, Y.-H.; Gao, J.; Zhang, X.-Q.; Gao, Y.; Wang, Z.-H.; Li, Y.-J.; Liu, G.-H.; Ma, X.-R.; Wang, A.-M.; Bai, J.-J.; et al. Synergistic effect of acidity and active phases for nickel nanoparticles supported HZSM-5 catalysts on lignin-related model compounds hydrodeoxygenation performance under mild conditions. *Ind. Crops Prod.* **2023**, *198*, 116704. [CrossRef]
145. Tian, J.-Y.; Hu, J.; Lin, F.; Ma, Y.-L.; Sun, Y.-G.; Zhu, Y.-B.; Wei, J.-P.; Lei, Y.-T.; Wu, J.-J. Effect of HZSM-5 Morphology on the Catalytic Properties of Ru/HZSM-5 for the Hydrodeoxygenation of Guaiacol to Cyclohexane. *Energy Fuels* **2024**, *38*, 18737–18747. [CrossRef]
146. Shu, R.; Zhong, Z.; You, H.; Tian, Z.; Chen, Y.; Ma, L. Hydrodeoxygenation of lignin-derived phenolic compounds over Ru/TiO_2–CeO_2 catalyst prepared by photochemical reduction method. *J. Energy Inst.* **2021**, *99*, 1–8. [CrossRef]
147. Ali, H.; Sharma, N.; Kumar, S.; Thybaut, J.W.; Lauwaert, J.; Zhang, X.; Kansal, S.K.; Saravanamurugan, S. Crucial role of oxygen vacancies for the efficient hydrodeoxygenation of lignin-based phenolic model compounds with Ni/$Ti_{1-x}Zr_xO_2$. *Catal. Sci. Technol.* **2025**, *15*, 3568–3580. [CrossRef]
148. Liu, W.; You, W.Q.; Sun, W.; Yang, W.S.; Korde, A.; Gong, Y.T.; Deng, Y.L. Ambient-pressure and low-temperature upgrading of lignin bio-oil to hydrocarbons using a hydrogen buffer catalytic system. *Nat. Energy* **2020**, *5*, 759–767. [CrossRef]
149. Xu, Y.; Liu, Z.; Liu, B.; Dong, B.; Li, Y.; Li, Y.; Guo, H.; Chai, Y.; Liu, C. Hydrodeoxygenation of guaiacol to bio-hydrocarbons over Ni catalyst supported on activated coconut carbon in alkaline condition. *Biomass Bioenergy* **2022**, *163*, 106506. [CrossRef]
150. Phan, D.-P.; Le, V.N.; Kim, J.; Lee, E.Y. Controlled hydrodeoxygenation of lignin-derived anisole over supported Pt on UiO-66 based-catalysts through defect engineering approach. *Fuel Process. Technol.* **2021**, *224*, 107001. [CrossRef]
151. Shi, Y.C.; Xing, E.H.; Wu, K.J.; Wang, J.L.; Yang, M.D.; Wu, Y.L. Recent progress on upgrading of bio-oil to hydrocarbons over metal/zeolite bifunctional catalysts. *Catal. Sci. Technol.* **2017**, *7*, 2385–2415. [CrossRef]

152. Cui, X.J.; Yuan, H.K.; Junge, K.; Topf, C.; Beller, M.; Shi, F. A stable and practical nickel catalyst for the hydrogenolysis of C-O bonds. *Green Chem.* **2017**, *19*, 305–310. [CrossRef]
153. Liu, M.J.; Wang, G.; Zhang, Z.D.; Li, Z.Y.; Xu, S.N.; Wang, R.P.; He, S.B. Catalytic pyrolysis performance of alkanes to light olefins over bifunctional ZSM-5 zeolites. *J. Anal. Appl. Pyrolysis* **2023**, *170*, 105924. [CrossRef]
154. Corma, A.; Orchillés, A.V. Current views on the mechanism of catalytic cracking. *Microporous Mesoporous Mater.* **2000**, *35–36*, 21–30. [CrossRef]
155. Chen, S.; Miao, C.X.; Luo, Y.; Zhou, G.L.; Xiong, K.; Jiao, Z.J.; Zhang, X.M. Study of catalytic hydrodeoxygenation performance of Ni catalysts: Effects of prepared method. *Renew. Energy* **2018**, *115*, 1109–1117. [CrossRef]
156. Li, S.; Chen, X.L.; Wang, J.; Yao, N.; Wang, J.G.; Cen, J.; Li, X.N. Construction the Ni@Carbon nanostructure with dual-reaction surfaces for the selective hydrogenation reaction. *Appl. Surf. Sci.* **2019**, *489*, 786–795. [CrossRef]
157. Kang, Y.H.; Wei, X.Y.; Li, J.; Jin, H.T.; Li, T.; Lu, C.Y.; Ma, X.R.; Zong, Z.M. Green and effective catalytic hydroconversion of an extractable portion from an oil sludge to clean jet and diesel fuels over a mesoporous Y zeolite-supported nickel catalyst. *Fuel* **2021**, *287*, 119396. [CrossRef]
158. Kang, Y.H.; Wei, X.Y.; Zhang, X.Q.; Li, Y.J.; Liu, G.H.; Ma, X.R.; Li, X.; Bai, H.C.; Li, Z.N.; Yan, H.J.; et al. Deep catalytic hydroconversion of straw-derived bio-oil to alkanes over mesoporous zeolite Y supported nickel nanoparticles. *Renew. Energy* **2021**, *173*, 876–885. [CrossRef]
159. Lee, H.; Kim, H.; Yu, M.J.; Ko, C.H.; Jeon, J.K.; Jae, J.; Park, S.H.; Jung, S.C.; Park, Y.K. Catalytic Hydrodeoxygenation of bio-oil model compounds over Pt/HY catalyst. *Sci. Rep.* **2016**, *6*, 28765. [CrossRef] [PubMed]
160. Ohta, H.; Yamamoto, K.; Hayashi, M.; Hamasaka, G.; Uozumi, Y.; Watanabe, Y. Low temperature hydrodeoxygenation of phenols under ambient hydrogen pressure to form cyclohexanes catalysed by Pt nanoparticles supported on H-ZSM-5. *Chem. Commun.* **2015**, *51*, 17000–17003. [CrossRef] [PubMed]
161. Niu, Z.Y.; Zhang, S.H.; Sun, Y.B.; Gai, S.L.; He, F.; Dai, Y.L.; Li, L.; Yang, P.P. Controllable synthesis of Ni/SiO_2 hollow spheres and their excellent catalytic performance in 4-nitrophenol reduction. *Dalton Trans.* **2014**, *43*, 16911–16918. [CrossRef] [PubMed]
162. Shu, R.Y.; Zhang, Q.; Xu, Y.; Long, J.X.; Ma, L.L.; Wang, T.J.; Chen, P.R.; Wu, Q.Y. Hydrogenation of lignin-derived phenolic compounds over step by step precipitated Ni/SiO_2. *RSC Adv.* **2016**, *6*, 5214–5222. [CrossRef]
163. Zhou, M.H.; Ye, J.; Liu, P.; Xu, J.M.; Jiang, J.C. Water-assisted selective hydrodeoxygenation of guaiacol to cyclohexanol over supported Ni and Co bimetallic catalysts. *ACS Sustain. Chem. Eng.* **2017**, *5*, 8824–8835. [CrossRef]
164. Wang, X.; Zhu, S.H.; Wang, S.; He, Y.; Liu, Y.; Wang, J.G.; Fan, W.B.; Lv, Y.K. Low temperature hydrodeoxygenation of guaiacol into cyclohexane over Ni/SiO_2 catalyst combined with Hβ zeolite. *RSC Adv.* **2019**, *9*, 3868–3876. [CrossRef] [PubMed]
165. Soltanian, S.; Lee, C.L.; Lam, S.S. A review on the role of hierarchical zeolites in the production of transportation fuels through catalytic fast pyrolysis of biomass. *Biofuel Res. J.* **2020**, *7*, 1217–1234. [CrossRef]
166. Shao, S.S.; Zhang, H.Y.; Shen, D.K.; Xiao, R. Enhancement of hydrocarbon production and catalyst stability during catalytic conversion of biomass pyrolysis-derived compounds over hierarchical HZSM-5. *RSC Adv.* **2016**, *6*, 44313–44320. [CrossRef]
167. Sirous-Rezaei, P.; Jae, J.; Ha, J.M.; Ko, C.H.; Kim, J.M.; Jeon, J.K.; Park, Y.K. Mild hydrodeoxygenation of phenolic lignin model compounds over a $FeReO_x/ZrO_2$ catalyst: Zirconia and rhenium oxide as efficient dehydration promoters. *Green Chem.* **2018**, *20*, 1472–1483. [CrossRef]
168. Resende, K.A.; Braga, A.H.; Noronha, F.B.; Hori, C.E. Hydrodeoxygenation of phenol over Ni/$Ce_{1-x}Nb_xO_2$ catalysts. *Appl. Catal. B Environ.* **2019**, *245*, 100–113. [CrossRef]
169. Ali, H.; Vandevyvere, T.; Lauwaert, J.; Kansal, S.K.; Saravanamurugan, S.; Thybaut, J.W. Impact of oxygen vacancies in Ni supported mixed oxide catalysts on anisole hydrodeoxygenation. *Catal. Commun.* **2022**, *164*, 106436. [CrossRef]
170. Xiao, X.; Bergstrom, H.; Saenger, R.; Johnson, B.; Sun, R.C.; Peterson, A. The role of oxygen vacancies in biomass deoxygenation by reducible zinc/zinc oxide catalysts. *Catal. Sci. Technol.* **2018**, *8*, 1819–1827. [CrossRef]
171. Wang, S.S.; Yang, G.Y. Recent advances in polyoxometalate-catalyzed reactions. *Chem. Rev.* **2015**, *115*, 4893–4962. [CrossRef] [PubMed]
172. Weinstock, I.A.; Schreiber, R.E.; Neumann, R. Dioxygen in polyoxometalate mediated reactions. *Chem. Rev.* **2018**, *118*, 2680–2717. [CrossRef] [PubMed]
173. Enferadi-Kerenkan, A.; Do, T.O.; Kaliaguine, S. Heterogeneous catalysis by tungsten-based heteropoly compounds. *Catal. Sci. Technol.* **2018**, *8*, 2257–2284. [CrossRef]
174. Kozhevnikov, I.V. Catalysis by heteropoly acids and multicomponent polyoxometalates in liquid-phase reactions. *Chem. Rev.* **1998**, *98*, 171–198. [CrossRef] [PubMed]
175. Zhong, J.W.; Pérez-Ramírez, J.; Yan, N. Biomass valorisation over polyoxometalate-based catalysts. *Green Chem.* **2021**, *23*, 18–36. [CrossRef]
176. Alharbi, K.; Alharbi, W.; Kozhevnikova, E.F.; Kozhevnikov, I.V. Deoxygenation of ethers and esters over bifunctional Pt-heteropoly acid catalyst in the gas phase. *ACS Catal.* **2016**, *6*, 2067–2075. [CrossRef]

177. Althikrallah, H.; Kozhevnikova, E.F.; Kozhevnikov, I.V. Facile gas-phase hydrodeoxygenation of 2,5-dimethylfuran over bifunctional metal-acid catalyst Pt-$Cs_{2.5}H_{0.5}PW_{12}O_{40}$. *Chem. Commun.* **2021**, *57*, 227–230. [CrossRef] [PubMed]
178. Zhang, B.; Sun, G.; Ding, S.P.; Asakura, H.; Zhang, J.; Sautet, P.; Yan, N. Atomically dispersed Pt_1-polyoxometalate catalysts: How does metal-support interaction affect stability and hydrogenation activity? *J. Am. Chem. Soc.* **2019**, *141*, 8185–8197. [CrossRef] [PubMed]
179. Alharbi, K.; Kozhevnikova, E.F.; Kozhevnikov, I.V. Hydrogenation of ketones over bifunctional Pt-heteropoly acid catalyst in the gas phase. *Appl. Catal. A-Gen.* **2015**, *504*, 457–462. [CrossRef]
180. Besson, M.; Gallezot, P.; Pinel, C. Conversion of Biomass into Chemicals over Metal Catalysts. *Chem. Rev.* **2014**, *114*, 1827–1870. [CrossRef] [PubMed]
181. Deng, W.P.; Zhang, Q.H.; Wang, Y. Polyoxometalates as efficient catalysts for transformations of cellulose into platform chemicals. *Dalton Trans.* **2012**, *41*, 9817–9831. [CrossRef] [PubMed]
182. Poole, O.; Alharbi, K.; Belic, D.; Kozhevnikova, E.F.; Kozhevnikov, I.V. Hydrodeoxygenation of 3-pentanone over bifunctional Pt-heteropoly acid catalyst in the gas phase: Enhancing effect of gold. *Appl. Catal. B Environ.* **2017**, *202*, 446–453. [CrossRef]
183. Giannakoudakis, D.A.; Barczak, M.; Florent, M.; Bandosz, T.J. Analysis of interactions of mustard gas surrogate vapors with porous carbon textiles. *Chem. Eng. J.* **2019**, *362*, 758–766. [CrossRef]
184. Florent, M.; Giannakoudakis, D.A.; Bandosz, T.J. Mustard gas surrogate interactions with modified porous carbon fabrics: Effect of oxidative treatment. *Langmuir* **2017**, *33*, 11475–11483. [CrossRef] [PubMed]
185. Simancas, R.; Chokkalingam, A.; Elangovan, S.P.; Liu, Z.D.; Sano, T.; Iyoki, K.; Wakihara, T.; Okubo, T. Recent progress in the improvement of hydrothermal stability of zeolites. *Chem. Sci.* **2021**, *12*, 7677–7695. [CrossRef] [PubMed]
186. Wang, S.B.; Lu, G.Q.M. Effects of promoters on catalytic activity and carbon deposition of Ni/γ-Al_2O_3 catalysts in CO_2 reforming of CH_4. *J. Chem. Technol. Biotechnol.* **2000**, *75*, 589–595. [CrossRef]
187. Jamil, A.K.; Muraza, O.; Osuga, R.; Shafei, E.N.; Choi, K.H.; Yamani, Z.H.; Somali, A.; Yokoi, T. Hydrothermal stability of one-dimensional pore ZSM-22 zeolite in hot water. *J. Phys. Chem. C* **2016**, *120*, 22918–22926. [CrossRef]
188. Ballesteros-Plata, D.; Infantes-Molina, A.; Rodríguez-Castellón, E. Study of bifunctionality of Pt/SBA-15 catalysts for HDO of dibenzofuran reaction: Addition of Mo or use of an acidic support. *Appl. Catal. A-Gen.* **2019**, *580*, 93–101. [CrossRef]
189. Yan, P.H.; Mensah, J.; Adesina, A.; Kennedy, E.; Stockenhuber, M. Highly-dispersed Ni on BEA catalyst prepared by ion-exchange-deposition-precipitation for improved hydrodeoxygenation activity. *Appl. Catal. B Environ.* **2020**, *267*, 118690. [CrossRef]
190. Phan, D.P.; Lee, E.Y. Controlled hydrogenolysis over heterogeneous catalysts for lignin valorization. *Catal. Rev.* **2020**, *62*, 607–630. [CrossRef]
191. Liu, J.W.; Chen, L.F.; Cui, H.; Zhang, J.Y.; Zhang, L.; Su, C.Y. Applications of metal-organic frameworks in heterogeneous supramolecular catalysis. *Chem. Soc. Rev.* **2014**, *43*, 6011–6061. [CrossRef] [PubMed]
192. Kang, Y.S.; Lu, Y.; Chen, K.; Zhao, Y.; Wang, P.; Sun, W.Y. Metal-organic frameworks with catalytic centers: From synthesis to catalytic application. *Coord. Chem. Rev.* **2019**, *378*, 262–280. [CrossRef]
193. Zhang, H.B.; Nai, J.W.; Yu, L.; Lou, X.W. Metal-organic-framework-based materials as platforms for renewable energy and environmental applications. *Joule* **2017**, *1*, 77–107. [CrossRef]
194. Jrad, A.; Abu Tarboush, B.J.; Hmadeh, M.; Ahmad, M. Tuning acidity in zirconium-based metal organic frameworks catalysts for enhanced production of butyl butyrate. *Appl. Catal. A-Gen.* **2019**, *570*, 31–41. [CrossRef]
195. Dhakshinamoorthy, A.; Santiago-Portillo, A.; Asiri, A.M.; Garcia, H. Engineering UiO-66 Metal Organic Framework for Heterogeneous Catalysis. *ChemCatChem* **2019**, *11*, 899–923. [CrossRef]
196. Vo, T.K.; Le, V.N.; Yoo, K.S.; Song, M.; Kim, D.; Kim, J. Facile synthesis of UiO-66(Zr) using a microwave-assisted continuous tubular reactor and its application for toluene adsorption. *Cryst. Growth Des.* **2019**, *19*, 4949–4956. [CrossRef]
197. Wang, Y.; Li, L.J.; Dai, P.C.; Yan, L.T.; Cao, L.; Gu, X.; Zhao, X.B. Missing-node directed synthesis of hierarchical pores on a zirconium metal-organic framework with tunable porosity and enhanced surface acidity via a microdroplet flow reaction. *J. Mater. Chem. A* **2017**, *5*, 22372–22379. [CrossRef]
198. Valekar, A.H.; Cho, K.H.; Chitale, S.K.; Hong, D.Y.; Cha, G.Y.; Lee, U.H.; Hwang, D.W.; Serre, C.; Chang, J.S.; Hwang, Y.K. Catalytic transfer hydrogenation of ethyl levulinate to γ-valerolactone over zirconium-based metal-organic frameworks. *Green Chem.* **2016**, *18*, 4542–4552. [CrossRef]
199. Hao, L.D.; Li, X.Y.; Hurlock, M.J.; Tu, X.M.; Zhang, Q. Hierarchically porous UiO-66: Facile synthesis, characterization and application. *Chem. Commun.* **2018**, *54*, 11817–11820. [CrossRef] [PubMed]
200. Yang, C.H.; Nguyen, Q.D.; Chen, T.H.; Helal, A.S.; Li, J.; Chang, J.K. Functional group-dependent supercapacitive and aging properties of activated carbon electrodes in organic electrolyte. *ACS Sustain. Chem. Eng.* **2018**, *6*, 1208–1214. [CrossRef]
201. Wen, D.T.; Hao, X.H.; Zheng, X.S.; Yu, J.J. UiO-66-NH_2-catalyzed biodiesel production: Mechanistic insights from molecular dynamics simulation. *J. Mol. Model.* **2026**, *32*, 137. [CrossRef] [PubMed]

202. Jing, H.Y.; Zhu, P.; Zheng, X.B.; Zhang, Z.D.; Wang, D.S.; Li, Y.D. Theory-oriented screening and discovery of advanced energy transformation materials in electrocatalysis. *Adv. Powder Mater.* **2022**, *1*, 100013, Erratum in *Adv. Powder Mater.* **2022**, *1*, 100078. [CrossRef]
203. Sun, Z.H.; Fridrich, B.; De Santi, A.; Elangovan, S.; Barta, K. Bright side of lignin depolymerization: Toward new platform chemicals. *Chem. Rev.* **2018**, *118*, 614–678. [CrossRef] [PubMed]
204. Zhang, J.; Zheng, C.Y.; Zhang, M.L.; Qiu, Y.J.; Xu, Q.; Cheong, W.C.; Chen, W.X.; Zheng, L.R.; Gu, L.; Hu, Z.P.; et al. Controlling N-doping type in carbon to boost single-atom site Cu catalyzed transfer hydrogenation of quinoline. *Nano Res.* **2020**, *13*, 3082–3087. [CrossRef]
205. Zhang, K.L.; Meng, Q.L.; Wu, H.H.; Yan, J.; Mei, X.L.; An, P.F.; Zheng, L.R.; Zhang, J.; He, M.Y.; Han, B.X. Selective hydrodeoxygenation of aromatics to cyclohexanols over Ru single atoms supported on CeO_2. *J. Am. Chem. Soc.* **2022**, *144*, 20834–20846. [CrossRef] [PubMed]
206. Li, C.C.; Nakagawa, Y.; Yabushita, M.; Nakayama, A.; Tomishige, K. Guaiacol hydrodeoxygenation over iron-ceria catalysts with platinum single-atom alloy clusters as a promoter. *ACS Catal.* **2021**, *11*, 12794–12814. [CrossRef]
207. Xia, J.; Dong, L.; Liu, X.H.; Chernikov, R.; Shakouri, M.; Hu, Y.F.; Guo, Y.; Wang, J.J.; Song, K.P.; Hu, P.J.; et al. Identifying the activity origin of a single-atom Au_1/Nb_2O_5 catalyst for hydrodeoxygenation of methylcatechol: A stable substitutional au plus site. *ACS Catal.* **2023**, *13*, 6093–6103. [CrossRef]
208. Dai, Q.; Xu, Z.; Wang, S.; Zeng, X.; He, F.; Yue, F.; Zhang, Z.; Ye, C.; Wang, Y.; Liu, C.; et al. Fine-tuned charge density of Pt single-atom sites for controllable hydrodeoxygenation of lignin. *Angew. Chem. Int. Ed.* **2025**, *64*, e202504347. [CrossRef] [PubMed]
209. Gao, X.; Ma, R.; Liu, Z.; Wang, S.; Wu, Y.; Song, G. Hydrodeoxygenation of lignin-derived phenols into cycloalkanes by atomically dispersed Pt-polyoxometalate catalysts. *Appl. Catal. B Environ.* **2024**, *352*, 124059. [CrossRef]
210. Hu, H.; Ma, D.; Yi, M.; Li, H.; Yuan, Z.; Liu, J.; Luo, Q.; Zhong, Q.; Wei, J.; Liu, G.; et al. Unveiling the enhancement of catalytic activity and stability by single-atom Mo anchored to cationic vacancy for the catalytic hydrodeoxygenation of lignin to naphthenes. *Chem. Eng. J.* **2025**, *505*, 159303. [CrossRef]
211. Hwu, H.H.; Chen, J.G.G. Surface chemistry of transition metal carbides. *Chem. Rev.* **2005**, *105*, 185–212. [CrossRef] [PubMed]
212. Murugappan, K.; Anderson, E.M.; Teschner, D.; Jones, T.E.; Skorupska, K.; Román-Leshkov, Y. Operando NAP-XPS unveils differences in MoO_3 and Mo_2C during hydrodeoxygenation. *Nat. Catal.* **2018**, *1*, 960–967. [CrossRef]
213. Ma, Y.F.; Guan, G.Q.; Hao, X.G.; Cao, J.; Abudula, A. Molybdenum carbide as alternative catalyst for hydrogen production—A review. *Renew. Sustain. Energy Rev.* **2017**, *75*, 1101–1129. [CrossRef]
214. Ding, W.M.; Yuan, S.B.; Yang, Y.; Li, X.M.; Luo, M. Defect engineering: The role of cationic vacancies in photocatalysis and electrocatalysis. *J. Mater. Chem. A* **2023**, *11*, 23653–23682. [CrossRef]
215. Xu, Q.; Guo, C.X.; Li, B.B.; Zhang, Z.D.; Qiu, Y.J.; Tian, S.B.; Zheng, L.R.; Gu, L.; Yan, W.S.; Wang, D.S.; et al. Al^{3+} dopants induced Mg^{2+} vacancies stabilizing single-atom Cu catalyst for efficient free-radical hydrophosphinylation of alkenes. *J. Am. Chem. Soc.* **2022**, *144*, 4321–4326. [CrossRef] [PubMed]
216. Yang, Y.S.; Ren, Z.; Zhou, S.J.; Wei, M. Perspectives on multifunctional catalysts derived from layered double hydroxides toward upgrading reactions of biomass resources. *ACS Catal.* **2021**, *11*, 6440–6454. [CrossRef]
217. Zhai, P.L.; Xia, M.Y.; Wu, Y.Z.; Zhang, G.H.; Gao, J.F.; Zhang, B.; Cao, S.Y.; Zhang, Y.T.; Li, Z.W.; Fan, Z.Z.; et al. Engineering single-atomic ruthenium catalytic sites on defective nickel-iron layered double hydroxide for overall water splitting. *Nat. Commun.* **2021**, *12*, 4587. [CrossRef] [PubMed]
218. Li, X.; Liu, J.Q.; Wu, J.G.; Zhang, L.P.; Cao, D.; Cheng, D.J. Constructing a highly active Pd atomically dispersed catalyst for cinnamaldehyde hydrogenation: Synergistic catalysis between Pd-N_3 single atoms and fully exposed Pd clusters. *ACS Catal.* **2024**, *14*, 2369–2379. [CrossRef]
219. Luo, G.Y.; Song, M.; Zhang, Q.; An, L.L.; Shen, T.; Wang, S.; Hu, H.Y.; Huang, X.; Wang, D.L. Advances of Synergistic electrocatalysis between single atoms and nanoparticles/clusters. *Nano-Micro Lett.* **2024**, *16*, 241. [CrossRef] [PubMed]
220. Wu, R.Z.; Meng, Q.L.; Yan, J.; Zhang, Z.R.; Chen, B.F.; Liu, H.Z.; Tai, J.; Zhang, G.K.; Zheng, L.R.; Zhang, J.; et al. Intermetallic synergy in platinum-cobalt electrocatalysts for selective C-O bond cleavage. *Nat. Catal.* **2024**, *7*, 702–718. [CrossRef]
221. Xie, J.; Xi, Y.J.; Gao, W.S.; Zhang, H.; Wu, Y.K.; Zhang, R.H.; Yang, H.F.; Peng, Y.; Li, F.W.; Li, Z.L.; et al. Hydrogenolysis of lignin model compounds on Ni nanoparticles surrounding the oxygen vacancy of CeO_2. *ACS Catal.* **2023**, *13*, 9577–9587. [CrossRef]
222. Zhang, L.K.; Shang, N.Z.; Gao, S.T.; Wang, J.M.; Meng, T.; Du, C.C.; Shen, T.D.; Huang, J.Y.; Wu, Q.H.; Wang, H.J.; et al. Atomically dispersed Co catalyst for efficient hydrodeoxygenation of lignin-derived species and hydrogenation of nitroaromatics. *ACS Catal.* **2020**, *10*, 8672–8682. [CrossRef]
223. Zhang, T.J.; Walsh, A.G.; Yu, J.H.; Zhang, P. Single-atom alloy catalysts: Structural analysis, electronic properties and catalytic activities. *Chem. Soc. Rev.* **2021**, *50*, 569–588. [CrossRef] [PubMed]
224. Tang, C.; Chen, L.; Li, H.J.; Li, L.Q.; Jiao, Y.; Zheng, Y.; Xu, H.L.; Davey, K.; Qiao, S.Z. Tailoring acidic oxygen reduction selectivity on single-atom catalysts via modification of first and second coordination spheres. *J. Am. Chem. Soc.* **2021**, *143*, 7819–7827. [CrossRef] [PubMed]

225. Zhang, E.R.; Dong, A.Q.; Yin, K.; Ye, C.L.; Zhou, Y.; Tan, C.; Li, M.G.; Zheng, X.B.; Wang, Y.; Gao, X.W.; et al. Electron localization in rationally designed Pt_1Pd single-atom alloy catalyst enables high-performance Li-O_2 batteries. *J. Am. Chem. Soc.* **2024**, *146*, 2339–2344. [CrossRef] [PubMed]
226. Wang, B.Y.; Zhou, P.; Yan, X.M.; Li, H.; Wu, H.G.; Zhang, Z.H. Cooperative catalysis of Co single atoms and nanoparticles enables selective C_{Ar}-OCH_3 cleavage for sustainable production of lignin-based cyclohexanols. *J. Energy Chem.* **2023**, *79*, 535–549. [CrossRef]
227. Webber, M.S.; Watson, J.; Zhu, J.; Jang, J.H.; Çaglayan, M.; Heyne, J.S.; Beckham, G.T.; Róman-Leshkov, Y. Lignin deoxygenation for the production of sustainable aviation fuel blendstocks. *Nat. Mater.* **2024**, *23*, 1622–1638. [CrossRef] [PubMed]
228. Schutyser, W.; Renders, T.; Van Den Bosch, S.; Koelewijn, S.F.; Beckham, G.T.; Sels, B.F. Chemicals from lignin: An interplay of lignocellulose fractionation, depolymerisation, and upgrading. *Chem. Soc. Rev.* **2018**, *47*, 852–908. [CrossRef] [PubMed]
229. Fang, H.; Chen, W.; Li, S.; Li, X.; Duan, X.; Ye, L.; Yuan, Y. Tandem Hydrogenolysis-hydrogenation of lignin-derived oxygenates over integrated dual catalysts with optimized interoperations. *ChemSusChem* **2019**, *12*, 5199–5206. [CrossRef] [PubMed]
230. Wang, H.L.; Ben, H.X.; Ruan, H.; Zhang, L.B.; Pu, Y.Q.; Feng, M.Q.; Ragauskas, A.J.; Yang, B. Effects of lignin structure on hydrodeoxygenation reactivity of pine wood lignin to valuable chemicals. *ACS Sustain. Chem. Eng.* **2017**, *5*, 1824–1830. [CrossRef]
231. Mao, N.; Bai, X.; Liu, G.; Fu, W.; Tang, Y.; Dai, Z.; Zhao, Y.; Li, J. One-pot conversion of lignin into cycloalkane-rich sustainable aviation fuel precursors: Integrated catalytic depolymerization and hydrodeoxygenation over a bimetallic Ru–Ni/AlO_x catalyst. *Ind. Eng. Chem. Res.* **2025**, *64*, 16637–16650. [CrossRef]
232. Abdelaziz, O.Y.; Hulteberg, C.P. Lignin depolymerization under continuous-flow conditions: Highlights of recent developments. *ChemSusChem* **2020**, *13*, 4382–4384. [CrossRef] [PubMed]
233. Luo, Z.C.; Kong, J.C.; Ma, B.; Wang, Z.C.; Huang, J.; Zhao, C. Liquefaction and hydrodeoxygenation of polymeric lignin using a hierarchical Ni microreactor catalyst. *ACS Sustain. Chem. Eng.* **2020**, *8*, 2158–2166. [CrossRef]
234. Xu, Y.L.; Liu, Z.Y.; Liu, B.; Dong, B.; Pan, Y.; Li, Y.P.; Li, Y.C.; Guo, H.L.; Chai, Y.M.; Liu, C.G. Regulation of surface hydrophobicity and metal dispersion on Pt-based catalyst for the boosted hydrodeoxygenation of guaiacol into bio-hydrocarbons. *Mol. Catal.* **2024**, *553*, 113761. [CrossRef]
235. Rawat, S.; Kumar, A.; Ma, S.; Yang, Z.; Gieleciak, R.; Tan, E.C.D.; Heyne, J.; Wang, H.; Bhaskar, T.; Yang, B. Advancing technologies for lignin-based jet fuel production in aqueous phase. *Chem. Eng. J.* **2026**, *539*, 177150. [CrossRef]
236. Kumar, A.; Anushree; Kumar, J.; Bhaskar, T. Utilization of lignin: A sustainable and eco-friendly approach. *J. Energy Inst.* **2020**, *93*, 235–271. [CrossRef]
237. Shomal, R.; Zheng, Y. Development of processes and catalysts for biomass to hydrocarbons at moderate conditions: A comprehensive review. *Nanomaterials* **2023**, *13*, 2845. [CrossRef] [PubMed]

Disclaimer/Publisher's Note: The statements, opinions and data contained in all publications are solely those of the individual author(s) and contributor(s) and not of MDPI and/or the editor(s). MDPI and/or the editor(s) disclaim responsibility for any injury to people or property resulting from any ideas, methods, instructions or products referred to in the content.